AD-A141 319 ELECTRON EMISSION AND ION DESORPTION SPECTROSCOPY OF CLEAN AND OXIDIZED T.. (U) NATIONAL BUREAU OF STANDARDS WASHINGTON DC SURFACE SCIENCE DI.. E BERTEL ET AL. 1/2

UNCLASSIFIED 30 MAR 84 TR-35 N00014-94-F-0002 F/G 7/2 NL

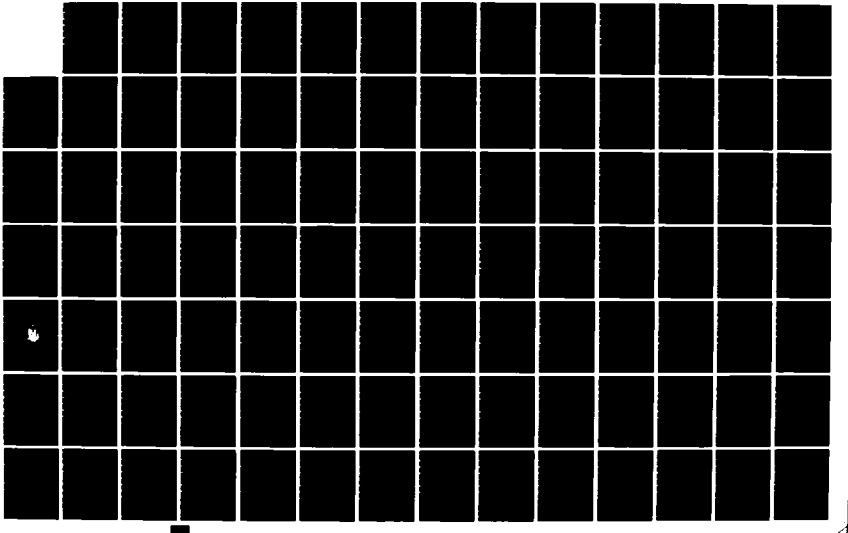

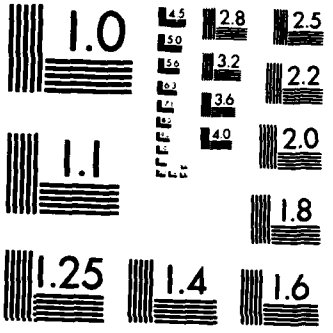

(12)

OFFICE OF NAVAL RESEARCH

Contract N00014-84-F0002

TECHNICAL REPORT NO. 35

ELECTRON EMISSION AND ION DESORPTION SPECTROSCOPY OF CLEAN AND OXIDIZED Ti(0001)

Erminald Bertel, Roger Stockbauer and Theodore E. Madey
Surface Science Division
National Bureau of Standards
Washington, DC 20234

March 30, 1984

Approved for Public Release; Distribution Unlimited

To be published in Surface Science

SECURITY CLASSIFICATION OF THIS PAGE (When Data Entered)

REPORT DOCUMENTATION PAGE	READ INSTRUCTIONS BEFORE COMPLETING FORM
1. REPORT NUMBER: 35 — 2. GOVT ACCESSION NO.: AD-A141319	3. RECIPIENT'S CATALOG NUMBER
4. TITLE (and Subtitle): Electron Emission and Ion Desorption Spectroscopy of Clean and Oxidized Ti(0001)	5. TYPE OF REPORT & PERIOD COVERED: Interim
	6. PERFORMING ORG. REPORT NUMBER
7. AUTHOR(s): Erminald Bertel, Roger Stockbauer and Theodore E. Madey	8. CONTRACT OR GRANT NUMBER(s): N00014-84-F0002
9. PERFORMING ORGANIZATION NAME AND ADDRESS: Surface Science Division, National Bureau of Standards, Washington, DC 20234	10. PROGRAM ELEMENT, PROJECT, TASK AREA & WORK UNIT NUMBERS
11. CONTROLLING OFFICE NAME AND ADDRESS: Office of Naval Research, Physical Science Program Office, Arlington, VA 22217	12. REPORT DATE: March 30, 1984
	13. NUMBER OF PAGES
14. MONITORING AGENCY NAME & ADDRESS(if different from Controlling Office)	15. SECURITY CLASS. (of this report): Unclassified
	15a. DECLASSIFICATION/DOWNGRADING SCHEDULE

16. DISTRIBUTION STATEMENT (of this Report)

Approved for Public Release; Distribution Unlimited

17. DISTRIBUTION STATEMENT (of the abstract entered in Block 20, if different from Report)

18. SUPPLEMENTARY NOTES

To be published in Surface Science

19. KEY WORDS (Continue on reverse side if necessary and identify by block number)

Direct recombination; oxidation; photoemission; resonant recombination; transition metals; titanium; titanium dioxide.

20. ABSTRACT (Continue on reverse side if necessary and identify by block number)

The electronic structure of Ti(0001) has been investigated by energy loss spectroscopy (ELS), Auger electron spectroscopy (AES), ultraviolet photoemission spectroscopy (UPS) using synchrotron radiation and electron stimulated desorption (ESD). Resonant electron emission due to a direct recombination process involving an atomic 3p - 3d interaction has been observed. Surface oxidation results in the formation of a thin protective TiO_2 layer which is stable to 250°C. In the oxide, the direct recombination process following 3p excitation gives rise to resonantly enhanced emission from the oxide. (Cont)

DD FORM 1 JAN 73 1473 EDITION OF 1 NOV 65 IS OBSOLETE

S/N 0102-LF-014-6601

SECURITY CLASSIFICATION OF THIS PAGE (When Data Entered)

Block 20. Abstract (Continued)

valence band. The cross section for electron and photon stimulated O^+ desorption is shown to be dominated by these atomic resonance effects as well.

Electron Emission and Ion Desorption Spectroscopy of Clean and Oxidized Ti(0001)

Erminald Bertel*, Roger Stockbauer and Theodore E. Madey

Surface Science Division

National Bureau of Standards

Washington, DC 20234

A1

* Visiting Professor, Dept. of Physics & Astronomy, University of Maryland, College Park, MD 20742, and NBS Visiting Scientist. Permanent address: Institut für Physikalische Chemie, Universität Innsbruck, A-6020 Innsbruck, Austria.

Abstract

The electronic structure of Ti(0001) has been investigated by energy loss spectroscopy (ELS), Auger electron spectroscopy (AES), ultraviolet photoemission spectroscopy (UPS) using synchrotron radiation and electron stimulated desorption (ESD). Resonant electron emission due to a direct recombination process involving an atomic 3p - 3d interaction has been observed. Surface oxidation results in the formation of a thin protective TiO_2 layer which is stable to 250°C. In the oxide, the direct recombination process following 3p excitation gives rise to resonantly enhanced emission from the oxide valence band. The cross section for electron and photon stimulated O^+ desorption is shown to be dominated by these atomic resonance effects as well.

1. INTRODUCTION

The structure and properties of titanium and its oxides are of great interest in various fields of science and technology ranging from electrocatalysis and photocatalysis to medicine. In the former cases, Ti oxides are used both as active catalysts (1) as well as supports for metal catalysts (2). In medical applications, titanium is an excellent biocompatible material, providing good conditions for osseointegration of implants in bone (3). The electronic structure of TiO_2 is of theoretical interest, because among other reasons, TiO_2 is believed to provide the classical example for the Knotek-Feibelman mechanism of electron- and photon-stimulated O^+ desorption (4,5).

In all of the above cases it is important to know the structures and properties of the (surface-) oxides involved. Most of the previous oxidation studies of Ti were carried out on polycrystalline material (6-15). The published results can be summarized as follows: Room temperature oxidation starts with immediate subsurface incorporation of oxygen. The depth profile of the oxygen concentration depends on the pressure during exposure. At saturation, however, the surface oxide is always a TiO_2-layer with estimated thickness of the order of 6 Å on top of lower oxides. At higher temperatures no TiO_2 layer is formed because the oxygen surface concentration is reduced by diffusion.

Characteristic changes in the photoemission spectra of Ti upon oxidation included a strong d-band attenuation, and core-level binding energy shifts. A maximum 2p level shift of 5 eV to higher binding energy has been associated with the formation of the TiO_2 layer.

There are only a few studies dealing with the surface oxidation of Ti single-crystals (5,16-18). A Ti(0001) p(2x2)-O structure was observed by low energy electron diffraction (LEED) after exposure to 1.25 - 5L O_2, depending on the particular crystal sample (16). At higher exposures the LEED pattern became streaky and finally a Ti(0001) (1x1)-O structure developed between 100 and 220 L O_2. At that stage the oxygen KLL Auger peak height saturated; hence the authors assumed completion

of the saturation oxide layer throughout the sampling depth. From a comparison of the Auger transitions around 400 eV with the corresponding bulk oxide spectrum reported by Solomon and Baun (19) the stoichiometry of the saturation oxide was assumed to be TiO. The exposures needed to achieve various stages of oxidation were pressure independent but were different for different samples. Recently, a stepped Ti(0001) surface has been investigated by Hanson et al (5). Work function measurements showed an initial decrease upon O_2 exposure, suggesting immediate oxygen subsurface incorporation in agreement with results on polycrystalline Ti (14,15,20). The UPS results showed a considerable d-band attenuation after exposure to 15 L O_2. For exposures performed at 90 K this attentuation was even more pronounced than at 300 K. Correspondingly, the O^+ ion yield in ESD and PSD was 5 times higher after the low temperature exposure. The O^+ ion energy distributions were similar for both reaction temperatures and the ion yield spectra were consistent with the behavior expected for the Knotek-Feibelman mechanism (4).

The goal of the present study was a detailed characterization of the Ti(0001)/O_2 system (preliminary accounts of parts of this work have been presented recently (21,22)). The electronic structure of the clean metal and of the oxidized surface have been investigated by electron and ion desorption spectroscopy. Electron energy loss spectroscopy (ELS) was used to probe the valence electron excitations [section 3] in the metal [3.1] and the surface oxide [3.2]. The characteristic loss structure in the valence region provided a fingerprint identifying the surface oxide as TiO_2. The variability of the sampling depth in ELS was exploited to show that the surface oxide obtained by saturation exposure to oxygen at room temperature covers the clean metal as a thin protective layer [3.3]. The thermal stability of this layer was studied by monitoring the changes in the electron energy loss spectra when the oxidized sample was heated [3.4].

The electron energy losses resulting from shallow core level (3p and 3s) excitations are reported in section 4. The 3p cross section near threshold and the 3s excitation cross section are strongly influenced by oxidation. Most remarkable however, the 3p cross section shows a pronounced maximum far above threshold, which remains nearly unaffected by oxidation. The stability of this loss structure against changes in the chemical environment is due to the strongly localized atomic character of the corresponding excitation which is discussed in more detail in section 8.

The decay channels of the 3p shell excitations have been monitored by electron-excited Auger spectroscopy [section 5]. In addition to the M_{23} VV Auger transition electron emission is observed to occur also at slightly higher energies in both the metal [5.1] as well as the oxide [5.2]. It is explained in terms of an auto-ionization process initiated by the localized 3p excitation.

Further progress in the explanation of the electronic structure of Ti(0001) and its surface oxide was achieved by UPS using synchrotron radiation from the SURF II facility at the National Bureau of Standards [section 6]. The changes in the electron distribution curves occurring upon oxidation are interpreted in a molecular orbital picture and show good qualitative agreement with cluster calculations (23). The TiO_2 stoichiometry of the surface oxide layer is confirmed by the observed chemical shift of the 3p core level. Resonant maxima in the valence electron photoemission and in the cross section of photon-excited Auger emission are observed [6.2]. This resonant photoemission corroborates the existence of the autoionization process as a decay channel for the 3p excitation in addition to the normal Auger process.

Secondary electron distribution curves are reported in section 6.3. For the clean surface we correlate the result with band structure calculations (24). Slight contamination is shown to produce significant changes in the secondary electron distribution.

Finally, electron and photon stimulated desorption of O^+ ions from the $Ti(0001)/O_2$ system has been studied [section 7]. The results are similar to the experiments on

the stepped Ti(0001) surface (5) and consistent with the Knotek-Feibelman interatomic Auger decay model (4).

Section 8 is devoted to a theoretical discussion of the nature of the localized 3p excitation far above threshold.

2. EXPERIMENTAL DETAILS

The measurements have been performed in a stainless steel UHV system at a base pressure of 1.5×10^{-10} Torr. The sample surface was prepared parallel to the (0001) plane with an accuracy of $\pm$ 0.5° by mechanical polishing only. Sample cleaning consisted of Ar sputtering (1 keV) and annealing ($\sim$ 700°C) cycles, followed by prolonged heating of the sample to about 800 °C to remove the bulk hydrogen. The only impurity left after this procedure was surface hydrogen, evidenced by UPS (17) and ESD-TOF (time-of-flight) measurements. The surface concentration of hydrogen could be significantly reduced by slight exposure to oxygen ($\sim$ 4 L) followed by heating to $\sim$ 700°C and quenching to room temperature. This procedure results in AES and UPS signals showing no signs of contamination, with only ESD able to detect small H^+ and F^+ signals.

Electron and ion spectra were recorded in a partially angle integrated mode with a double-pass cylindrical mirror analyzer (CMA). ELS, AES and ESD spectra were obtained by excitation with a coaxial electron gun. The AES and some of the ELS were collected with the sample surface perpendicular to the analyzer axis which produced angle-integrated spectra with respect to the azimuthal angle. The polar angle of emission of the analyzed electrons in this geometry is 52° (determined by the analyzer collection angle). The remaining spectra were obtained with the sample at some angle, usually 45°, to the analyzer axis which produced partially angle-integrated spectra. In this geometry the polar angle of emission of the analyzed electrons depends on the azimuthal angle. The mass distributions of desorbing ions were measured by TOF-mass spectrometry through the CMA as described in refs. (5) and (25). UPS spectra were recorded with mainly p polarization. The resolution of the toroidal grating monochromator was about 0.35 eV at $h\nu$ = 37 eV, 0.7 eV at $h\nu$ = 47 eV and 1.8 eV at $h\nu$ = 67 eV.

3. ELECTRON ENERGY LOSS: VALENCE REGION

3.1 Clean Metal

ELS spectra of clean Ti metal are shown in Fig. 1 (curves a and b). At 1150 eV primary energy (curve 1a) the spectrum is dominated by a peak at about 17 eV in good agreement with earlier data obtained in reflection (26) as well as transmission (27) geometry. This feature has been attributed to the volume plasmon excitation (26). Within a free electron approximation the position of the collective volume loss is calculated to be at 17.7 eV. An additional loss feature at about 8.5 eV becomes more prominent if the sampling depth is reduced by lowering the primary energy and going to off-normal incidence (curve b in Fig. 1). The fact that this loss feature is due to the electronic structure of the surface is demonstrated not only by its sampling-depth-dependence but also by its sensitivity to surface contamination. An exposure of 0.4 L O_2 is sufficient to reduce the intensity of the 8.5 eV loss considerably (curve c in Fig. 1). It is also reduced if surface hydrogen is present (after Ar sputtering and annealing without subsequent oxygen treatment).

Assignment of structures seen in ELS to either interband transitions or collective excitations is facilitated by comparison with optical data. The results of these optical experiments are usually expressed in terms of the complex dielectric response function $= \varepsilon_1 + i\varepsilon_2$. Lynch et al. (28) report such measurements for polycrystalline Ti, but from their sample preparation method one can expect heavy oxidation of the surface. The loss function ($-\mathrm{Im}(1/\varepsilon)$) reported by these authors is indeed quite different from the clean metal spectra shown in Fig. 1. Optical data obtained by Wall et al. (29) on polycrystalline Ti cleaned in UHV are in much better agreement with the present results. The loss intensity below 7 eV is attributed mainly to interband transitions by Wall et al. (29), although ε_1

goes through zero at around 4 eV and Lynch et al. (28) assume therefore collective contributions between 4 and 5 eV.

The surface sensitive loss at $\sim$ 8.5 eV observed in the present experiment cannot be identified unambiguously by comparison with optical data. It may, however, be related to surface states. Indeed, Feibelman et al. (30) predicted for the Ti(0001) surface a strong deviation from bulk values of the density of states, and this has been verified experimentally using UPS (31) and appearance potential spectroscopy (18).

The loss intensity around 13 eV could be associated with a surface plamson, The results of Wall et al. (29), however, indicate substantial bulk contributions to the loss function in this energy range as well.

3.2 Surface Oxidation Monitored by ELS

The changes of the ELS spectrum in the 0-30 eV range occurring upon exposure to oxygen at room temperature are shown in Fig. 2. A primary energy of 150 eV and off-normal incidence have been used to obtain the highest possible surface sensitivity. Even small exposures to oxygen (4 L) cause a decrease of the loss feature at 8.5 eV. Simultaneously a maximum is formed at 12.5 eV. At higher exposures this maximum shifts to lower energy and increases in height, resulting in a dominant peak at 10 eV after 40 L O_2 exposure. A shoulder at 12.5 eV persists up to saturation exposure. For exposures larger than 5 L O_2 a substantial reduction of the loss intensity between 2 and 5 eV is observed, while features at 1.5 and 5.5 eV emerge. Finally a continuous increase in loss intensity is observed at $\sim$ 23.5.

The decrease in loss intensity between 2 and 5 eV is most easily interpreted by comparison with UPS spectra described below in Sec. 6. The oxygen exposure results in a decrease of the Ti 3d electron density due to formation

of surface oxides. Consequently intraband excitations involving 3d electrons are reduced in intensity and the loss spectrum shows a minimum around 3.5 eV. The subsequent increase in loss intensity towards higher energies can be associated with the onset of excitations across the band gap of the Ti-oxide formed. Kurtz and Henrich (32a) observed in vacuum-cleaved Ti_2O_3 a loss peak at 6.2 eV (dN/dE-mode) which they associated with an $O(2p) \rightarrow e_g^{\pi}$ transition. Upon O_2 adsorption, this loss shifted to 5.6 eV. In TiO_2 a peak of similar origin is observed at 5.5 eV (32b, 33). Consequently, the 5.5 eV feature appearing in the present experiment indicates the formation of a surface oxide with an oxidation state beyond Ti_2O_3.

The peak at 10 eV has been observed by Henrich et al. (32a) in oxygen-exposed Ti_2O_3 and in vacuum fractured TiO_2 and has been attributed to $O(2p) \rightarrow Ti(3d)$ charge transfer excitations by Kurtz and Henrich (32a). In ELS experiments on freshly-cleaved Ti_2O_3 the 10 eV peak does not appear and therefore seems to be characteristic of Ti^{4+} species (32a) in the surface oxide. In contrast the feature at about 13 eV appears in various Ti-oxides. Kurtz and Henrich (32a) propose an $O(2p) \rightarrow O(3s)$ excitation to be responsible for this structure.

The optical data of Wall et al. (29) for oxidized polycrystalline Ti show that ε_1 is close to zero from 9 to 14 eV and the calculated loss function has a maximum at about 14 eV. In the loss function given by Lynch et al. (28) for polycrystalline Ti which was certainly oxidized due to the preparation method, a similar peak also appears at $\sim$ 13.5 eV. From their optical data, Lynch et al. (28) derive plasmon energies of 4.7 and 13.7 eV and surface plasmon energies of 4.2 and 10.7 eV. Thus the optical data suggest that the loss spectrum of the Ti surface oxide is modified by collective effects between 4 and 14 eV and should not be interpreted on the basis of single electron excitations only.

The 23 eV structure is apparently too broad to be detected in the derivative mode used by Kurtz and Henrich (32a). It has been attributed to a volume plasmon

excitation involving all the valence electrons (36). There is a surprisingly close agreement with free electron values of $\hbar\omega_p$ (22.8 eV for Ti_2O_3 and 23.8 eV for TiO_2).

The above results strongly suggest the build-up of a TiO_2-like surface oxide for exposures larger than 40 L. However, the 1.5 eV loss shown in Fig. 2 is not observed in bulk TiO_2, whereas a very intense feature is observed at this energy in Ti_2O_3 (32). Supposedly the 1.5 eV loss in Fig. 2 originates either from surface defects containing Ti^{3+} or from the metal-oxide interface.

Finally, a comparison of the present spectra with transmission high-energy loss data (36) shows good agreement for the observed losses. The double peak at 10 and 13 eV is not resolved in the high energy data but nevertheless Frandon et al. (36) assign single electron excitations around 10 eV to the $3e_g$ and $2t_{2g}$ states and a collective loss at 12 eV which is consistent with the conclusions presented here. A bulk plasmon loss appears in the high energy data at 26 eV, i.e., 2.5 eV above the corresponding loss peak in the present work. The difference may be due to the thin-layer structure of the surface oxide formed on Ti(0001).

3.3 The Structure of the Surface Oxide as Probed with ELS

In Fig. 3 ELS spectra of the Ti(0001) surface are shown for intermediate (20 L) and "saturation" exposures (10^3 L) of oxygen. The surface sensitivity has been varied by changes in both primary energy and angle of incidence. Due to the partially angle integrated collection mode, influences from anisotropic scattering are deemed to be small. Spectrum 3a was obtained after 20 L O_2 exposure with 1000 eV primary energy and normal incidence. The clean metal plasmon feature at 17 eV is dominant, but there is already considerable intensity around 12.5 eV indicating the presence of oxide. If the surface sensitivity is increased by increasing the angle of incidence to 55° (Fig. 3b), the intensity ratios of

clean metal and oxide features change dramatically. The metal plasmon nearly disappears and the ELS spectrum resembles closely those shown for intermediate exposures in Fig. 2. Note, that with 150 eV primary energy the surface sensitivity is larger than with 1000 eV primary energy; hence, the spectrum obtained using 150 eV primary energy after 10 L O_2 exposure in Fig. 2 shows the same features as that obtained using 1000 eV primary energy after dosing with 20 L O_2 in Fig. 3b.

Spectra recorded after saturation exposure (10^3 L O_2) are shown in Fig. 3, lower panel. Spectrum 3e was measured with high surface sensitivity (Ep = 150 eV, 65° angle of incidence) and shows the characteristic loss features of the saturation surface oxide as discussed above. If the direction of the primary electron beam is changed to normal incidence (Fig. 3d), the most significant change is a reduction in intensity of the 10 eV feature. A slight increase in loss intensity around 3.5 eV appears to occur also. If a primary energy of 1000 eV is used, however, the ELS spectrum changes in a dramatic way (Fig. 3c). The metal bulk plasmon peak at 17 eV reappears, the 10 eV peak is reduced further, and the gap in loss intensity around 3.5 eV nearly disappears.

The presence of the metal plasmon peak as well as oxide peaks at intermediate and saturation exposure indicate the coexistence of both the clean metal and the oxide phase near the surface. This is consistent with two different models of oxide formation: either island growth or overlayer formation. The variation of the sampling depth, which can easily be achieved in ELS spectroscopy, provides a powerful tool to distinguish between these two different modes of oxide growth. In the case of overlayer growth only the oxide signal is detected if the spectra are taken with high surface sensitivity. If the probing depth is increased, however, the metal underneath starts to contribute to the signal and for sufficiently thin overlayers it might even dominate at high primary energies. This is in contrast to the probing depth dependence in the case of island growth, where at subsaturation exposures, the metal signal is observed together with the oxide features even at low primary energies (small

sampling depth) and the differences between low and high primary energy spectra are much less pronounced (37). The results presented in Fig. 3 show a strikingly different ratio of metal to oxide signal for different probing depths, the metal signal being absent at low primary energy. Therefore, overlayer growth is clearly favored in the case of the O/Ti(0001) system. In addition, from the presence of discrete metal and oxide features at high primary energy it can be concluded that the interface between metal and oxide is quite sharp. Assuming a mean free path of 12-15 Å for 1000 eV electrons and 5 Å for 150 eV electrons in TiO_2 the oxide layer is estimated to be only of the order of 10 Å (or approximately 3 atomic layers) in thickness. Accordingly, the change in oxygen concentration from TiO_2 stoichiometry to the clean Ti-metal takes place within about 2 atomic layers.

3.4. The Thermal Stability of the Oxide Overlayer

In order to check the thermal stability of the surface oxide formed during exposure of Ti(0001) to oxygen at room temperature, the changes in the oxide ELS spectrum have been observed as a function of temperature. In Fig. 4 a series of ELS spectra is presented which have been recorded at 1000 eV primary energy and 55° angle of incidence at successively higher temperatures up to 450 °C. The last one has been taken after cooling down again to T_R ($\sim$ 25°C). The top spectrum was recorded after room temperature exposure and shows the characteristic oxide features at 23.5, 12.5 and 10 eV as well as the gap at 3.5 eV. Small contributions from the metal beneath the oxide are evidenced by the slightly enhanced intensity around 17 eV, by the ratio of the 12.5 eV and 10 eV peak and by the residual intensity in the low energy loss region at 3.5 eV.

Heating to 160 °C does not change the loss structure, but at 250 °C the 3.5 eV loss intensity starts to increase and the 10 eV peak decreases. Both changes indicate reduction of Ti^{4+} to lower oxidation states. At 390 °C the minimum at

3.5 eV and the peak at 10 eV have virtually vanished but the high energy plasmon at 23 eV and the 12.5 eV peak are still present, which suggests a stoichiometry between TiO and Ti_2O_3. Between 390 °C and 450 °C, however, a dramatic change occurs. The high energy plasmon as well as the 12.5 eV peak disappear leaving a broad structure around 15 eV with a poorly defined shoulder at 8 eV. After cooling to room temperature the shoulder shifts to 6 eV and is more pronounced. Probably, this spectrum is typical of either TiO or Ti with oxygen dissolved in the metal lattice.

3.5 Summary: Electron Energy Losses-Valence Region

In summary the electron energy losses in the valence region are strongly influenced by collective effects in both metal and oxide. A definite peak assignment is not possible in all cases, but the metal and oxide spectra show distinctly different features. The sampling depth dependence of their intensity ratio indicates oxide overlayer formation saturating at about 10 Å thickness under conditions of the present experiment. Comparison with ELS spectra of bulk-Ti_2O_3 and bulk-TiO_2 suggests the formation of Ti^{4+} in the outermost layers.

4. ELECTRON ENERGY LOSS: SHALLOW CORE LEVEL REGION

In Fig. 5a an ELS spectrum of surface oxidized Ti is shown again but now including the shallow core level region. A broad peak is observed at about 47 eV which is associated with Ti 3p → 3d excitations (38). In the lower half of Fig. 5 the 3p losses are shown on an enlarged scale for Ti metal (5b) and oxide (5c).

The first feature in the metal spectrum (5b), a small peak at ∿ 34 eV, is too sharp to be a double plasmon excitation. It has been observed on polycrystalline Ti as well and was attributed to a 3p → conduction band excitation, the peak shape being due to band structure effects (39). This assignment will be discussed below. The threshold for the 3p excitation is given as 33 eV by Ross and Gaugler (39)

thus coinciding with the UPS binding energy of the 3p level observed here (see below). In the present ELS data, however, the threshold occurs at slightly lower energy consistent with the observations of Erickson and Powell (40) for primary electron energies of approximately 200 eV.

After passing through a minimum at 37 eV the loss intensity in the metal spectrum rises again to a broad but pronounced peak at about 47 eV. This peak has been detected in a variety of soft x-ray absorption spectroscopy (SXAS) and ELS experiments (26,38,39,41). A similar broad maximum in the 3p excitation cross section 10-15 eV above threshold is a common feature in all transition metals with less than half filled 3d shells (26,38,41,42). The peak at 60 eV loss energy is attributed to Ti 3s excitations (XPS binding energy of 58.7 eV (43)). Grunes and Leapman (44) found similar, though much less intense peaks in angularly resolved transition electron energy loss spectra on the 3d transition metals. The momentum transfer dependence of the peak intensities led to an identification of the losses as dipole forbidden 3s → 3d excitations. This assignment is consistent with the observation of the peak in ELS at E_p = 217 eV and the absence of a corresponding feature in the photoexcited spectra (especially the CFS-photoabsorption spectrum). The surprisingly large oscillator strength of the 3s → 3d loss in the present data seems to be a further example of the behavior of optically forbidden transitions at intermediate energies (45).

The 3p-excitation spectrum obtained after oxidation of the Ti(0001) surface is shown in Fig. 5c. The small loss peak at ∿ 34 eV in the metal has disappeared (Note that the 3p binding energy is shifted in the oxidized surface to 38 eV as shown below). The main peak in the 3p cross section (∿ 47 eV in Ti metal) is a little bit sharper and shifted to 46 eV. The Ti 3s loss appears much less pronounced in the oxide with an intensity comparable to that reported by Grunes and Leapman (44). The shift of the 3s loss peak amounts to at most 2.5 eV in the present data. The strong reduction of the intensity of the 3s → 3d transition after oxidation is not yet understood, because the $2t_{2g}$ and $3e_g$ levels

should provide a significant d-projected density of states even in the oxide.

The broad maximum in the 3p excitation cross section at 47 eV in the metal has been interpreted as an atomic effect (46), namely excitation of high lying multiplet terms of the atomic $3p^5 3d^{n+1}$ configuration. These terms are driven up in energy by a strong exchange interaction and draw a large oscillator strength in transition metals with less than half filled 3d shells. We discuss this phenomenon in section 8. In the following the symbol $3p^5 3d^*$ will be used to designate this localized state 14 eV above threshold.

The atomic character of the main 3p resonance at 47 eV seems to be in contrast to the explanation of the near threshold structure at $\sim$ 34 eV in the metal as a 3p $\rightarrow$ conduction band excitation. In order to describe the whole 3p excitation spectrum consistently in an atomic picture one could also try to associate the small 3p-loss peak near threshold with dipole forbidden excitations of atomic multiplet terms. The photon absorption spectrum reported by Hanson et al. (5) shows, similar to the ELS spectrum, a slight shoulder near 35 eV which is at variance with the assignment to optically non-allowed transitions. However, the spin-orbit interaction will relax this restriction rendering some of the near threshold transitions weakly dipole-allowed. But in any case, the near threshold states are expected to interact strongly with conduction band states. Therefore the discrimination between an atomic and a solid state picture may be artificial.

In the photon excited spectra presented in Fig. 10 no structure appears in this energy range. Consequently the decay process following a near-threshold excitation of the 3p shell does not enhance the direct 3d emission. Instead, the resulting electron emission probably appears in the Auger peak near threshold (47). The CFS curve tuned to the Auger peak (Fig. 10c) does not show such a contribution around 35 eV, but only a close inspection of subtle changes in the

AES peak shape near threshold could provide conclusive evidence as to which decay channel is operating.

The ELS spectrum of the oxidized sample is nearly featureless between 33 eV and 41 eV. In contrast to the persistence of the main peak at 47 eV the small peak at 35 eV has disappeared in the oxide. A 3p → conduction band excitation in the oxide, however, would require at least 38 eV (see section 6). Theforefore the associated peak may be masked by the onset of the main 3p resonance in the oxide.

In summary, the electron energy loss spectrum associated with 3p excitations in the metal and the oxide is explained in terms of a 3p → conduction band excitation near threshold and an excitation to a localized state far above threshold which may be considered a "remnant" of high lying atomic $3p^5 3d^{n+1}$ multiplet terms as will be discussed in section 8.

5. AUGER ELECTRON SPECTROSCOPY

5.1. Low Energy Region: Ti Metal

In Fig. 6a the low energy (0-100 eV) dN/dE - Auger spectrum is shown obtained by electron excitation with a primary energy E_p = 217 eV. The spectrum is dominated by a very intense transition at ϵ' = 25 eV (inflection point of the dN/dE - AES peak referenced to the vacuum level). Using the UPS derived binding energies (Fig. 7) and bearing in mind that the 3d hole-hole Coulomb-correlation energy is small in the lower transition metals (48), the 25 eV emission is readily identified as $M_{23}M_{45}M_{45}$ super Coster-Kronig (SCK) Auger emission. The calculated energy

$$\epsilon' = E_{3p} - 2E_{3d} - U_{eff} - \phi = 26.4 \text{ eV} - U_{eff}$$

with E_{3p} = 33 eV, E_{3d} = 1 eV, and analyzer work function ϕ = 4.6 eV, is in

perfect agreement with the measured energy, if U_{eff} is assumed to be 1.4 eV, which is a reasonable value.

Another broad feature, however, appears between 37 and 45 eV in the metal AES spectrum. It has been noted previously by other groups (49,50,16) and was tentatively assigned to a transition in an already ionized atom (50).

A different explanation, however, has been proposed as a result of the present investigations (22). As discussed in the preceding section, the 3p shell can be resonantly excited to a final state 47 eV above the ground state. The excited state is 14 eV above the 3p ionization threshold in Ti metal. There are two possible de-excitation mechanisms. The first is the normal $M_{23}M_{45}M_{45}$ Auger decay, i.e., electron emission from the 3p shell followed by a SCK Auger transition. This mechanism results in the ejection of 2 electrons, the first one with a kinetic energy of ε = 9-10 eV, the second one with ε' = 25 eV (both energies referenced to the vacuum level). Due to the resonant character of the 3p excitation, the AES yield should show a resonant maximum at 47 eV photon energy in a photon excited Auger experiment. This is actually the case as shown in Fig. 11.

The second decay mechanism of the excited state at 47 eV is a direct recombination type process, where the excitation energy is completely transferred from the 3p shell to a 3d electron. In this case only one electron is emitted, but with substantially higher energy than in the Auger decay. The energy is expected to be

$$\varepsilon'' = E_{excit} - E_{3d} - \phi = 41.4 \text{ eV}$$

in good agreement with the higher energy peak observed in the metal Auger spectrum (Fig. 6a).

In a single electron notation the excitation and the two subsequent decay processes can be described as follows:

$$3p^6 3d^2 4s^2 \rightarrow 3p^5 3d^2 4s^2 3d^* \qquad (1)$$

$$3p^5 3d^2 4s^2 3d^* \rightarrow 3p^6 4s^2 + \varepsilon d + \varepsilon' \ell \qquad (2a)$$

(delocalization and SCK-decay)

$$3p^5 3d^2 4s^2 3d^* \rightarrow 3p^6 3d^1 4s^2 + \varepsilon'' \ell \qquad (2b)$$

(direct recombination)

where ℓ defines the angular momentum of the ejected electron with respect to the emitting atom.

If the peak at 42 eV in the electron excited AES-spectrum is actually due to a direct recombination (d.r.) process this should give rise to peculiar observations in photoemission spectroscopy. First, at a photon energy of around 47 eV a resonant enhancement of the 3d photoemission should occur. This is due to the fact that the kinetic energy ε'' carried off by an electron ejected in a direct recombination process at $h\nu = 47$ eV is exactly the same as the energy of a photoelectron from a direct 3d photoemission process at this photon energy (initial states and final states are identical in both processes). Second, a constant final state (CFS) spectrum monitoring the photon energy dependence of the SCK-Auger emission (analyzer kept at constant kinetic energy $E_k = 25$ eV) should trace the 3p ionization cross-section, whereas a CFS spectrum of the higher energy feature ($E_k = 42$ eV) should reveal a rather sharp structure peaking at 47 eV photon energy, namely the resonantly enhanced 3d-photoelectron peak passing through the CFS-window. Both experiments have been carried out and, as discussed in section 6, the results fully support the mechanism proposed above.

5.2. Low Energy Auger Region: Oxidized Ti

In Fig. 6b the dN/dE Auger spectrum of the oxidized Ti(0001) surface is presented. The 25 eV SCK emission is nearly completely suppressed. The broad feature around 43 eV in the clean metal is replaced by a slightly sharper structure around 36 eV kinetic energy in the oxide.

The attenuation of the $M_{23}M_{45}M_{45}$ Auger transition at 25 eV indicates a strong reduction of the 3d electron density. This is in agreement with the

conclusions inferred from the appearance of a pronounced minimum in ELS intensity at 3.5 eV (Fig. 2) and the disappearance of the 3d-emission in UPS (see below). All of these changes indicate that the thin surface oxide layer formed after only 40 L of O_2 exposure has a stoichiometry close or equal to TiO_2.

The emission at 36 eV is readily explained in terms of the direct recombination model. As already discussed in Section 4 the 3p cross section in the oxide shows a resonant peak at 46 eV similar to the clean metal. In a direct recombination process analogous to that proposed in the metal but in this case involving an oxide-valence-band electron, an electron is ejected with a kinetic energy

$$\epsilon''_{oxide} = E_{excit} - E_{OVB} - \phi = 36 \text{ eV}$$

where E_{OVB} is the energy of the oxide valence band = 6 eV. This is in good agreement with the energy observed in the electron-excited AES spectrum (Fig. 6b). Such a de-excitation process involving an interaction between the 3p core level and the oxide valence band is expected to be dominant only if no intraatomic interaction with 3d electrons is possible (51). Hence the 36 eV emission in the electron-excited oxide Auger spectrum is another indication of Ti^{4+} formation.

After having explained the electron excited Auger spectra of both clean and oxidized Ti(0001) in terms of a conventional SCK-Auger emission and a direct recombination process following resonant 3p-excitation, it remains now to show that an explanation involving only conventional Auger transitions is impossible.

In clean Ti metal possible low-energy Auger processes are $M_1M_{45}M_{45}$ ($E_K \tilde{\approx} 50$ eV), $M_1M_{23}M_{45}$ ($E_K \tilde{\approx} 19$ eV) and $M_{23}M_{45}M_{45}$ ($E_K \tilde{\approx} 25$ eV). None of these transitions causes electron emission at 37-45 eV. Auger emission originating from doubly ionized atoms (50) is expected to be weak, possibly below the detection limit. Furthermore, in this case the $M_{23}M_{45}M_{45}$ peak at 25 eV and the broad 42 eV feature should show different primary energy dependences in the electron excited AES, which was not observed.

For the oxidized Ti sample, calculations of Auger energies are slightly less reliable than for the metal because the chemical shift of the 3s level has not been

determined in the present experiment and the oxide valence band has a large energy spread resulting in a broad range of possible Auger energies. The only Auger transition in the oxide, however, which could cause emission at 34-39 eV is the M_1VV process. If we assume a 3s core level shift of 5 eV upon oxidation similar to what has been observed for the 2p (52) and the 3p levels (Fig. 9), the 3s binding energy in the oxide is estimated to be 63 eV. The interaction should be strongest with the lower part of the oxide valence band where the bonding orbitals have a 10-20 percent admixture of Ti levels in contrast to the nonbonding orbitals in the upper part of the oxide valence band (23). If we further assume a Coulomb correlation energy of the two final state holes in the valence band of roughly 4 eV, the M_1VV Auger energy is then estimated to be approximately 39 eV. This is in the energy range of the observed transition, but the cross section for such an M_1VV process in the oxide should be smaller than for the corresponding intra-atomic M_1VV transition in the metal (51). Such an emission (at about 50 eV) in the metal, however, is not observed, hence a major contribution of the M_1VV Auger process to the 36 eV peak in the oxide spectrum can be ruled out.

6. ULTRAVIOLET PHOTOEMISSION SPECTROSCOPY

6.1. Electron Distribution Curves (EDC)

Electron distribution curves of clean Ti(0001) recorded at 3 different photon energies are shown in Fig. 7. At $h\nu$ = 37 eV a weak d-emission is observed peaking below 1 eV binding energy. The steplike increase of the electron yield at 5 eV (for this photon energy) is associated with the $M_{23}M_{45}M_{45}$ Auger emission. This feature remains at constant electron kinetic energy as the photon energy is increased.

At 47 eV photon energy the d-band emission is strongly enhanced and much broader. At 57 eV the 3d yield has decreased again but the deeper parts of the d band contribute more than at 37 eV photon energy.

Exposure to 1.5 L oxygen causes a narrowing of the d-band (Fig.8) while the maximum in d-band emission at 47 eV remains unchanged. An oxygen 2p-derived peak appears at about 6.2 eV binding energy with a FWHM of roughly 1.8 eV and a shoulder at the higher binding energy side extending to 9 eV. At photon energies around 47 eV a slight change of the O 2p peak shape is observed but its yield does not increase in passing through the resonance energy of 47 eV. Beyond that energy the cross section for O 2p emission drops off quite sharply.

Further exposure to oxygen reduces the metallic d-band emission considerably. At exposures exceeding 40 L O_2 no further change in the UPS spectra is observed. A series of EDCs obtained from an oxygen saturated Ti(0001) surface is displayed in Fig. 9. 3d emission is nearly absent at 37 and 57 eV. An enhancement of this residual emission occurs at $h\nu$ = 47 eV but even then the 3d peak is much smaller than the oxygen 2p-derived oxide valence band peak. This oxide valence band has its onset at about 3.8 eV binding energy and extends down to 9.5 eV. Compared to the slightly oxidized surface the emission has increased mainly between 3.8 and 5.5 eV corresponding to the non-bonding and weakly bonding 2p(π)-derived levels, and in the region between 7 and 9 eV corresponding to the 2p-3d-hybridized orbitals of strongly σ-bonding character (23) (shaded areas in Fig. 9, bottom curve). At 47 eV the oxide valence band emission in the saturated surface oxide exhibits strong enhancement between 6 and 8 eV (shaded areas in Fig. 9, middle curve). A comparison with the MO-diagram for TiO_6^{-8} (23) suggests that the enhancement is associated with the $2e_g$ and the $1t_{2g}$ levels. Both have strong 3d admixture but are different in bonding character (σ and π, respectively). Tossell et al. (23) calculated the spatial distribution of the electron density: the $2e_g$ orbital has 21 percent, the $1t_{2g}$ 12 percent of its charge density inside the "Ti-sphere", the charge fraction in the "O-sphere" being 58 and 57 percent, respectively. (The remaining change is distributed in the interatomic space.) It is the comparatively large wave function amplitude on the Ti site which is

responsible for the participation of the $2e_g$ and $1t_{2g}$ orbital in the core hole decay. The positive charge remaining after resonant emission from these orbitals, however, is mainly concentrated inside the oxygen sphere. In that sense, the resonant photoemission from the oxide valence band can be called a "cross-autoionization". It should be mentioned that the orbital assignment made above does not take into account the slight distortion of the oxygen octahedra, which reduces the symmetry (53) and produces an additional splitting of the e_g into a_{1g} and b_{1g} levels and of the t_{2g} into a_{1g} and e_g levels. These details, however, cannot be resolved in angular integrated photoelectron spectroscopy.

The strong attenuation of the d-band emission after only 48 L O_2 exposure is a further corroboration of the oxide overlayer model which was proposed earlier (Section 3.3) based on the ELS results. A comparison with UPS spectra measured on bulk-Ti_2O_3 and TiO_2 samples (54, 32a) indicates an oxidation state beyond Ti_2O_3 for the surface oxide formed in the present experiment. The residual emission at the Fermi level seems to be slightly higher than in bulk-TiO_2 and can be attributed to Ti^{3+} surface defects and contributions from the metal-oxide interface, as already discussed in section 3.2 for the 1.5 eV electron energy loss.

Additional information about the oxidation state of the surface is available from core level chemical shifts. Fig. 7 (insert) shows the position of the 3p level in the clean metal at 33 eV. After 48 L O_2 exposure the 3p emission appears at 38 eV binding energy (Fig. 9, insert). This 5 eV binding energy shift agrees very well with 2p-core level shifts observed in TiO_2 bulk samples (52). The $2p_{3/2}$ peak was measured at 5.2 eV higher binding energy in TiO_2 as compared to the metal, whereas the chemical shift of the $2p_{3/2}$ level in Ti_2O_3 is only about 4.3 eV (52).

The O 2s peak in Ti(0001) + 48 L O_2 is shown in Fig. 9 (insert). The binding energy is 22.6 eV. The chemical shift between the lightly (1.5 L) and

heavily oxidized (48 L O_2) surface could not be measured, because the O 2s emission from the lightly oxidized surface was too weak to be measured precisely.

6.2. Resonant Photoemission in Ti and TiO_2

It was pointed out in section 5.1 that a direct energy transfer from the resonantly excited 3p shell to the valence electrons with subsequent electron emission according to equation (2b) (i.e., a direct recombination process), should result in resonant photoemission. The process can be described by the equation

$$Ti + h\nu_{res} \rightarrow Ti^{*} \rightarrow Ti^{+} + e^{-} \ (\varepsilon'') \qquad (3)$$

with $h\nu_{res}$ being a photon at the resonance energy, $\sim$ 47 eV, in both metal and oxide. Ti^{*} is the intermediate state with a resonantly excited 3p shell. The resonant enhancement of the Ti-metal 3d photoemission at 47 eV has been observed and is shown in Fig. 7. Likewise in the lightly oxidized sample a similar enhancement of the 3d emission occurs (Fig. 8). In the saturated surface oxide the residual 3d emission has a maximum at 47 eV but some parts of the oxygen 2p-derived oxide valence band exhibit resonant emission as well (Fig. 9).

The spectra in Figs. 7-9 represent the photoemission behavior only at selected discrete photon energies. In order to obtain more complete information constant initial state (CIS) spectra have been recorded for the metal and the surface oxide. The CIS spectrum of clean Ti(0001) has been measured by tuning the electron analyzer energy in harmony with the photon energy so as to monitor the 3d photoemission yield at all photon energies between 30 and 70 eV (i.e., the difference between photon energy $h\nu$ and analyzer energy E_a was kept constant: $h\nu - E_a = E_{3d} + \phi = 5.5$ eV). The CIS curve of the oxide has been measured by tuning the analyzer to the emission from 7 eV below the Fermi level ($h\nu - E_a = E_{OVB} + \phi = 11.6$ eV). $E_{OVB} = 7$ eV is the binding energy of the oxide valence band levels which experience the largest resonant enhancement.

The CIS spectra recorded in this way are presented in Fig. 10. The spectra are corrected for the photon monochromator transmission but not for the electron analyzer collection efficiency. In the clean metal (curve a) the 3d emission has a minimum near 35 eV photon energy, rises subsequently to a broad maximum around 47 eV and then falls at 60 eV photon energy to below 20% of the maximum emission. The FWHM of the resonance peak is approximately 11 eV. A comparison with the 3p ELS spectrum in Ti metal (Fig. 5b) reveals a similar peak shape (apart from the energy region near threshold which has been discussed in section 4).

In Ti(0001) + 48 L O_2 the resonant emission of the valence band has its onset at higher energies than that of the metal (Fig. 10). It peaks at about the same energy as in the metal but the peak has a smaller FWHM. This behavior again agrees well with the results from ELS spectroscopy apart from different intensities of the resonance in ELS and in photoemission. In ELS the resonant loss peak in the oxide is similar in magnitude to the 3p loss peak in the metal while in photoemission the resonance in the oxide valence band emission is less pronounced than in the metal. This might indicate a different branching ratio between

Auger-deexcitation and direct recombination in metal and oxide, respectively. On the other hand, the CIS spectra presented as curves a and b of Fig. 10 show only spectral dependence, not the magnitude of the photoemission intensity because they trace peak heights but not the areas. Furthermore, a different angular dependence of the resonant electron emission in metal and oxide might well cause differences in the collection efficiency. Hence from the CIS spectra alone, a reliable determination of branching ratios is not possible.

The intensity of the $M_{23}M_{45}M_{45}$ Auger emission from clean Ti(0001) as a function of photon energy is shown as the dashed curve of Fig. 10c. The Auger yield has been measured with CFS-spectroscopy keeping the analyzer energy constant at 27 eV which corresponds to the inflection point of the steplike Auger feature in Fig. 7. The Auger cross-section behavior is quite similar to the 3d photoemission. Hence the branching ratio between Auger and resonant photo-emission seems to be nearly independent of photon energy. Slight differences in the resonance peak shape of ELS spectra, CIS spectra and CFS spectra are possibly indicated but an exact assessment would require lower noise levels than obtained in the present study.

The data presented so far consistently point to the direct recombination process as an additional deexcitation channel in addition to the ordinary Auger transition. The peaks at 42 eV and 36 eV in the electron excited Auger spectra of Ti metal and oxide, respectively, have been attributed in section 5.1 to electron emission resulting from this process. Photoelectron spectroscopy using synchrotron radiation can provide additional insight into the origin of these peaks based on their photon energy dependence. A true Auger emission should slowly vary with photon energy in a CFS spectrum reflecting the photon-energy dependence of the cross-section for core-hole ionization. Resonant electron emission in a direct recombination type process, however, should result in a sharply peaked CFS spectrum, the peak originating from resonantly enhanced direct photoemission passing through the CFS analyzer-energy window just at the resonant photon energy (55).

In Fig. 11 the result of such an experiment on Ti metal is shown as a three-dimensional plot of CFS-spectra taken at different kinetic energies. At 25 eV kinetic energy the electron yield is dominated by the SCK-Auger emission for photon energies above threshold. The corresponding CFS curve matches quite closely the dashed curve in Fig. 10. A small feature appearing at $\sim$ 35 eV photon energy is due to residual bulk hydrogen which had not been completely removed from the Ti-sample in the present experiment (17). The shaded curves recorded at higher kinetic energies are similar in appearance to UPS spectra with "reversed" energy scales. The 3d-emission peak shifts from 34 eV photon energy at E_K = 28 eV to 58 eV photon energy at E_K = 52 eV thereby passing through a maximum at 47 eV photon energy (E_K = 41 eV). The set of CFS spectra presented in Fig. 11 can be related to an electron-excited Auger spectrum by recalling that an electron beam acts as a white light source (55). Therefore, it can be looked upon as exciting all these spectra simultaneously. This results in an electron emission maximum at E_K = 25 eV due to the $M_{23}M_{45}M_{45}$ Auger emission and a second (much smaller) maximum at E_K = 41 eV due to resonant electron emission from the 3d shell in good agreement with the AES spectrum shown in Fig. 6a.

If the peak at 41 eV in the electron-excited Auger spectrum had its origin in any true Auger process whatsoever it would have a cross-section behavior resembling the 25 eV CFS curve rather than the sharply peaked spectrum actually observed at E_K = 41 eV. In this context it is interesting to note that resonant electron emission via direct recombination following 4d $\rightarrow$ 4f excitation in rare earths has already been observed by electron-excited Auger spectroscopy (56).

6.3. True Secondary Electrons

The secondary electron distribution at low kinetic energies is determined mainly by inelastic electron-electron scattering processes. Intensity variations in the energy distribution of the secondary electrons can be related to the

single-particle density of states above the Fermi level (57). However, these structures are strongly angle dependent and tend to be obscured in a partially angle-integrated experiment.

In Fig. 12 full electron distribution curves including the low energy secondary electrons are shown for clean Ti(0001), Ti(0001) + 1.5 L O_2 and Ti(0001) + 48 L O_2. These curves are plotted on an electron kinetic energy rather than an electron binding energy scale.

In clean Ti a pronounced minimum is observed just a few electron volts above the vacuum level E_v (E_k = 0). In the spectrum excited with 37 eV photon energy it appears at 3.5 eV above E_v. At 42 eV photon energy it is obscured by the direct 3p emission, but with further increasing photon energies the minimum broadens and shifts to higher kinetic energies. The secondary electron yield near zero kinetic energy increases drastically when the photon energy exceeds the 3p threshold. (The secondary electron yield at zero kinetic energy has been measured previously (5) and shows the same resonant behavior as the 3d yield and the $M_{23}M_{45}M_{45}$ Auger yield.) It should be pointed out that the minimum in the secondary electron distribution disappears in hydrogen-contaminated titanium.

In the lightly oxidized Ti a minimum in the secondary electron yield is still recognizable whereas in the fully oxidized Ti surface the secondary electron distribution appears as a nearly featureless single peak at 3.5 eV above E_v independent of photon energy. The secondary electron yield clearly peaks at resonance ($\sim$ 47 eV) as described previously (5).

Using a work function value for the clean Ti(0001) surface of 4.58 eV (18) the minimum in the secondary electron distribution of the clean metal at 37 eV is localized approximately 8.1 eV above the Fermi level.

The apparent shift in the minimum of the secondary yield with increasing photon energy occurs only in the metal spectra which show a strong, sharply-peaked direct 3p emission. An intense electron energy loss tail is associated with the sharp 3p emission and might cause the observed modifications in the secondary electron distribution. Ti K absorption spectra (58) show only slight (if any) structure at 8 eV above the Fermi level, but hydrogen contamination is likely and would suppress the effect.

7. ELECTRON- AND PHOTON-STIMULATED ION DESORPTION

Electron- and photon-stimulated ion desorption from a stepped Ti(0001) surface have been studied recently (5). The ion yield versus photon energy curve was similar to the photoabsorption curve of Ti metal, both reflecting the 3p ionization cross section. Surprisingly, however, the O^+ ion yield in the surface oxide peaked at 46 eV photon energy, i.e., 1 eV below the photoabsorption maximum of Ti metal. This is in marked contrast to the 3p binding energy shift, which is 5 eV to higher energies in the oxide.

From the results of the ELS experiments in the present study (Fig. 5) and the discussion in Section 4, it appears that the O^+ ion desorption behaves in exactly the same way as the 3p electron energy loss in the oxide. Therefore, similar to the ELS spectrum, the O^+ yield spectrum is strongly modified by final state effects, i.e., the atomic $3p \rightarrow 3d^*$ resonance (unfortunately it is impossible to compare the ion yield curve directly to the $M_{23}VV$ Auger yield in the oxide, because the Auger electron energy distribution is too broad to be separated from the secondary electron background).

The results of supplementary experiments with electron stimulated desorption on the Ti(000) + O system are summarized in Fig. 13. The O^+ ion yield as a function of room temperature oxygen exposure has been measured at 5 eV ion kinetic energy. Similar to the stepped Ti(0001) surface a sigmoidal

curve shape is observed (5). The ion signal onset is shifted slightly to higher exposures (i.e., 2.5 L) on the flat surface but saturation occurs at about 12 L O_2 on both the stepped and the flat basal plane. The kinetic energy distribution of O^+ ions desorbing under electron impact (E_p = 175 eV) is shown on the upper right of Fig. 13. The ESD O^+ ion yield as a function of electron energy also has been measured and is shown in Fig. 13 (upper left). The energy scale on the abscissa is the difference between the Fermi levels of the electron gun and the sample plus the gun filament work function (4.5 eV for W). Clearly the threshold is close to the 3p binding energy.

All ESD results obtained in the present study are consistent with the Knotek-Feibelman mechanism (4) i.e., interatomic Auger decay, giving rise to O^+ desorption. Knotek and Feibelman proposed this mechanism for TiO_2 because they assumed a formal charge between -1 and -2 to be associated with the oxygen ions in TiO_2. Hence, for O^+ desorption a transfer of 2 to 3 electrons is required, which is most easily accomplished in an interatomic Auger decay. The large core level shift in TiO_2 substantiates the assumption of a considerable charge transfer to the oxygen ions. However, the ionicity of the oxygen/metal bond is still an unresolved problem, different methods giving vastly different results (59). Thus other mechanisms for O^+ desorption providing a smaller rearrangement of the charge density than the Knotek-Feibelman mechanism should be considered, too. It has been pointed out in section 6.1 that a "cross-autoionization" (resonant photoemission from the oxide valence band) can remove charge from the strongly bonding $2e_g$ and $1t_{2g}$ orbitals. It is unlikely, however, that a mere ionization of a bonding orbital would result in O^+ desorption because the reduction in charge density on the oxygen site and the accompanying reduction of the bonding forces is too small to initiate such a process. An

additional shake-up of an electron from bonding to antibonding orbitals (i.e., a 2 hole-1 electron final state) might be sufficient to initiate O^+ desorption (60). In TiO_2, however, a corresponding satellite feature could not be detected unambiguously (core level satellites have been observed in TiO_2 and attributed to such charge transfer shake-up states (61) but it has been pointed out that extrinsic losses are likely to dominate the satellite structure (62)).

8. Atomic Effects Modifying the 3p Cross Section in Ti-Metal

Dehmer et al. (63) were the first to point out the close analogy of the 3p photo-absorption in the 3d transition metals and the 4d → 4f photo-absorption in the rare earth metals. In both cases the subshell absorption cross section shows a broad maximum above threshold, the delayed onset being more pronounced in metals with less than half-filled subshells. According to the explanation put forward by Dehmer et al. (63) for the rare earths, the large delay is caused by the exchange interaction between the 4d hole and the n+1 4f electrons. The Slater G^1 (4d, 4f) exchange integral for collapsed 4f-orbitals is large enough to raise some of the $4d^9\ 4f^{n+1}$ multiplet terms into the continuum. For the rare earth metals with less than half-filled 4f shells (n<7), the higher lying multiplet terms draw the largest oscillator strength (64). Therefore the 4d excitation cross section reaches its peak far above threshold for the rare earth metals from La to Sm. For the heavier rare earths (n>7) the clear separation into

high lying levels with large oscillator strength and low lying, weakly forbidden levels breaks down (64). Similarly, in the 3d-transition metal atoms with less than half filled 3d shells, the optically favoured $3p^5 3d^{n+1}$ multiplet terms are driven up in energy by 10-15 eV due to the large value of the $G^1(3p,3d)$ Slater integral. In the solid transition metals a similar effect occurs. The important role of exchange interactions in shaping the 3p excitation cross section in the 3d-transition metals is nicely demonstrated by the SXAS (Soft X-ray Absorption Spectra) (38) and the ELS spectra (41) of the transition metals. Whereas in the lower half of the series a broad maximum occurs far above threshold, the 3p cross section in Mn to Ni shows a sharp steplike onset with a maximum close to the threshold.

In Ti metal the 3p cross section peaks at 47 eV, i.e., 14 eV above threshold. It is important to note that the $3p^5 3d^*$ state is strongly localized. (As already pointed out, the large value of $G^1(3p,3d)$ is associated with localization of this state). According to the atomic energy levels tabulated by Corliss and Sugar (65), the separation between ^3P (lowest term of the $p^5 d$ configuration) and ^1P (highest term) is 15 eV in Ti^{4+}. This difference amounts to 4/3 $G^1(3p,3d)$ (66). Not only the spacing of the multiplet terms but also the absolute excitation energies in Ti^{4+} (34 eV for $^1S \rightarrow {}^3P$ and 49 eV for $^1S \rightarrow {}^1P$) compare very well with the corresponding excitations in Ti-metal (threshold: 31-33 eV, maximum of the 3p loss-structure: 47 eV). Therefore one must conclude that the excited state is similarly localized in both the Ti^{4+} ion and in Ti-metal.

The localized character of the excitation is additionally confirmed by the fact that changes in the chemical environment produce only small effects. In the oxide the screening response of the valence electrons is strongly reduced as is partly reflected by the 5 eV binding energy shift of the 2p (52) and 3p (see Sec. 6) core levels. In contrast, the 3p loss peak at 47 eV does not show a significant energy shift upon oxidation. This indicates that the chemical shift is nearly the

same for the initial (3p) and the excited $3d^*$-state, which again is only possible if the $3d^*$-level is strongly localized.

The picture of a direct recombination process is predicted on a localized, atomic-like core excitation which decays by an autoionization process to a filled-core final state. We have assumed all along that the 3d-orbital in the $3p^5\ 3d^{N+1}$ configuration of Ti is collapsed: no longer hydrogenic but localized within approximately 1.5 a.u. of the nucleus. In the case of isolated atoms this collapse occurs at Z=21 (ground state Sc). The work of Hansen (67) has shown that in the best independent scheme, different terms of a $3p^5$ 3d-type configuration might have orbitals with considerably different spatial extents. Thus cases exist where some terms of a given configuration have collapsed orbitals while others do not. However Ti ($3p^5\ 3d^{N+1}$) is sufficiently far from these "transitional" regions to be free of such term-dependent effects (68,69) and the orbitals of all the terms are collapsed.

A slightly different point of view as assumed by Zangwill and Soven (70). Using the time-dependent local density approximation they explained the behavior of subshell photoionization cross sections in cerium and barium in terms of a collective resonant dipole oscillation of the closed 4d shell. In the case of Ti and the other transition metals it is the 3p shell which shows a "giant" dipole resonance. The connection of this picture with the HF-approach is made by visualizing the resonant response of the 3p shell to the external field as virtual transitions to $3d^*$ states of the kind discussed above. Thus it is the availability of emply localized "3d-like" states which provides for the enormous polarizability of the 3p shell.

So far an understanding of the general shape of the 3p cross-section as a function of energy has been achieved by comparison with atomic data and calculations. A detailed understanding of how the solid state environment should modify the atomic cross-section behavior is still lacking (71). The controlled change of the chemical

environment performed in the present study provides some more insight. Apparently, excitations near threshold are much more strongly influenced by changes in the environment than the localized excitations far above threshold. This is demonstrated by the pronounced change in loss intensity at about 34 eV (3p excitation near threshold) and 60 eV (3s excitation near threshold) and the relatively small change of the 47 eV peak (3p excitation far above threshold) (72).

9. SUMMARY

The room temperature oxidation of a Ti(0001) surface has been investigated. UPS as well as ELS shows a nearly complete depletion of the metallic (3d,4s) conduction band in the surface oxide. The 3p core level undergoes a chemical shift of 5 eV upon oxidation which is the value expected for TiO_2. The $M_{23}M_{45}M_{45}$ Auger transition is nearly completely suppressed in the saturated oxide. Electron excited Auger spectra as well as CIS spectra of the oxide valence band show resonant electron emission from the metal-oxygen bonding orbitals, which is explained by a direct recombination process involving an energy transfer from the resonantly excited 3p shell to the oxide valence band. This process is only likely to occur if there is substantial transfer of 3d electrons into the oxide valence band, i.e., if TiO_2 is formed. A large ion yield is observed in both PSD and ESD from the surface oxide. The threshold and the photon-energy dependence are consistent with the Knotek-Feibelman process which involves an interatomic Auger transition. This, too, is expected only for the maximum valency compound TiO_2. ELS experiments show that the surface oxide grows into a thin protective overlayer which is stable up to 250°C.

In addition to the oxidation process, the electronic excitation spectrum of the metal and the oxide has been studied using ELS. Plasmon losses involving the valence electrons have been observed in both cases. The excitation spectrum of the 3p core level shows a maximum high above threshold which is caused by atomic effects

3p → conduction band excitations seem to be important. The resonant 3p shell excitation can decay by an $M_{23}VV$ Auger process or by direct energy transfer to valence electrons which results in resonant enhancement of 3d emission in the metal and of the oxide valence band emission in the surface oxide.

10. ACKNOWLEDGEMENTS

We wish to acknowledge extensive discussions with T.B. Lucatorto and C.J. Powell and a critical reading of the manuscript by F.P. Netzer, University of Innsbruck, Austria. E.B. acknowledges the financial support of the Max Kade Foundation, New York. This work was supported in part by the Office of Naval Research.

References

1. A. Fujishima and K. Honda, Nature 238, 37 (1972).
2. B.J. Tatarchuk and J.A. Dumesic, J. Catalysis 70, 308 (1981) and references therein.
3. J.E. Sundgren, M.K. Hibbs, U. Helmersson, B. Jacobson and H.T.G. Hentzell, J. Vac. Sci. Technol. (1983), in press.
4. M.L. Knotek and P.J. Feibelman, Phys. Rev. Lett. 40, 964 (1978).
5. D.M. Hanson, R. Stockbauer and T.E. Madey, Phys. Rev. B 24, 5513 (1981).
6. D.E. Eastman, Solid State Comm. 10, 933 (1972).
7. T. Smith, Surf. Sci. 38, 292 (1973).
8. P.J. Bassett and T.E. Gallon, J. Elec. Spec. Rel. Phenom. 2, 101 (1973).
9. L. Porte, M. Demosthenous and Tran Minh Duc, J. Less-Common Met. 56, 183 (1977).
10. A. Muller and A. Benninghoven, Surf. Sci. 41, 493 (1974).
11. L.I. Johansson, A.L. Hagstrom, A. Platau and S.E. Karlsson, Phys. Stat. Sol. (b) 83, 77 (1977).
12. A. Platau, L.I. Johansson, A.L. Hagstrom, S.E. Karlsson and S.B.M. Hagstrom, Surf. Sci. 63, 153 (1977).
13. B. Kasemo and E. Tornqvist, Surf. Sci. 77, 209 (1978).
14. Y. Fukuda, W.T. Elam and R.L. Park, Appl. Surf. Sci. 1, 278 (1978).
15. J.B. Bignolas, M. Bujor and J. Bardolle, Surf. Sci. 108, L453 (1981).
16. H.D. Shih and F. Jona, Appl. Phys. 12, 311 (1977).
17. Y. Fukuda, F. Honda and J.W. Rabalais, Surf. Sci. 91, 165 (1980).
18. B.T. Jonker, J.F. Morar and R.L. Park, Phys. Rev. B 24, 2951 (1981).
19. J.S. Solomon and W. L. Baun, Surf. Sci. 51, 228 (1975).
20. W. Brearly and N.A. Surplice, Surf. Sci. 64, 372 (1977).
21. E. Bertel, R. Stockbauer and T.E. Madey, J. Vac. Sci. Technol. A1, 1075 (1983).

22. E. Bertel, R. Stockbauer and T.E. Madey, Phys. Rev. B 27, 1939 (1983).

23. J.A. Tossell, D.J.Vaughan and K.H. Johnson, Am. Mineral. 59, 319 (1974).

24. L.F. Matheiss, Phys. Rev. 134, A970 (1964).

25. T.E. Madey, and R. Stockbauer, "Experimental Methods in Electron and Photon Stimulated Desorption," to be published.

26. J.L. Robins and J.B. Swan, Proc. Phys. Soc. (London) 76, 857 (1960).

27. C. Wehenkel and B. Gauthe, Phys. Stat. Sol. (b) 64, 515 (1974).

28. D.W. Lynch, C.G. Olson and J.H. Weaver, Phys. Rev. B 11, 3617 (1975).

29. W.E. Wall, M.W. Ribarski and J.R. Stevenson, J. Appl. Phys. 51, 661 (1980).

30. P.J. Feibelman, J.A. Appelbaum and D.R. Hamann, Phys. Rev. B 20, 1433 (1979).

31. P.J. Feibelman and F.J. Himpsel, Phys. Rev. B 21, 1394 (1980).

32a. R.L. Kurtz and V.E. Henrich, Phys. Rev. B 25, 3563 (1982), and references therein.

b. V.E. Henrich, H.J. Zeiger and G. Dresselhaus, Electron Energy Loss Spectroscopy of Surface States on Titanium and Vanadium Oxides, in: Electrocatalysis on Non-metallic Surfaces, Nat. Bureau of Standards, Special Publication 455, (U.S. GPO, Washington, D.C. 1976).

33. Y.W. Chung, W.J. Lo and G.A. Somorjai, Surface Sci. 64, 588 (1977).

34. E. Bertel, G. Strasser and F.P. Netzer, Surf. Sci. 118, 387 (1982) and references therein.

35. Y. Sakisaka, H. Kato and M. Onchi, Surf. Sci. 120, 150 (1982).

36. J. Frandon, B. Brousseau and F. Pradal, J. Physique 39, 839 (1978).

37. E. Bertel, G. Strasser, F.P. Netzer, J.A.D. Matthew, Surf. Sci. 118, 387 (1982).

38. B. Sonntag, R. Haensel and C. Kunz, Sol. St. Comm. 7, 597 (1969).

39. P.N. Ross and K.A. Gaugler, Surf. Sci. 122, L579 (1982).

40. N.E. Erickson and C.J. Powell, J. Vac. Sci. Tech. (in press).

41. C. Wehenkel and B. Gauthé, Phys. Lett. 47A, 253 (1974).

42. D.L. Misell and A.J. Atkins, Phil. Mag. 27, 95 (1973).

43. D.A. Shirley, R.L. Martin, S.P. Kowalczyk, F.R. McFeely and L. Ley, Phys. Rev. B 15, 544 (1977).

44. L.A. Grunes and R.D. Leapman, Phys. Rev. B22, 3778 (1980).

45. F.P. Netzer, G. Strasser and J.A.D. Matthew, Phys. Rev. Lett. 51, 211 (1983).

46. F. Combet-Farnoux and M. Lamoureux, in: VUV Radiation Physics, Proc. 4th Int. Conf., Eds., E.E. Koch et al. (Hamburg 1974) p. 89.

47. L.C. Davis and L.A. Feldkamp, Phys. Rev. B. 23, 6239 (1981).

48. D.E. Ramaker, Auger Spectroscopy as a Probe of Valence Bonds and Bands, in: Chemistry and Physics of Solid Surfaces IV, eds.: R. Vanselow and R. Howe (Springer, Berlin 1982).

49. T.W. Haas, J.T. Grant and G.J. Dooley, Phys. Rev. B 1, 1449 (1970).

50. H.E. Bishop, J.C. Riviere and J.P. Coad, Surf. Sci. 24, 1 (1971).

51. J.A.D. Matthew and Y. Komninos, Surf. Sci. 53, 716 (1975).

52. R.L. Kurtz and V.E. Henrich, Chem. Phys. Lett. (1983).

53. J.B. Goodenough, Metallic Oxides, in: Progress in Solid State Chemistry, Vol. 5, ed. H. Reiss (Pergamon, Oxford 1971).

54. V.E. Henrich and R.L. Kurtz, Phys. Rev. B 23, 6280 (1981).

55. J.A.D. Matthew and S.M. Girvin, Phys. Rev. B 24, 2249 (1981).

56. F.P. Netzer, E. Bertel and J.A.D. Matthew, Surf. Sci. 103, 1 (1981).

57. R.F. Willis and N.E. Christensen, Phys. Rev. B 18, 5140 (1978).

58. K. Tsutsumi, O. Aita and K. Ichikawa, Phys. Rev. B 15, 4638 (1977).

59. K. Wandelt, Surf. Sci. Rep. 2, 1 (1982).

60. D.E. Ramaker, J. Chem. Phys. 78, 2998 (1983) and Chem. Phys. 80, 183 (1983).

61. D.C. Frost, C.A. McDowell and B. Wallbank, Chem. Phys. Lett. 40, 189 (1976).

62. H. Chermette, P. Pertosa and F.M. Michel-Calendini, Chem. Phys. Lett. 69, 240 (1980).

63. J.L. Dehmer, A.F. Starace, U. Fano, J. Sugar and J.W. Cooper, Phys. Rev. Lett. 25, 1521 (1971).

64. J. Sugar, Phys. Rev. B 5, 1785 (1972).

65. Ch. Corliss and J. Sugar, J. Phys. Chem. Ref. Data 8, 1 (1979).

66. R.D. Cowan, The Theory of Atomic Structure and Spectra, Univ. of California Press (Berkeley 1981) p. 354.

67. J.E. Hansen, J. Phys. B 5, 1083 (1972).

68. M.W.D. Mansfield and G.H. Newsom, Proc. Roy. Soc. Lond. A 357, 77 (1977).

69. A.W. Weiss and T.B. Lucatorto, personal communication.

70. A. Zangwill and P. Soven, Phys. Rev. Lett 45, 204 (1980).

71. T.B. Lucatorto, T.J. McIllrath, W.T. Hill and C.J. Clark, Proc. Int. Conf. on X-Ray and Atomic Inner-Shell Physics (Eugene, Oregon 1982).

72. B. Sonntag, J. de Physique, 39, C4-9 (1978).

Figure Captions

Fig. 1. Electron energy loss spectra of Ti(0001).

a: Clean surface, normal incidence, 1150 eV primary energy (bulk sensitive).

b. Clean surface, angle of incidence 55°, 150 eV primary energy (surface sensitive).

c. Lightly oxidized surface (Ti(0001) + 0.4 L O_2), angle of incidence 55°, 150 eV primary energy (surface sensitive).

Fig. 2. Electron energy loss spectra of Ti(0001) at various stages of oxidation. Angle of incidence 65°, 150 eV primary energy (high surface sensitivity).

Fig. 3. Sampling depth dependence of the electron energy loss spectra of Ti(0001) after partial (upper panel) and complete oxidation (lower panel).

a. Ti(0001) + 20 L O_2, normal incidence, 1000 eV primary energy (bulk sensitive).

b. Ti(0001) + 20 L O_2, angle of incidence 55°, 1000 eV primary energy (increased surface sensitivity).

c. Ti(0001) + 10^3 L O_2, normal incidence, 1000 eV primary energy (bulk sensitive).

d. Ti(0001) + 10^3 L O_2, normal incidence, 150 eV primary energy (increased surface sensitivity).

e. Ti(0001) + 10^3 L O_2, angle of incidence 65°, 150 eV primary energy (highly surface sensitive).

Fig. 4. Thermal stability of the Ti surface oxide: ELS spectra as a function of temperature. Ti(0001) + 10^3 L, angle of incidence 55°, 1000 eV primary energy (moderate surface sensitivity).

Fig. 5. 3p excitation in clean and oxidized Ti monitored by electron energy loss spectroscopy.

a. Ti(0001) + 48 L O_2 (saturation exposure), angle of incidence 55°, 217 eV primary energy (highly surface sensitive).

b. Shallow core level losses in clean Ti (3p and 3s). Normal incidence.

c. Shallow core level losses in Ti + 48 L O_2. Angle of incidence 55° (highly surface sensitive).

Fig. 6. Electron excited $M_{23}VV$ Auger spectra of (a) clean Ti(0001) and (b) Ti(0001) + 48 L O_2 (E_p = 217 eV).

Fig. 7. UPS spectra of clean Ti(0001) recorded at various photon energies. Insert: Ti 3p emission ($h\nu$ = 57 eV).

Fig. 8. UPS spectra of lightly oxidized Ti(0001) (oxygen exposure: 1.5 L) recorded at various photon energies.

Fig. 9. UPS spectra of heavily oxidized Ti(0001) recorded at various photon energies. The hatched areas of the 37 eV spectrum show the increase only of the oxide valence band emission with respect to the 37 eV spectrum of lightly oxidized titanium (Fig. 8). The hatched area of the 47 eV spectrum shows the resonant enhancement of the oxide valence band emission with respect to the 37 eV spectrum of the same surface (lower curve). Inserts: The Ti 3p and O 2s emission in Ti(0001) + 48 L O_2 recorded at 57 eV photon energy.

Fig. 10. CIS spectra of (a) the 3d photoemission in Ti(0001) and (b) the oxide valence-band photoemission in Ti(0001) + 48 L O_2; (c) CFS spectrum of the $M_{23}V_{45}V_{45}$ Auger yield in Ti(0001).

Fig. 11. CFS spectra of the electron yield at various kinetic energies. The spectrum at E_K = 25 eV shows the $M_{23}V_{45}V_{45}$ Auger cross-section, the

spectrum at E_K = 41 eV shows the resonantly enhanced 3d emission passing through the analyzer window at a photon energy of 47 eV. The small feature appearing at 5 eV higher photon energies than the 3d emission is due to residual H contamination.

Fig. 12. The secondary electron distribution in (a) clean Ti(0001), (b) Ti(0001) + 1.5 L O_2 and (c) Ti(0001) + 48 L O_2.

Fig. 13. Electron stimulated desorption of O^+ from oxidized Ti(0001): O^+ yield as a function of O_2 exposure. Inserts: O^+ yield at 4.3 eV ion kinetic energy as a function of electron energy (left) and the energy distribution of the desorbing O^+ ions (right).

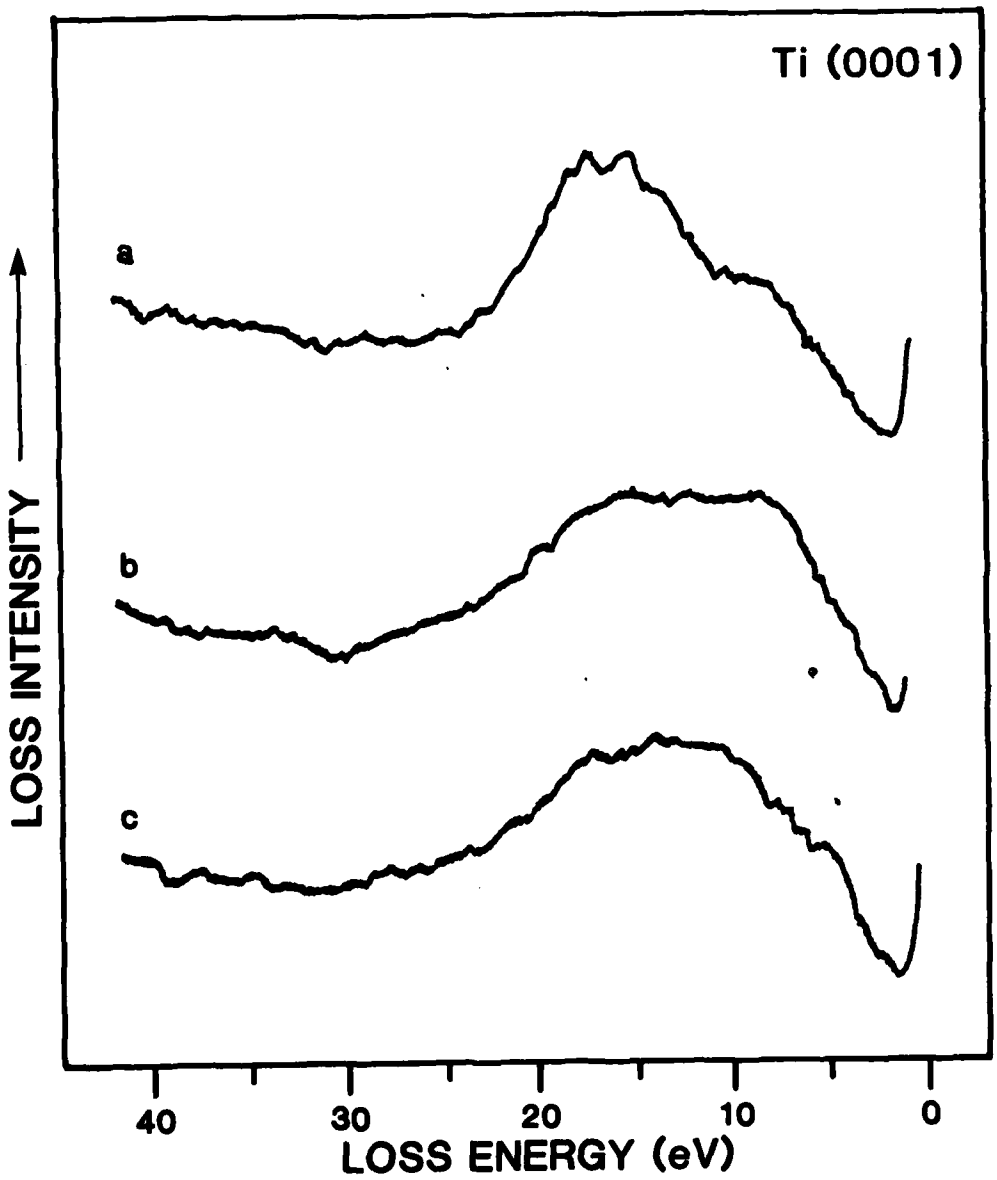

Fig. 1

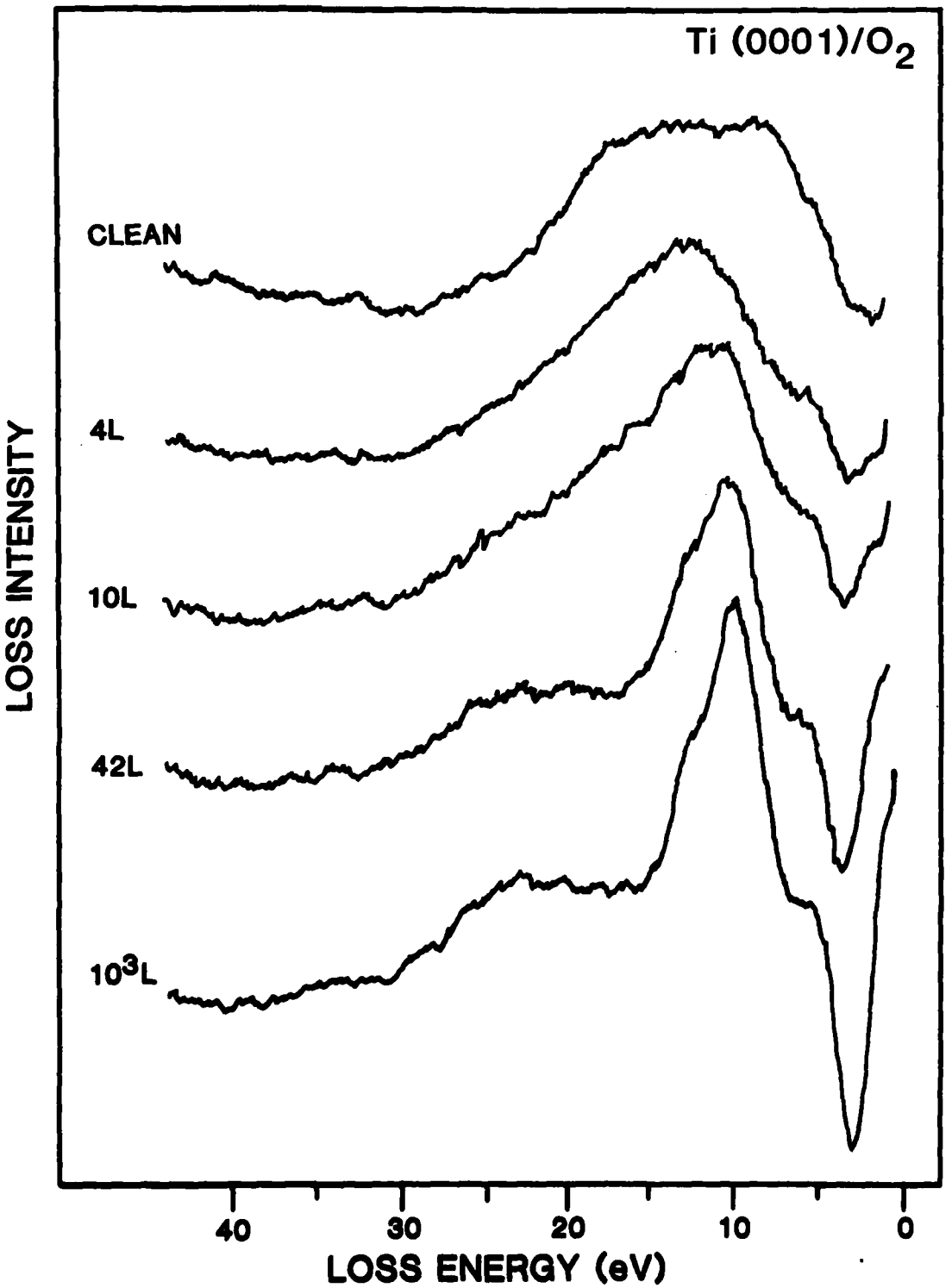
Ti (0001)/O2
CLEAN
4L
10L
42L
10^3L
LOSS INTENSITY
40
30
20
10
0
LOSS ENERGY (eV)

Fig. 2

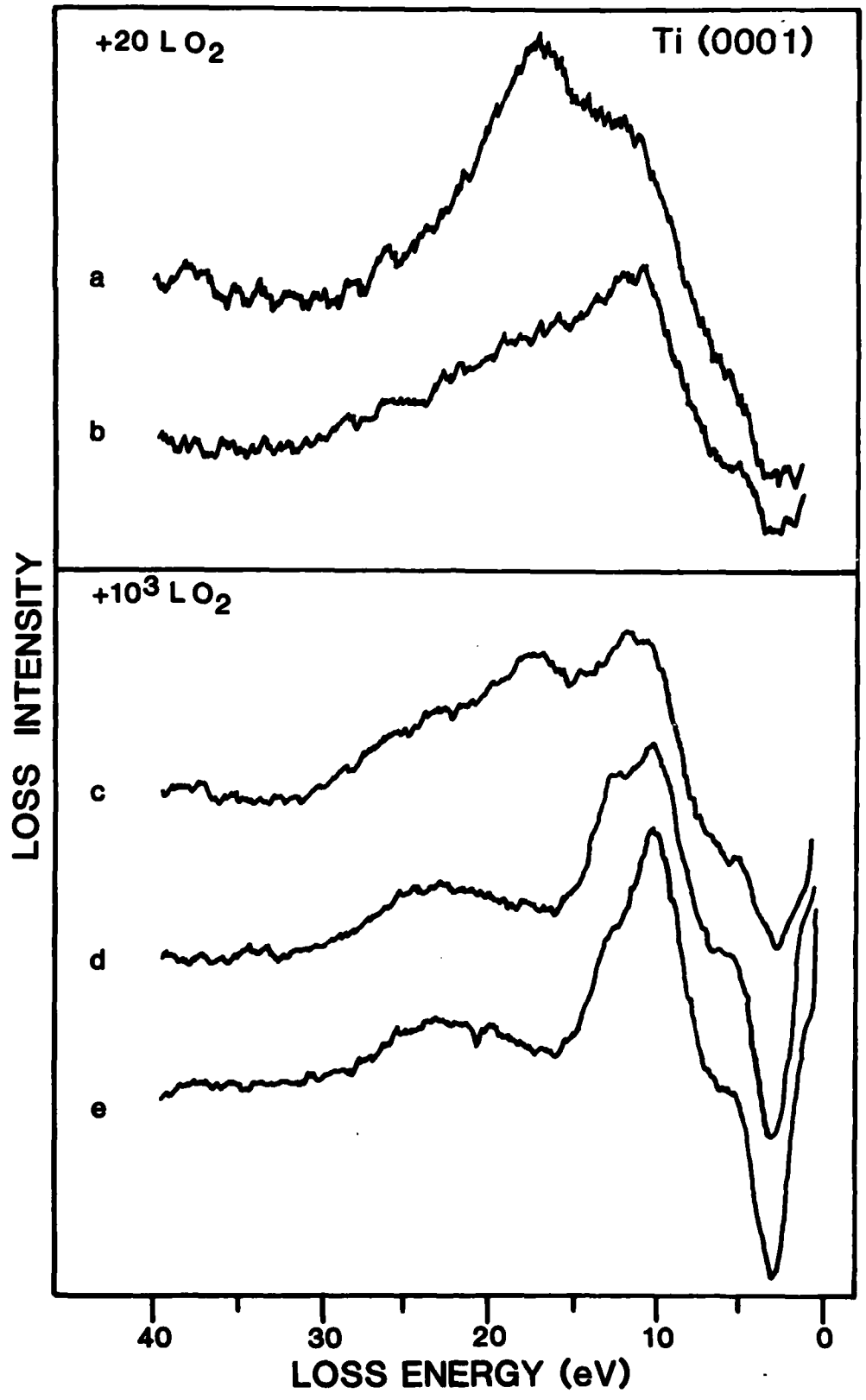
+20 L O2
Ti (0001)
a
b
+10^3 L O2
c
d
e
LOSS INTENSITY
40
30
20
10
0
LOSS ENERGY (eV)

Fig. 3

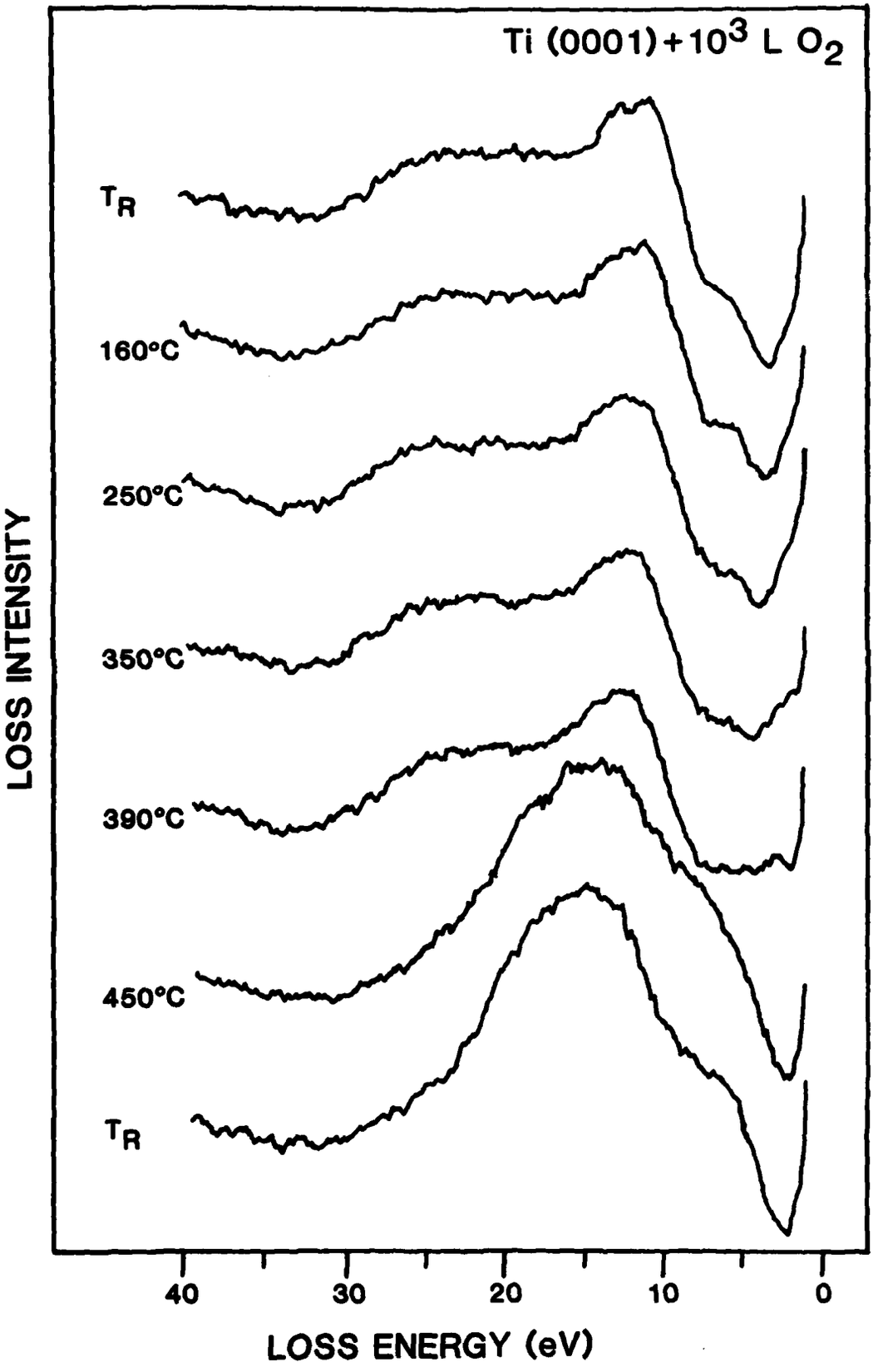
Ti (0001)+10³ L O₂
T_R
160°C
250°C
350°C
390°C
450°C
T_R
LOSS INTENSITY
40
30
20
10
0
LOSS ENERGY (eV)

Fig. 4

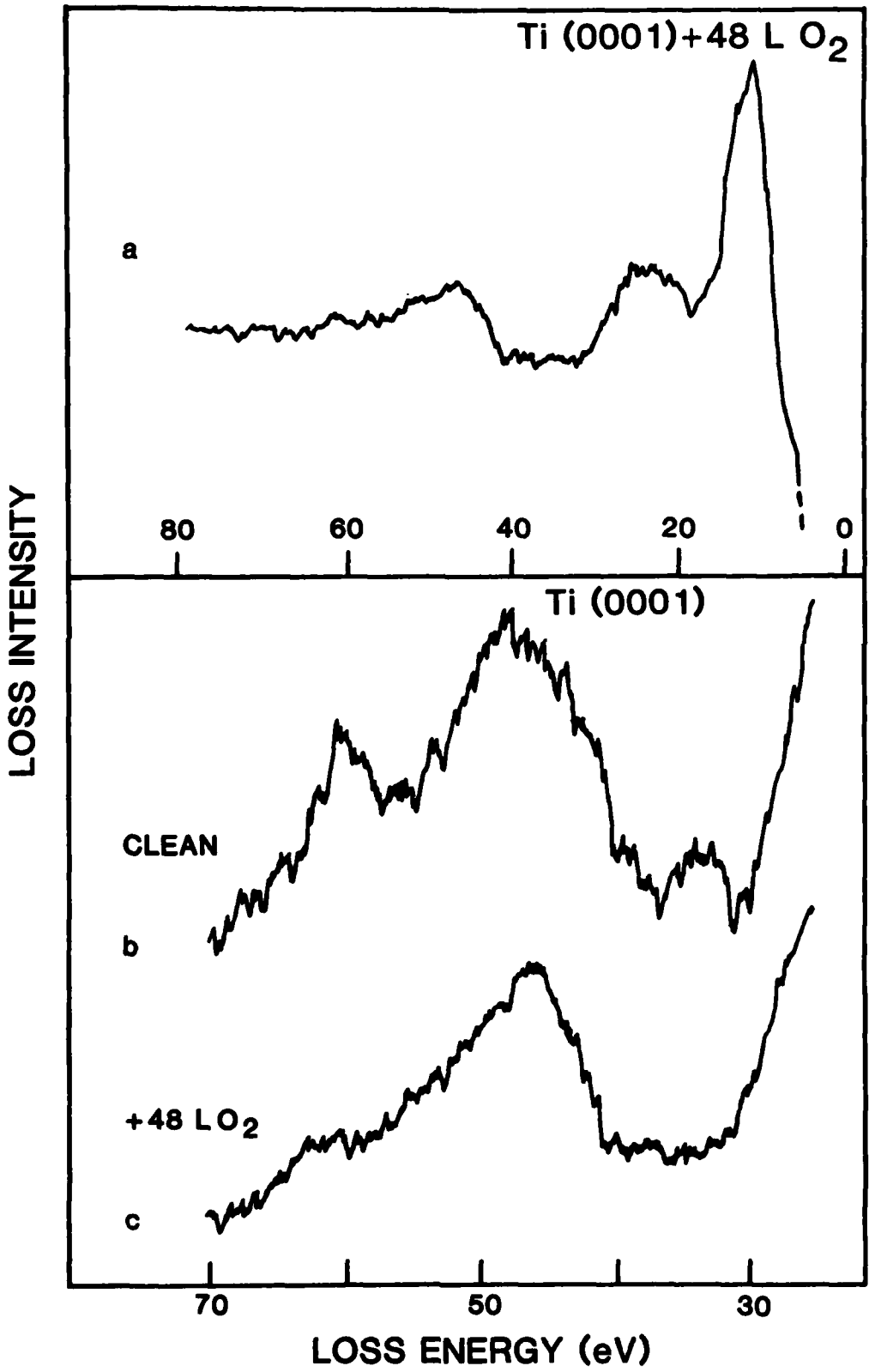
Ti (0001)+48 L O_2
a
80
60
40
20
0
Ti (0001)
CLEAN
b
+48 L O_2
c
70
50
30
LOSS INTENSITY
LOSS ENERGY (eV)

Fig. 5

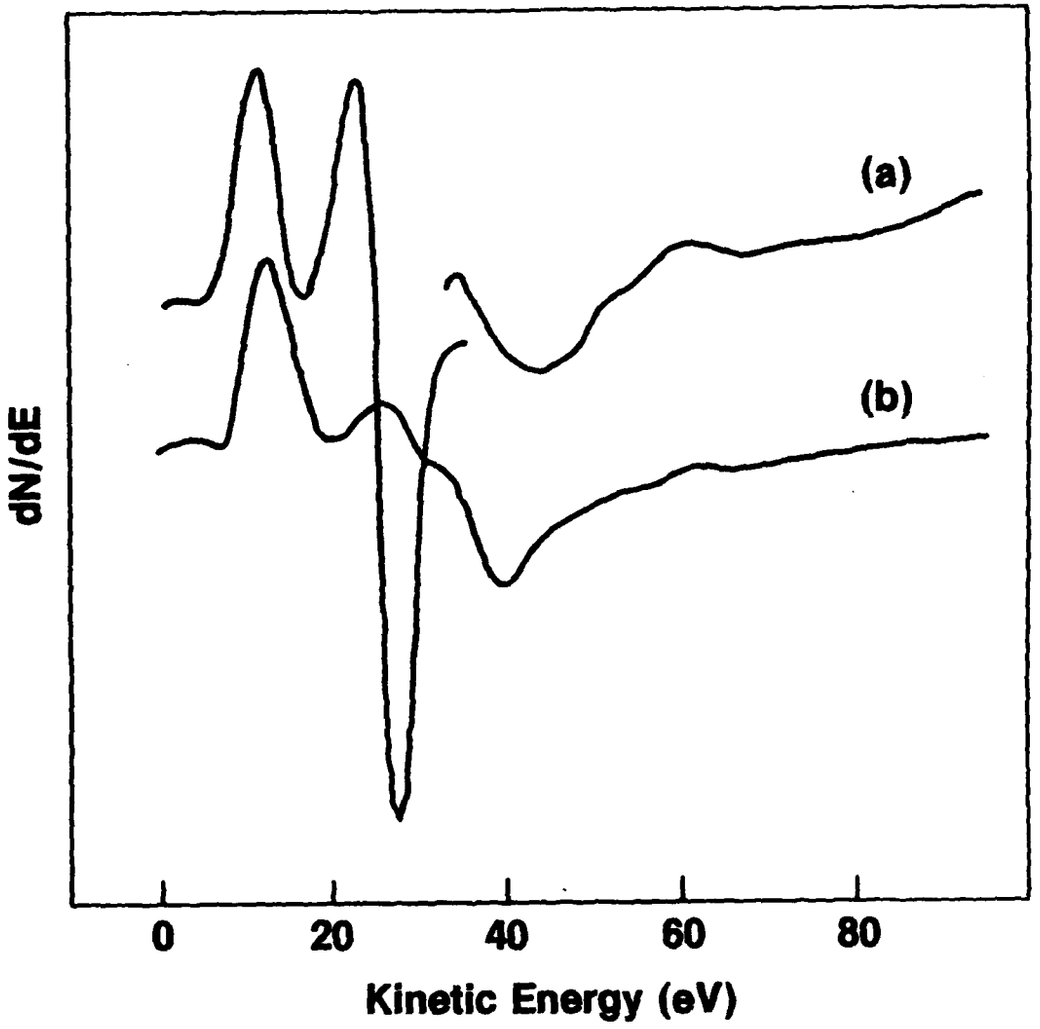

Fig. 6

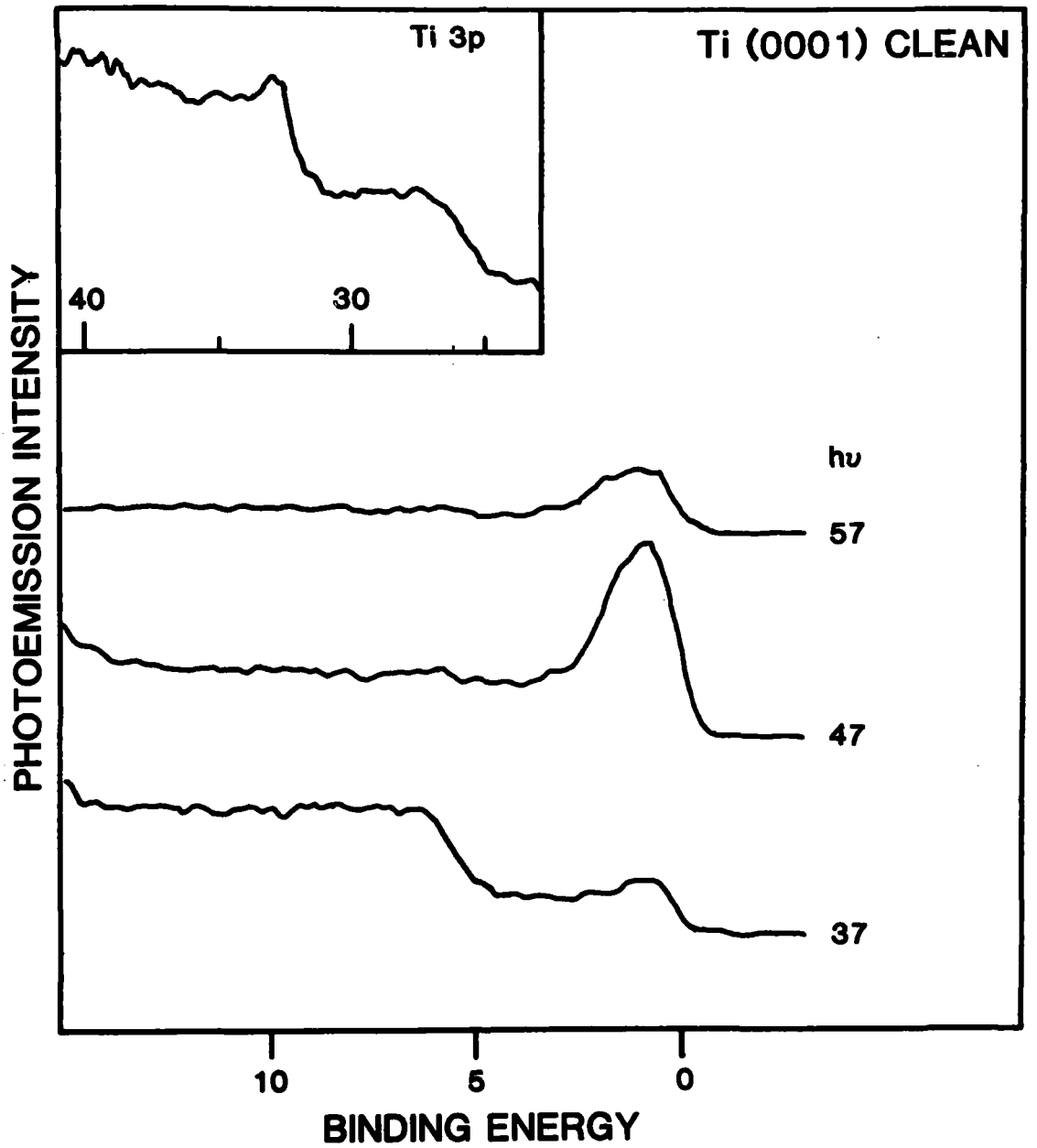
Ti 3p
Ti (0001) CLEAN
40
30
PHOTOEMISSION INTENSITY
hυ
57
47
37
10
5
0
BINDING ENERGY

Fig. 7

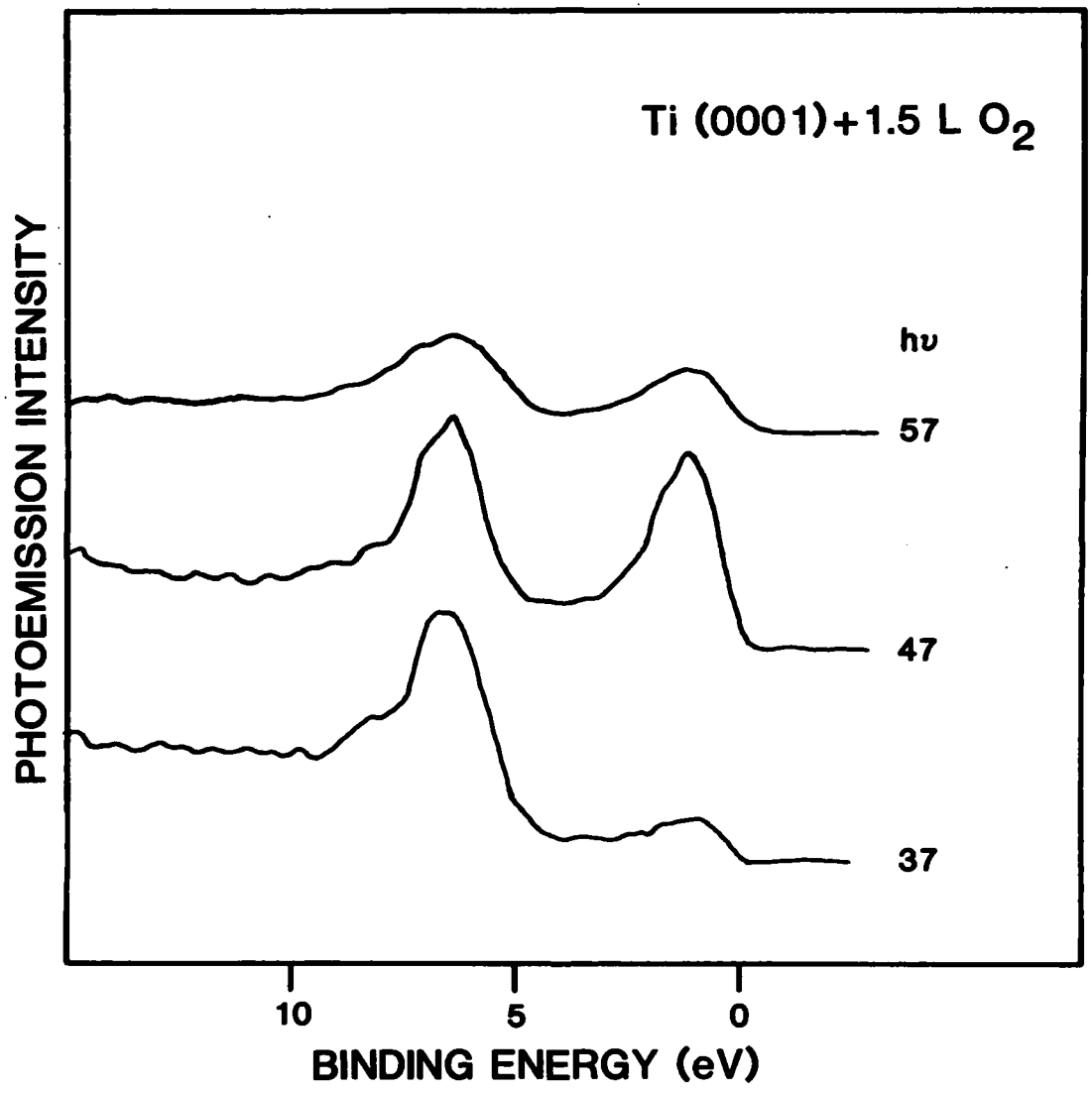
Ti (0001)+1.5 L O_2
hυ
57
47
37
PHOTOEMISSION INTENSITY
10
5
0
BINDING ENERGY (eV)

Fig. 8

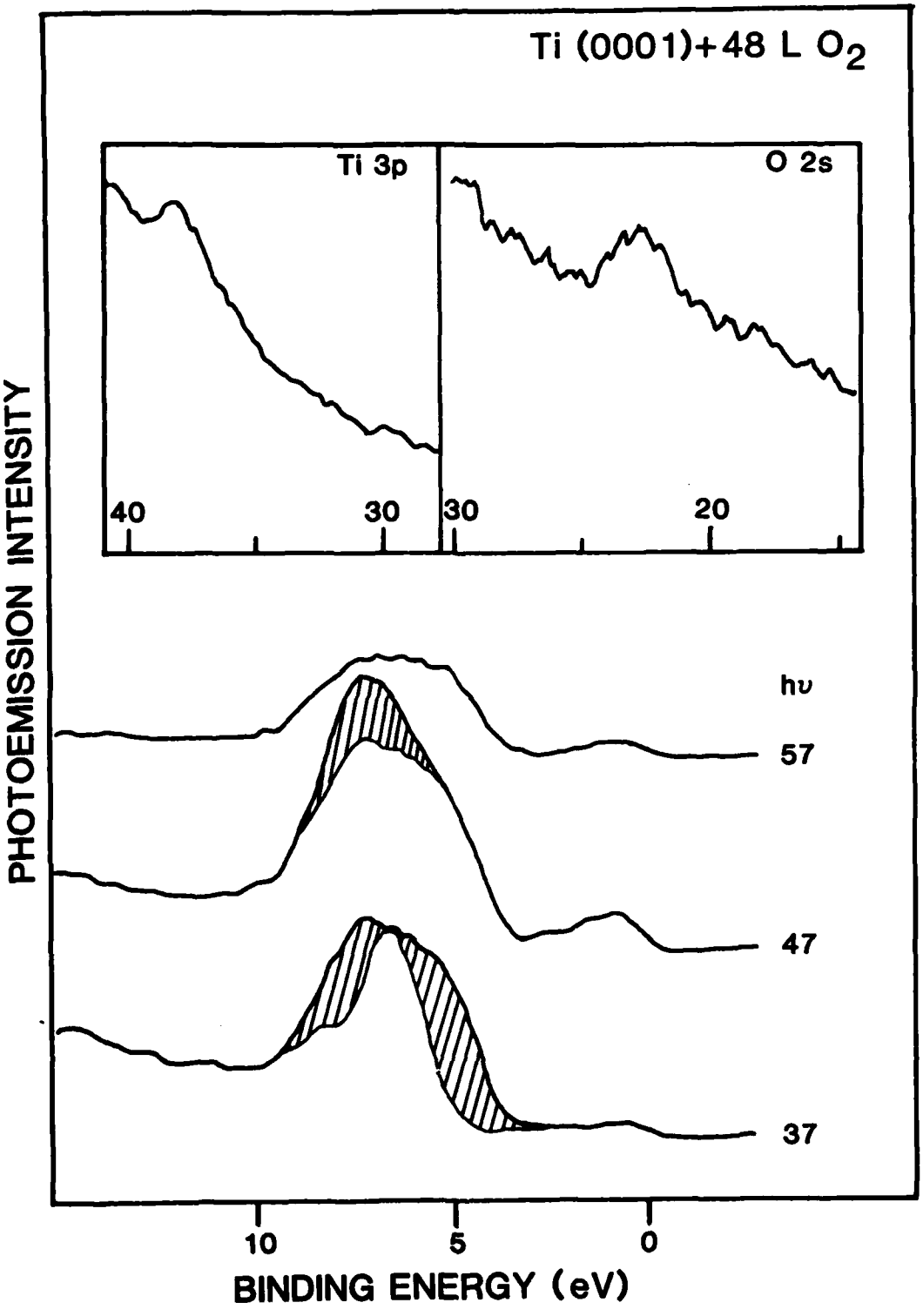
Ti (0001)+48 L O_2
Ti 3p
O 2s
40
30
30
20
PHOTOEMISSION INTENSITY
hυ
57
47
37
10
5
0
BINDING ENERGY (eV)

Fig. 9

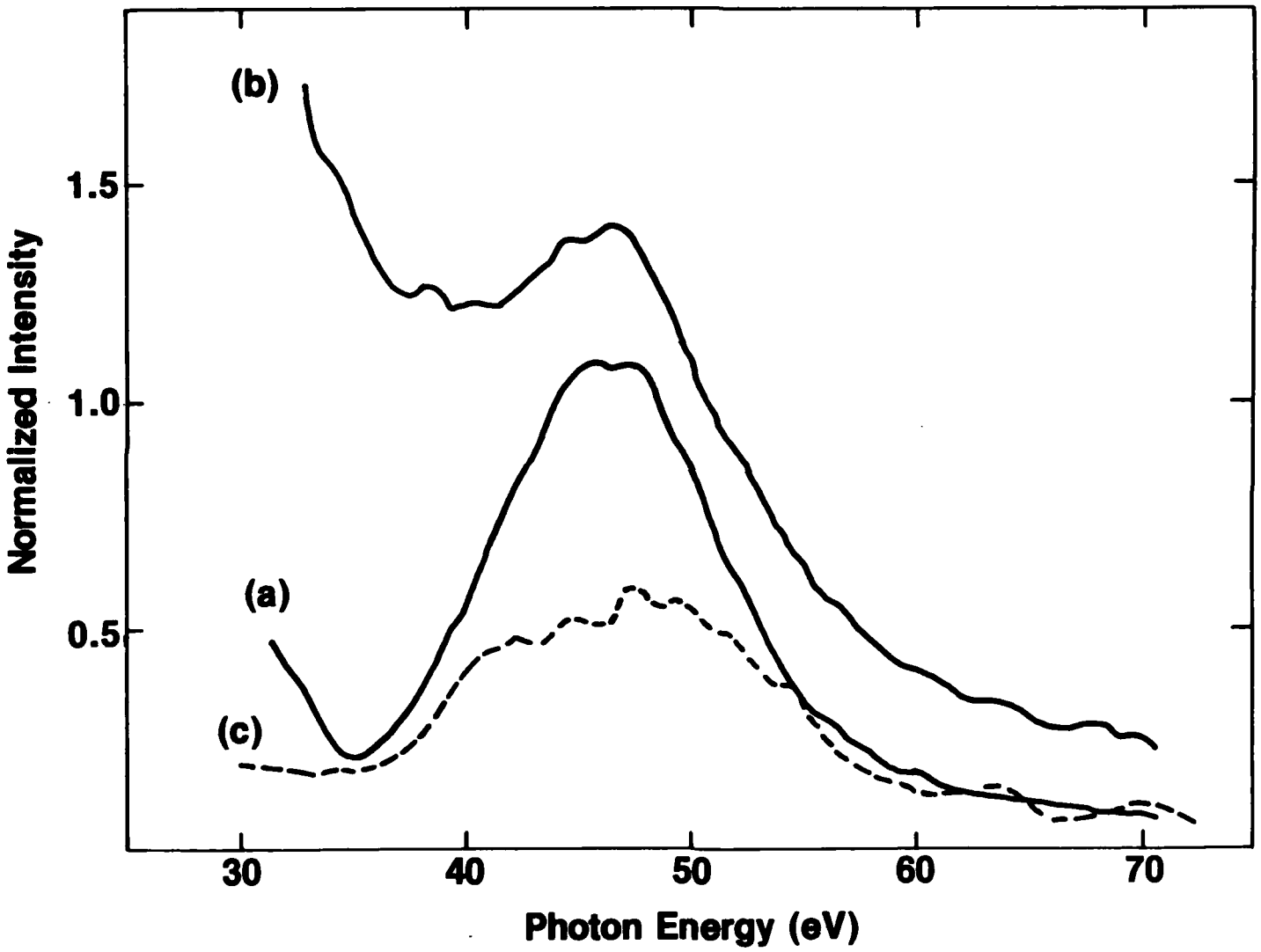
(b)
(a)
(c)
1.5
1.0
0.5
Normalized Intensity
30
40
50
60
70
Photon Energy (eV)

Fig. 10

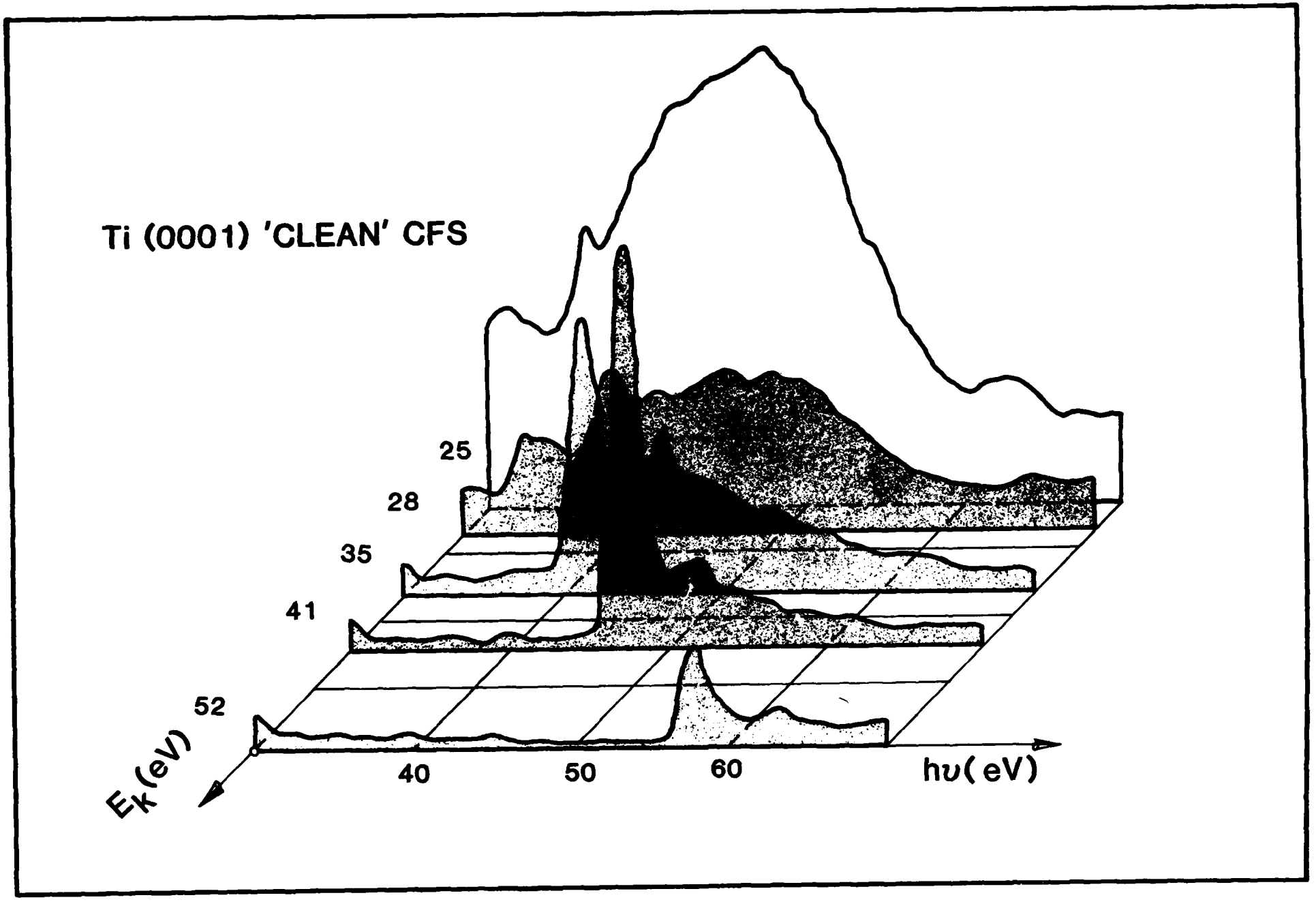

Fig. 11

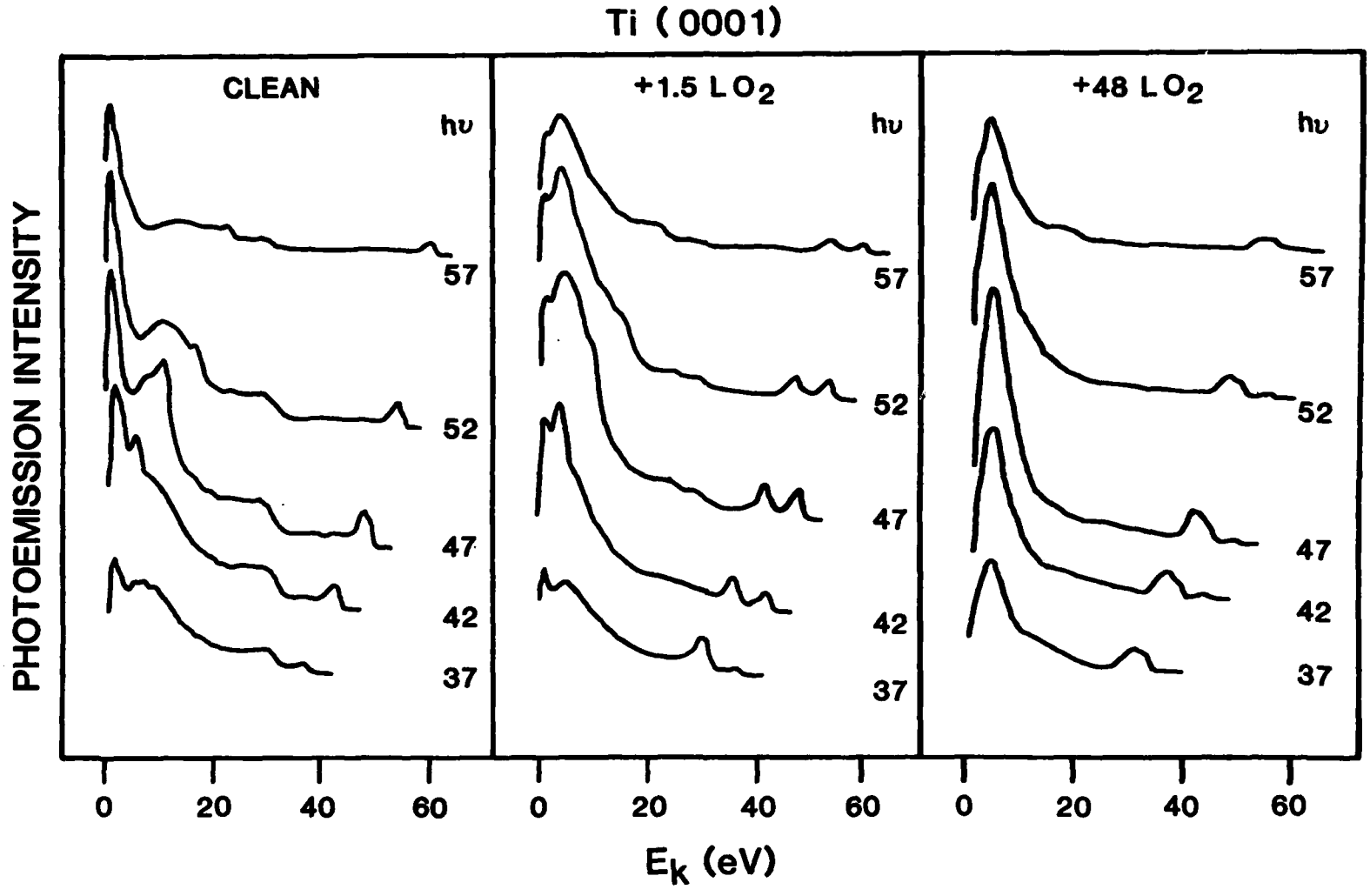
Ti (0001)
CLEAN
+1.5 L O2
+48 L O2
hυ
57
52
47
42
37
PHOTOEMISSION INTENSITY
0
20
40
60
Ek (eV)

Fig. 12

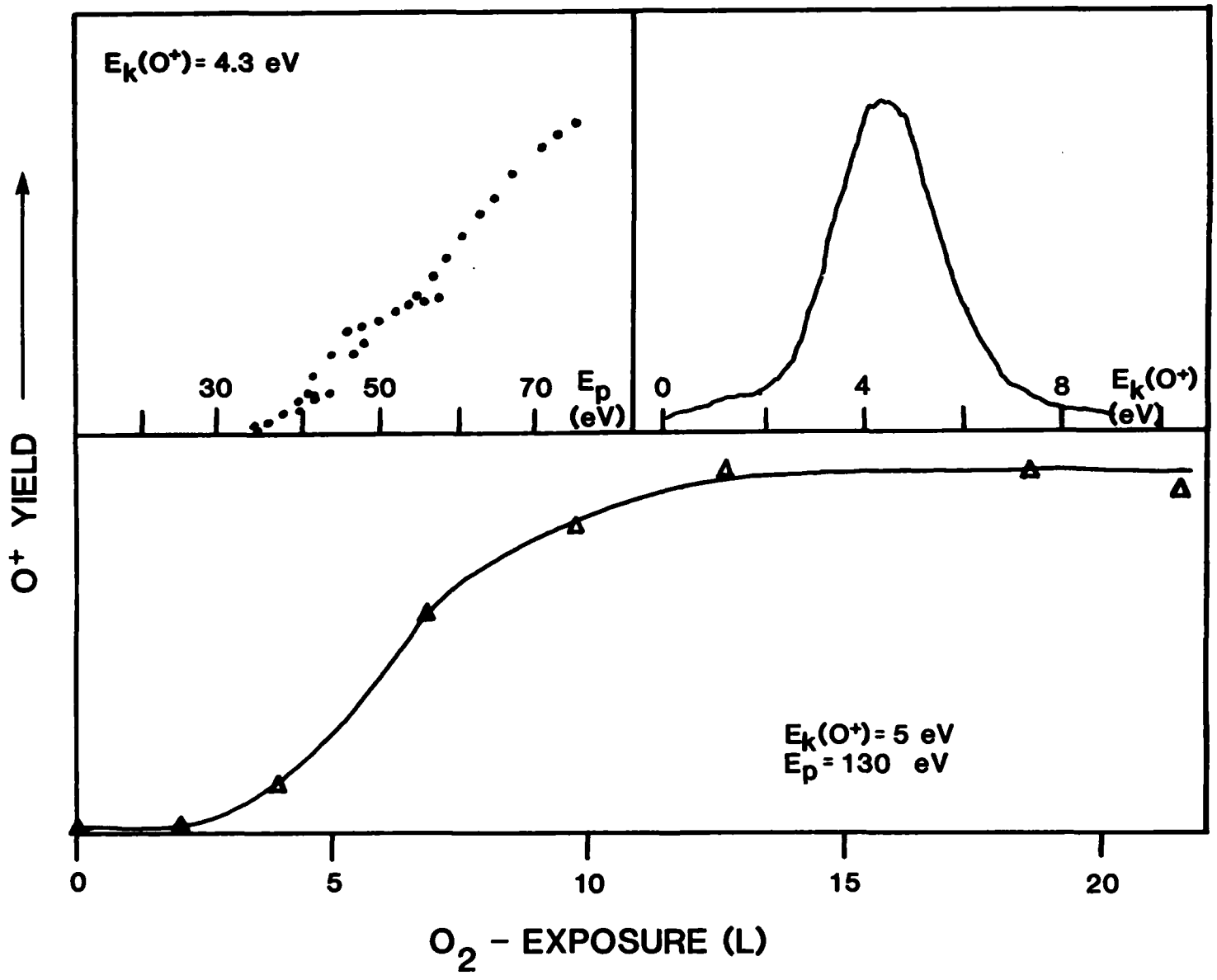
$E_k(O^+)$= 4.3 eV
30
50
70
E_p (eV)
0
4
8
$E_k(O^+)$ (eV)
O^+ YIELD
$E_k(O^+)$= 5 eV
E_p = 130 eV
0
5
10
15
20
O_2 – EXPOSURE (L)

Fig. 13

OFFICE OF NAVAL RESEARCH

Contract N00014-84-F0002

TECHNICAL REPORT NO. 36

ELECTRON AND PHOTON STIMULATED DESORPTION OF CONDENSED MOLECULAR FILMS: RELEVANCE TO THE MECHANISMS OF ION FORMATION AND DESORPTION

Roger Stockbauer, Erminald Bertel, and Theodore E. Madey
Surface Science Division
National Bureau of Standards
Washington, DC 20234

March 30, 1984

Journal of Vacuum Science and Technology A, 1, 1075 (1983).

SECURITY CLASSIFICATION OF THIS PAGE (When Data Entered)

REPORT DOCUMENTATION PAGE		READ INSTRUCTIONS BEFORE COMPLETING FORM
1. REPORT NUMBER 36	2. GOVT ACCESSION NO.	3. RECIPIENT'S CATALOG NUMBER
4. TITLE (and Subtitle) Electron and Photon Stimulated Desorption of Condensed Molecular Films: Relevance to the Mechanisms of Ion Formation and Desorption		5. TYPE OF REPORT & PERIOD COVERED Interim 6. PERFORMING ORG. REPORT NUMBER
7. AUTHOR(s) Roger Stockbauer, Erminald Bertel, and Theodore E. Madey		8. CONTRACT OR GRANT NUMBER(s) N00014-84-F0002
9. PERFORMING ORGANIZATION NAME AND ADDRESS Surface Science Division National Bureau of Standards Washington, DC 20234		10. PROGRAM ELEMENT, PROJECT, TASK AREA & WORK UNIT NUMBERS
11. CONTROLLING OFFICE NAME AND ADDRESS Office of Naval Research Physical Science Program Office Arlington, VA 22217		12. REPORT DATE March 30, 1984 13. NUMBER OF PAGES
14. MONITORING AGENCY NAME & ADDRESS(if different from Controlling Office)		15. SECURITY CLASS. (of this report) Unclassified 15a. DECLASSIFICATION/DOWNGRADING SCHEDULE

16. DISTRIBUTION STATEMENT (of this Report)

Approved for Public Release; Distribution Unlimited

17. DISTRIBUTION STATEMENT (of the abstract entered in Block 20, if different from Report)

18. SUPPLEMENTARY NOTES

Journal of Vacuum Science and Technology A, 1, 1075 (1983).

19. KEY WORDS (Continue on reverse side if necessary and identify by block number)

Cyclohexane; electron stimulated desorption; hydrogen bonding; methanol; photon stimulated desorption; synchrotron radiation; ultraviolet-photoemission spectroscopy; water.

20. ABSTRACT (Continue on reverse side if necessary and identify by block number)

We have used electron-stimulated desorption (ESD) and photon-stimulated desorption (PSD) techniques to study the electronic processes which lead to desorption of ions from condensed films of hydrogen-containing molecules C_6H_{12} (cyclohexane), CH_3OH (methanol), and H_2O. In the condensed state, C_6H_{12} is bound primarily by van der Waals' forces, whereas, CH_3OH and H_2O are both hydrogen-bonded. We see striking differences in the mass distribution of ESD ions from these two classes of condensed films.

DD FORM 1 JAN 73 1473 EDITION OF 1 NOV 65 IS OBSOLETE

S/N 0102-LF-014-6601

SECURITY CLASSIFICATION OF THIS PAGE (When Data Entered)

Summary Abstract: Electron- and photon-stimulated desorption of condensed molecular films: Relevance to the mechanisms of ion formation and desorption

Roger Stockbauer, Erminald Bertel,[a] and Theodore E. Madey

Surface Science Division, National Bureau of Standards, Washington, D.C. 20234

(Received 23 September 1982; accepted 5 November 1982)

PACS numbers: 68.45.Da, 79.90. + b

We have used electron-stimulated desorption (ESD) and photon-stimulated desorption (PSD) techniques to study the electronic processes which lead to desorption of ions from condensed films of hydrogen-containing molecules C_6H_{12} (cyclohexane), CH_3OH (methanol), and H_2O. In the condensed state, C_6H_{12} is bound primarily by van der Waals' forces, whereas, CH_3OH and H_2O are both hydrogen-bonded. We see striking differences in the mass distribution of ESD ions from these two classes of condensed films.

ESD of the nonhydrogen-bonded C_6H_{12} has been studied as a function of film thickness on a clean Cu(100) substrate using time-of-flight (TOF) mass spectrometry. An electron energy of 100 eV was used with a beam current on the sample of approximately 10^{-9} A. For thin layers (corrected exposures $\lesssim 2.5$ L, where $1\ \text{L} = 1\times10^{-6}$ Torr s) predominantly H^+ ions are seen. The H^+ ions have a most probable kinetic energy of 4 eV, and the H^+ yield increases to a plateau value for exposures $\gtrsim 4$ L. For exposures $\gtrsim 2$ L, heavier ions appear in the ESD mass spectrum ($C_1H_n^+ \cdots C_6H_n^+$) having a most probable kinetic energy ~ 1 eV [Fig. 1(a)]; the yield of heavy ions increases with both increasing film thickness and electron beam energy to > 150 eV. Beam damage[1] was negligible under conditions of these experiments. These results are qualitatively consistent with a model by which ions close to the metal surface are preferentially neutralized. The low kinetic energies and high masses of heavy fragments result in substantially lower velocities and, therefore, longer residence times near the metal surfaces than for H^+, so the heavy ions have a higher probability of reneutralization. The reneutralization rate decreases with increasing film thickness, causing an increased yield of higher mass fragments. The ESD ion mass spectrum from a thick layer of C_6H_{12} is *qualitatively similar* to the gas phase mass spectrum.

In strong contrast, ESD of hydrogen-bonded films of H_2O and CH_3OH yields only trace levels of high mass ions. The dominant ESD ion from condensed layers of both molecules is H^+, with yields of higher mass ions $\lesssim 2\%$ of H^+ [Fig. 1(b)]. In addition, cluster ions from the water film [$(H_2O)_n H^+$] were at the 0.1% level or less. The results are independent of film thickness. These observations are *quantitatively different* from the gas phase results, where high mass ions dominate in the mass spectrum.

Evidence for the mechanism of H^+ formation in condensed CH_3OH and H_2O comes from PSD in combination with ESD. PSD of ions from the condensed methanol has been studied over the photon energy range 15 to 75 eV.[2] The threshold for H^+ desorption is at 18 eV, with the maximum yield at 25 eV. This suggests that ionization of the $4a'$ level is the underlying mechanism, because its onset occurs near the 18 eV threshold. In order to determine if the H^+ desorption is due to C–H or O–H bond cleavage (or both), we studied low energy ESD of isotopically labeled CH_3OH films.[3] It was found that low-energy (< 70 eV) electron excitation and fragmentation of CH_3OH results overwhelmingly in H^+ ejection by C–H bond cleavage. This is additional evidence for involvement of the $4a'$ level since it is dominantly a C–H bonding orbital. In contrast, the gas-phase fragmentation shows H^+ arising from both O–H and C–H bond cleavage.[4]

PSD of H^+ from H_2O films[5] has higher threshold and maximum yield energies (25 and 30 eV, respectively) than CH_3OH, and may arise from excitation of a two-hole shake-up state of H_2O.[6]

The absence of heavy ion fragments in the ESD mass spectra of H_2O and CH_3OH films may be related to hydrogen bonding in the condensed layers. Hydrogen bonding could provide an effective deexcitation mechanism for heavy ion fragments, via a strong coupling between adjacent molecules through which the electronic or vibronic excitation becomes delocalized. The reduced yield of heavy ions may also be due

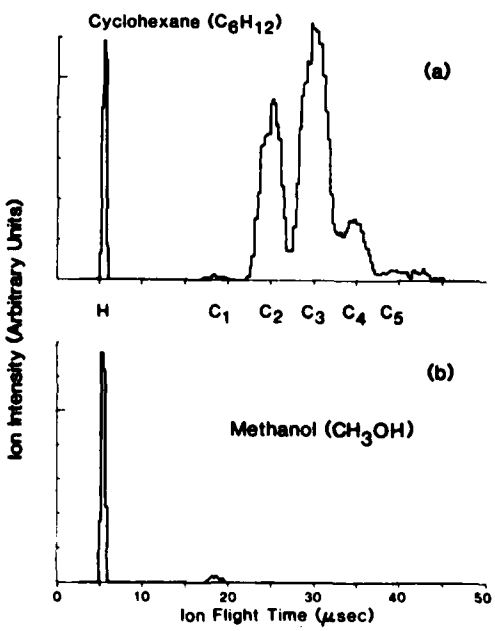

FIG. 1. Comparison of time-of-flight mass spectra from electron-stimulated desorption of (a) cyclohexane taken at 1.5 eV ion kinetic energy and (b) methanol at 3.8 eV ion kinetic energy.

to proton transfer reactions occurring at the surface of the film before or during desorption, a process which could effectively reneutralize the desorbed heavy ions. Hydrogen bonding, however, is not significant in condensed C_6H_{12}, nor do proton transfer processes[7] occur with high probability in ion-molecule collisions of C_6H_{12} and its fragments. Thus, in agreement with the proposed model, heavy ion fragments are not strongly suppressed in ESD of C_6H_{12}.

This work was conducted at the National Bureau of Standards synchrotron light source, SURF-II. E.B. acknowledges financial support from the Max Kade Foundation. This work was supported in part by the Office of Naval Research.

[a]National Bureau of Standards guest scientist and visiting professor, Department of Physics, University of Maryland. Permanent address: Institute fur Physikalische Chemie, Universität Innsbruck, A-6020 Innsbruck, Austria.

[1]T. E. Madey and J. T. Yates, Jr., Surf. Sci. 76, 397 (1978).
[2]D. M. Hanson, R. Stockbauer, and T. E. Madey, J. Chem. Phys. 77, 1569 (1982).
[3]R. Stockbauer, E. Bertel, and T. E. Madey, J. Chem. Phys. 76, 5639 (1982).
[4]M. D. Burrows, S. R. Ryan, W. E. Lamb, Jr., and L. C. McIntyre, Jr., J. Chem. Phys. 71, 4931 (1979).
[5]R. A. Rosenberg, V. Rehn, V. O. Jones, A. K. Green, C. C. Parks, G. Loubriel, and R. H. Stulen, Chem. Phys. Lett. 80, 488 (1981).
[6]D. E. Ramaker, J. Vac. Sci. Technol. A (these proceedings).
[7]K. R. Ryan, L. W. Sieck, and J. H. Futrell, J. Chem. Phys. 41, 111 (1964).

OFFICE OF NAVAL RESEARCH

Contract N00014-84-F0002

TECHNICAL REPORT NO. 37

OXIDATION OF THE Ti(0001) SURFACE

Erminald Bertel, Roger Stockbauer, and Theodore E. Madey
Surface Science Division
National Bureau of Standards
Washington, DC 20234

March 30, 1984

Jornal of Vacuum Science and Technology A, 1, 1075 (1983).

SECURITY CLASSIFICATION OF THIS PAGE (When Data Entered)

REPORT DOCUMENTATION PAGE		READ INSTRUCTIONS BEFORE COMPLETING FORM
1. REPORT NUMBER 37	2. GOVT ACCESSION NO.	3. RECIPIENT'S CATALOG NUMBER
4. TITLE (and Subtitle) Oxidation of the Ti(0001) surface		5. TYPE OF REPORT & PERIOD COVERED Interim 6. PERFORMING ORG. REPORT NUMBER
7. AUTHOR(s) Erminald Bertel, Roger Stockbauer, and Theodore E. Madey		8. CONTRACT OR GRANT NUMBER(s) N00014-84-F0002
9. PERFORMING ORGANIZATION NAME AND ADDRESS Surface Science Division National Bureau of Standards Washington, DC 20234		10. PROGRAM ELEMENT, PROJECT, TASK AREA & WORK UNIT NUMBERS
11. CONTROLLING OFFICE NAME AND ADDRESS Office of Naval Research Physical Science Program Office Arlington, VA 22217		12. REPORT DATE March 30, 1984 13. NUMBER OF PAGES
14. MONITORING AGENCY NAME & ADDRESS(if different from Controlling Office)		15. SECURITY CLASS. (of this report) Unclassified 15a. DECLASSIFICATION/DOWNGRADING SCHEDULE

16. DISTRIBUTION STATEMENT (of this Report)

Approved for Public Release; Distribution Unlimited

17. DISTRIBUTION STATEMENT (of the abstract entered in Block 20, if different from Report)

18. SUPPLEMENTARY NOTES

Journal of Vacuum Science and Technology A, 1, 1075 (1983).

19. KEY WORDS (Continue on reverse side if necessary and identify by block number)

Oxidation; photoemission; direct recombination; titanium; titanium dioxide.

20. ABSTRACT (Continue on reverse side if necessary and identify by block number)

Previous studies on polycrystalline Ti samples showed that exposure to $\gtrsim$ 100 L O_2 produced thin layers of TiO_2 on top of lower Ti oxides. On Ti(0001) an earlier report indicated TiO rather than TiO_2 stoichiometry for the surface oxide formed at saturation exposure. The aim of the present study on Ti(0001) was to clarify the structure and the composition of this surface oxide by use of electron-stimulated ion desorption (ESD), Auger electron spectroscopy (AES), electron energy loss spectroscopy (ELS), and ultra-violet photoelectron spectroscopy (UPS) using synchrotron (continued)

DD FORM 1 JAN 73 1473 EDITION OF 1 NOV 65 IS OBSOLETE

S/N 0102-LF-014-6601

SECURITY CLASSIFICATION OF THIS PAGE (When Data Entered)

Block 20. Abstract (Continued)

radiation at the NBS SURF II facility.

Summary Abstract: Oxidation of the Ti(0001) surface

Erminald Bertel,[a)] Roger Stockbauer, and Theodore E. Madey

Surface Science Division, National Bureau of Standards, Washington, D.C. 20234

(Received 22 September 1982; accepted 15 October 1982)

PACS numbers: 81.60.Bn, 79.20.Fv, 79.20.Kz, 79.60.Cn

Previous studies on polycrystalline Ti samples showed that exposure to $\gtrsim 100$ L O_2 produced thin layers of TiO_2 on top of lower Ti oxides (e.g., Refs. 1–6). On Ti(0001) an earlier report indicated TiO rather than TiO_2 stoichiometry for the surface oxide formed at saturation exposure.[7] The aim of the present study on Ti(0001) was to clarify the structure and the composition of this surface oxide by use of electron-stimulated ion desorption (ESD), Auger electron spectroscopy (AES), electron energy loss spectroscopy (ELS), and ultraviolet photoelectron spectroscopy (UPS) using synchrotron radiation at the NBS SURF II facility. Key experimental results are:

(a) ESD: Exposure of the clean Ti(0001) surface to oxygen caused a slight increase of O^+ ion yield during the first 4 L of exposure followed by a rapid increase and saturation after only 12 L exposure. The sigmoidal curve shape was very similar to that observed earlier on a stepped Ti(0001) surface.[8]

(b) AES: The *MMM* spectrum of the clean metal shows the dominant super Coster–Kronig emission at 25 eV and a small peak at 43 eV. Both features disappear after exposure to only 40 L O_2. A small new peak is observed at 36 eV in the oxide. Further O_2 exposure caused no significant changes.

(c) ELS: The Ti metal bulk plasmon is observed at 17 eV. Considerable loss intensity between 1–4 eV is due to intraband excitations in the conduction band. After exposure to 40 L O_2 the spectra show a marked dependence on the sampling depth. With highest surface sensitivity (primary energy $E_p = 150$ eV, angle of incidence $\theta = 55°$) an oxide bulk plasmon is observed at 23 eV. Increasing the probing depth ($E_p = 1000$ eV, normal incidence) results in the appearance of both the metal and the oxide plasmon in the ELS spectra. The low-energy-loss intensity is much-attenuated, consistent with the formation of a band gap in the oxide. In the gap a residual loss at about 2.4 eV is observed to increase in intensity with increasing electron irradiation time.

(d) UPS: The $3p$ level in the clean Ti appears at 33 eV binding energy (BE). Both $3p$ and $3d$ emission show a reso-

nant enhancement peaking at 47 eV photon energy. After exposure to 1.5 L O_2 a sharp oxygen-induced feature appears at 6.5 eV BE, which is much more intense than the 3*d* emission off resonance, but similar in intensity at resonance. After exposure to 40 L O_2 the 3*d* emission is hardly detectable off resonance but slightly enhanced at $h\nu = 47$ eV; the 3*p* level is shifted to 38 eV BE. The oxide valence band appears now as a broad-structured feature between 4 and 9 eV BE showing significant enhancement at $h\nu = 47$ eV.

The following conclusions can be drawn. The observation of both the clean metal and the oxide plasmon in ELS spectra taken at high-primary energy proves the presence of both phases within the sampling depth. Oxide island growth can be ruled out, because the metal plasmon does not appear in low-primary-energy ELS spectra. The ELS data are consistent, however, with a continuous oxide overlayer of less than 10 Å thickness. All oxygen-induced features observable with the techniques mentioned above saturate at or below 40 L exposure, which confirms the protective nature of this thin overlayer for oxygen pressures below 5×10^{-7} Torr. The thickness of the surface oxide at saturation is smaller than the sampling depth of the Ti *LMM* Auger emission. Hence, this signal cannot be used independently to characterize the oxide layer in contrast to earlier suggestions.[7] The Ti M_{23} M_{45} M_{45} emission has a smaller escape depth and is nearly completely suppressed in Ti(0001) + 40 L O_2, indicating an oxidation state beyond the TiO stoichiometry. The *d*-band emission of the saturation oxide in UPS is considerably smaller than the *d* emission from vacuum-cleaved Ti_2O_3[9] which is consistent with TiO_2 stoichiometry. The small residual *d* emission corresponds to the loss intensity observed in the band gap and can be attributed to Ti^{3+} defects in the oxide.

The resonant enhancement of the metal 3*d* emission at photon energies around 47 eV is due to the interaction with the 3*d* shell in a direct recombination-type process.[10] The 3*p* shell is excited to a final state 47 eV above the ground state. Deexcitation is possible via two channels. Autoionization leaves the 3*p* shell with a hole, decaying in a subsequent super-Coster–Kronig transition. Alternatively, the excited 3*p* shell can transfer the energy directly to the 3*d* shell, kicking out a 3*d* electron with substantially higher energy than in the Auger process (i.e., 43 vs 25 eV). This is the process giving rise to the 3*d* resonant enhancement. The resonant enhancement of the oxide valence band in Ti(0001) + 40 L O_2 is an additional indication of TiO_2 stoichiometry because it implies an interatomic interaction between Ti 3*p* shell and oxide valence band. With an intraatomic channel available as in Ti_2O_3 one would expect the latter to be dominant, giving rise mainly to enhanced 3*d* emission as it is actually observed in Ti(0001) + 1.5 L O_2. A similar consideration holds for the ESD O^+ yield. Only in the maximum-valency compound TiO_2 is the Ti 3*p* core hole likely to decay via the interatomic channel which creates two holes on the oxygen site causing the high O^+ ion yield observed in ESD (Knotek–Feibelman mechanism[11]). Finally, the large binding energy shift of the 3*p* level (5 eV) also suggests TiO_2 formation rather than Ti_2O_3.

Acknowledgments: E. B. acknowledges financial support by the Max Kade Foundation, New York. The work has been in part supported by the Office of Naval Research.

[a] Visiting Professor, Department of Physics and Astronomy, University of Maryland. Permanent Address: Inst. f. Physikalische Chemie, Universitat Innsbruck, A-6020 Innsbruck, Austria.

[1] T. Smith, Surf. Sci. **38**, 292 (1973).
[2] P. J. Bassett and T. E. Gallon, J. Electron. Spectrosc. Relat. Phenom. **2**, 101 (1973).
[3] L. Porte, M. Demosthenous, and T. M. Duc, J. Less Common Met. **56**, 183 (1977).
[4] L. I. Johansson, A. L. Hagstrom, A. Platau, and S. E. Karlsson, Phys. Status Solidi B **83**, 77 (1977).
[5] A. Platau, L. I. Johansson, A. L. Hagstrom, S. E. Karlsson, and S. B. M. Hagstrom, Surf. Sci. **63**, 153 (1977).
[6] B. Kasemo and E. Tornqvist, Surf. Sci. **77**, 209 (1978).
[7] H. D. Shih and F. Jona, Appl. Phys. **12**, 311 (1977).
[8] D. M. Hanson, R. Stockbauer, and T. E. Madey, Phys. Rev. B **24**, 5513 (1982).
[9] R. L. Kurtz and V. E. Henrich, Phys. Rev. B **25**, 3563 (1982).
[10] E. Bertel, R. Stockbauer, and T. E. Madey, Phys. Rev. B (submitted).
[11] M. L. Knotek and P. J. Feibelman, Phys. Rev. Lett. **40**, 964 (1978).

OFFICE OF NAVAL RESEARCH

Contract N00014-84-F0002

TECHNICAL REPORT NO. 38

DESORPTION OF IONS FROM SURFACES:

MECHANISMS OF PHOTON STIMULATED DESORPTION

Roger Stockbauer and Theodore E. Madey
Surface Science Division
National Bureau of Standards
Washington, DC 20234

March 30, 1984

Annals of the Israel Physical Society, 6, 483 (1983).

SECURITY CLASSIFICATION OF THIS PAGE (When Data Entered)

REPORT DOCUMENTATION PAGE		READ INSTRUCTIONS BEFORE COMPLETING FORM
1. REPORT NUMBER 38	2. GOVT ACCESSION NO.	3. RECIPIENT'S CATALOG NUMBER
4. TITLE (and Subtitle) DESORPTION OF IONS FROM SURFACES: MECHANISMS OF PHOTON STIMULATED DESORPTION		5. TYPE OF REPORT & PERIOD COVERED Interim
		6. PERFORMING ORG. REPORT NUMBER N00014-84-F0002
7. AUTHOR(s) Roger Stockbauer and Theodore E. Madey		8. CONTRACT OR GRANT NUMBER(s)
9. PERFORMING ORGANIZATION NAME AND ADDRESS Surface Science Division National Bureau of Standards Washington, DC 20234		10. PROGRAM ELEMENT, PROJECT, TASK AREA & WORK UNIT NUMBERS
11. CONTROLLING OFFICE NAME AND ADDRESS Office of Naval Research Physical Science Program Office Arlington, VA 22217		12. REPORT DATE March 30, 1984
		13. NUMBER OF PAGES
14. MONITORING AGENCY NAME & ADDRESS(if different from Controlling Office)		15. SECURITY CLASS. (of this report) Unclassified
		15a. DECLASSIFICATION/DOWNGRADING SCHEDULE

16. DISTRIBUTION STATEMENT (of this Report)

Approved for Public Release; Distribution Unlimited

17. DISTRIBUTION STATEMENT (of the abstract entered in Block 20, if different from Report)

18. SUPPLEMENTARY NOTES

Published in the Annals of the Israel Physical Society, 6, 483 (1983).

19. KEY WORDS (Continue on reverse side if necessary and identify by block number)

Cyclohexane; hydrogen bonding; methanol; photon stimulated desorption; synchrotron radiation; ultraviolet photoemission spectroscopy; water.

20. ABSTRACT (Continue on reverse side if necessary and identify by block number)

A review is given of the mechanisms of Photon Stimulated Desorption (PSD) from ionic, covalent and van der Waals bonded surface molecules. An interatomic Auger decay process describes desorption from ionically bonded, maximal valency compounds. The mechanism for ion desorption from covalently bonded systems is thought to involve relatively long-lived two hole states. Ion desorption from thick molecular films presents a challenge to theory since heavy fragments (C_xH_y) desorb from some (cyclohexane) and not from others (water, methanol).

DD FORM 1 JAN 73 1473 EDITION OF 1 NOV 65 IS OBSOLETE

S N 0102-LF-014-6601

SECURITY CLASSIFICATION OF THIS PAGE (When Data Entered)

PACS: 81.60.Bn; 79.20.Fv; 79.20Kz

DESORPTION OF IONS FROM SURFACES: MECHANISMS OF PHOTON STIMULATED DESORPTION

Roger Stockbauer and Theodore E. Madey
National Bureau of Standards
Washington, D.C. 20234 USA

ABSTRACT

A review is given of the mechanisms of Photon Stimulated Desorption (PSD) from ionic, covalent and van der Waals bonded surface molecules. An interatomic Auger decay process describes desorption from ionically bonded, maximal valency compounds. The mechanism for ion desorption from covalently bonded systems is thought to involve relatively long-lived two hole states. Ion desorption from thick molecular films presents a challenge to theory since heavy fragments (C_xH_y) desorb from some (cyclohexane) and not from others (water, methanol).

1. INTRODUCTION

With synchrotron radiation sources becoming readily available and accessible, Photon Stimulated Desorption (PSD) of ions from surfaces has become a viable scientific technique. The field is relatively young, the first successful experiment being reported in 1979[1]. The primary thrust of PSD experiments to date has been the investigation of the mechanism by which ions are desorbed from surfaces with a view toward developing PSD as a surface characterization technique.

Besides the availability of synchrotron radiation sources, two events in the mid 1970's spurred the development of PSD. The first was the discovery that in electron stimulated desorption (ESD), ions were emitted in well defined cones of emission in directions determined by the orientation of surface bonds, and hence ESDIAD (Electron Stimulated Desorption Ion Angular Distribution) could be used to determine the bonding geometry of surface species[2]. This resulted in attempts to better understand ion desorption mechanisms to predict the systems to which ESDIAD could be applied. The second event was the development of a mechanistic theory of ion desorption from ionically bonded compounds[3] based on an interatomic Auger decay process initiated by production of a core hole. It was soon realized that theories

for ion desorption could best be tested by comparing PSD ion yields (ion intensity vs. photon energy) with excitation cross sections[4,5]. This paper will concern itself with such comparisons with a view toward illuminating the mechanisms of ion desorption. The comparisons will be made for three classes of compounds: ionically bonded maximal valency compounds where the ion desorption is dominated by excitations in the substrate, covalently bonded systems where the substrate influence is minimal or non-existent, and thick molecular films where there is no substrate influence on the ion desorption[6].

2. IONICALLY BONDED SYSTEMS

In 1978, Knotek and Feibelman[3] proposed an interatomic Auger decay mechanism to explain ion desorption from maximal valency compounds by ESD. They described the desorption as a three step process illustrated in Fig. 1 for the maximal valency compound TiO_2. The initial step is the formation of a core hole in the Ti atom. Normally, this hole would be filled by a Ti valence electron with the subsequent ejection of a second valence electron (Auger decay process). In a maximal valency compound, this process has low probability since the metal valence electrons are depleted. Instead the Ti core hole is filled by an electron from the oxygen (step 2) accompanied by the ejection of one or two more oxygen valence electrons into the vacuum (step 3). The oxygen atom which was initially coordinated in a -2 charge state finds itself in a 0 or +1 charge state in close proximity to the positively charged Ti ion. The Coulomb repulsion expels the oxygen ion from the surface.

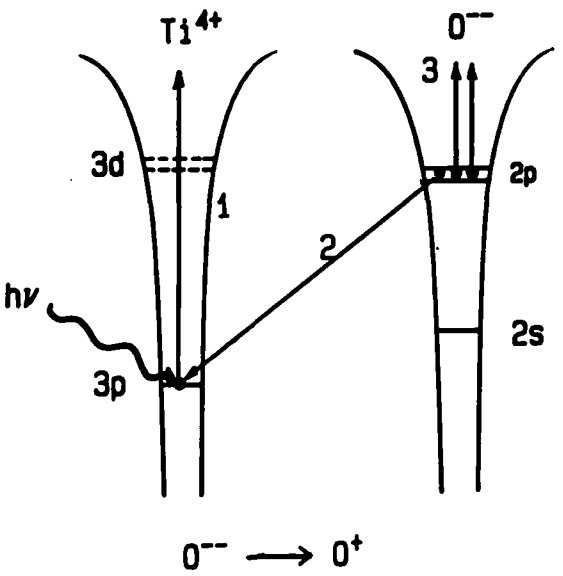

Fig. 1. Schematic showing the steps involved in the Knotek-Feibelman interatomic Auger decay mechanism (Ref. 3).

This theory leads to three predictions. The first is that ion desorption is independent of how the core hole is produced, i.e., desorption should occur whether the core hole was produced by electron, photon or ion impact. The second, which follows from the first, is that the cross section for ion production should be proportional to the cross section for core hole production. The third is that ion desorption from non-maximal valency ionic compounds, e.g., Ti_2O_3, should be greatly reduced.

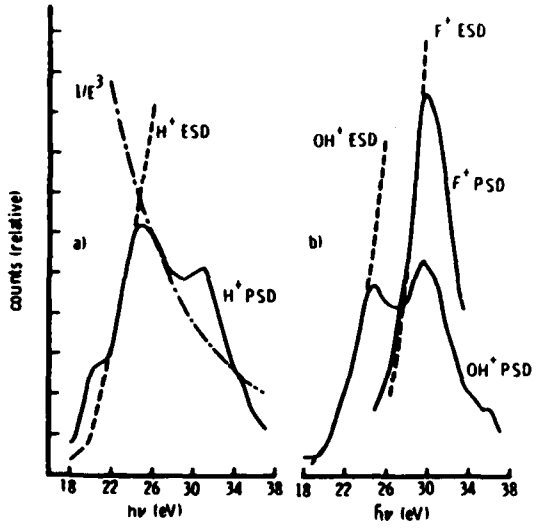

Fig. 2. PSD and ESD ion yields from TiO_2 (Ref. 1).

Fig. 2 presents data obtained by Knotek, Jones and Rehn[1] which verifies the first prediction. The solid lines are PSD ion yields for H^+, OH^+ and F^+ from a TiO_2 surface while the dashed lines are the ESD ion yields for the same surface. The thresholds and shape of the curves directly above onset are nearly identical showing the equivalence of electron and photon impact in stimulating ion desorption. The difference in the shape of the curves at higher energy is due to the difference in ionization cross section for electrons and photons and points out the advantage of using photons for this type of measurement. The photoionization cross section decreases as $\sim 1/E^3$ whereas the electron impact ionization cross section falls off much slower, as $\ln E/E$. Energy levels which appear as peaks in photoionization appear only as changes in slope in electron impact ionization and are therefore easier to identify using photon impact.

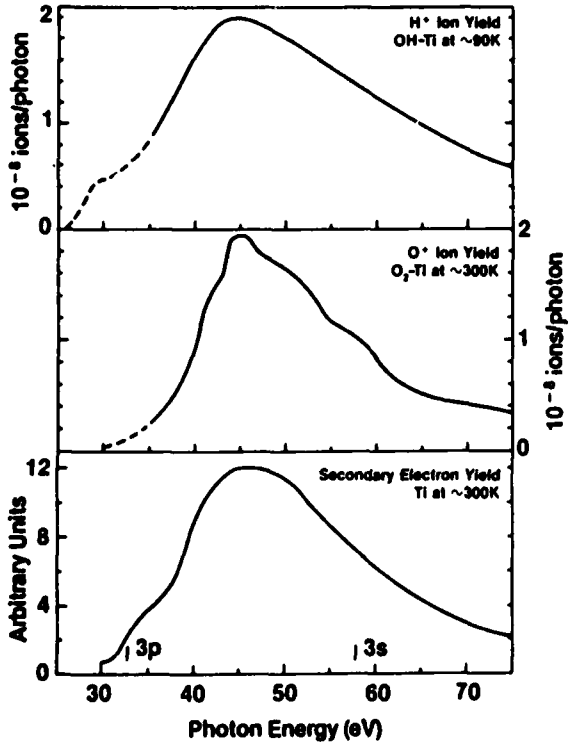

Fig. 3. H^+ from OH and O^+ from O on Ti compared with Ti core hole production (Ref. 7, 15).

The confirmation of the second prediction of the Knotek-Feibelman theory is illustrated in the lower two frames of Fig. 3.[7] The middle is the O^+ ion yield from a thin film of TiO_2 on a Ti(001) substrate. The bottom is the secondary electron yield of Ti(001) which is proportional to the probability of producing a core hole in the metal. The close similarily between the two curves strongly suggests that the ion desorption is directly related to the production of a core hole in the metal in agreement with the second prediction. Differences in detail are due to the fact that ionization of Ti^{4+} contributes to

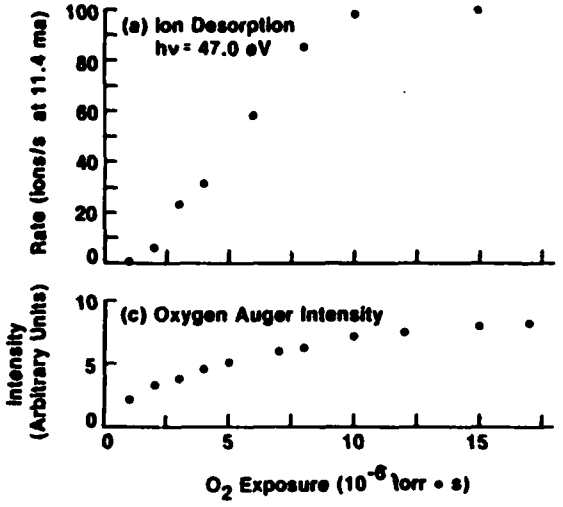

Fig. 4. O^+ ion yield and O Auger intensity vs. oxygen exposure on a Ti(001) surface (Ref. 7).

the O^+ yield, whereas ionization of metallic Ti contributes to the secondary electron yield.

Confirmation of the third prediction is illustrated in Fig. 4 which shows the O^+ ion intensity as a function of exposure for the same Ti(001) + O_2 system discussed above. Separate studies have shown that the Ti metal when exposed to O_2 progressively oxidizes[8], i.e., it goes through several stages of oxidation before forming the maximal valency TiO_2 oxide. In the early stages of oxidation, e.g., where chemisorbed O and sub-maximal-valency Ti oxides are formed, no ion desorption is observed.

Similar agreement between PSD ion yields and core hole cross sections have been observed for shallow core levels in maximal valency oxides of tungsten[4,5] and niobium[9] and for the deeper core levels in TiO_2[10], BeO, SiO_2, Al_2O_3[11] and oxygen on molybdenum[12]. An interesting application of PSD was reported by Benbow, Thuler and Hurych[13]. For the mixed metal compound Na_xWO_3 they determined the surface oxygen was bonded to W by observing that O^+ was desorbed at the W core levels but not the Na core levels.

The ion yield curves do not always exactly follow the core level cross sections. Competition between PSD and normal Auger, resonant decay and resonant photoemission processes can result in differences between the curves[6,14].

3. COVALENTLY BONDED SYSTEMS

The top frame of Fig. 3 shows that not all ion desorption is initiated by substrate core hole events. The system is OH produced by dissociation of H_2O on the same Ti(001) crystal discussed above [15]. At photon energies above 35 eV, it appears that the Ti core hole is involved in the H^+ ion desorption. However, the onset for the desorption is some 5 eV below the onset for the core hole production in Ti(001). This difference indicates that the Ti core hole is not involved in the ion desorption at onset.

A more extreme case of the noninvolvement of the substrate core hole in ion desorption is illustrated in Fig. 5[16]. The solid line is the O^+ ion yield from CO bonded covalently on a Ru(001) crystal while the dashed line is proportional to the metal core hole production. There is little correlation between the two curves indicating that the ruthenium core holes are not involved in the ion desorption.

The theory for ion desorption from covalently bonded systems is not yet fully developed. Ramaker[17] has suggested that the ion desorption shown in Fig. 5 is due to processes in the adsorbed CO bond involving two hole (2h) or two hole, one electron (2hle) excitations. Similar 2hle excitations are thought to be responsible for the low energy onset of H^+ from OH on Ti(001) in Fig. 3.

In general, this mechanism involves forming two holes in the adsorbed molecule. This is similar to forming a doubly charged ion state in a gas phase molecule. This can lead to a strong Coulomb repulsion resulting in bond rupture with subsequent ion desorption. A necessary condition for ion desorption is that the two hole state remain localized on a single adsorbed molecule long enough for the electronic energy to be converted to internuclear motion. One hole hopping times are on the order of 10^{-16} seconds while ion desorption times are on the order of 10^{-14} seconds. In contrast, two hole hopping times can be longer than

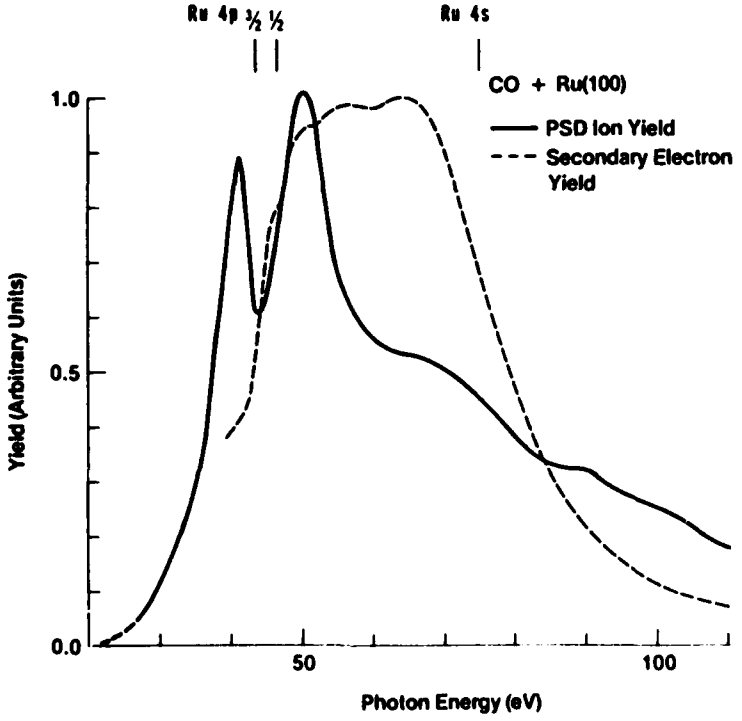

Fig. 5. O^+ ion yield from CO compared with Ru core hole production (Ref. 16).

one-hole hopping times by orders of magnitude. For long-lived two hole states ($\sim 10^{-14}$s), the Coulomb hole-hole correlation energy U is much larger than the width of the single particle band W which the holes occupy, and it is not energetically favorable for them to dissipate their energy by separating[18]. The correlation energy in effect keeps the holes together long enough for desorption to occur.

4. MOLECULAR FILMS

Ion desorption from molecular films has been studied by a number of groups using both electron and photon impact[15,19-21]. Fig. 6 shows the ion yield from a thick film of methanol on Ti along with the Ti core hole production[19]. There is little correlation between the two curves indicating that the ion yield is independent of core hole excitations in the substrate. This is not surprising since the films are thick enough ($\sim$ 20Å) to suppress the influence of the substrate. This represents, in effect, PSD from a molecular solid.

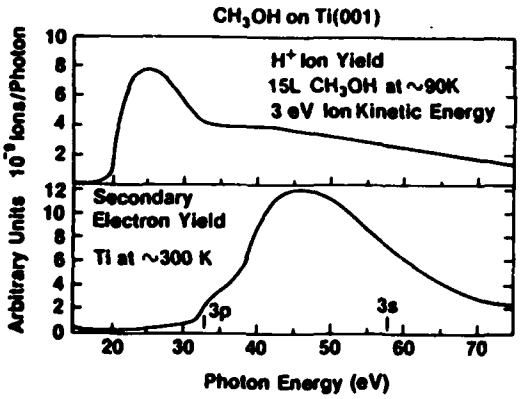

Fig. 6. H^+ ion yield from condensed methanol compared with Ti core hole production (Ref. 19).

An interesting contrast has been noted in the mass spectrum of ions desorbed from water, methanol and cyclopropane[22]. Only H^+ is observed from water and methanol even though their gas phase mass spectra are dominated by heavier ions. In contrast, the mass spectrum of desorbed ions from thick films of cyclohexane are dominated by C_xH_y fragments as shown in Fig. 7. The lack of heavy fragments in the water and methanol ion desorption may arise from hydrogen bonding providing an efficient energy delocalization pathway leading to deexcitation of the states involved in the heavy ion desorption. Also, proton transfer in water and methanol could effectively neutralize the heavy ions. Reactions such as

$$CH_2OH^+ + CH_3OH \rightarrow CH_2O + CH_3OH{\cdot}H^+$$

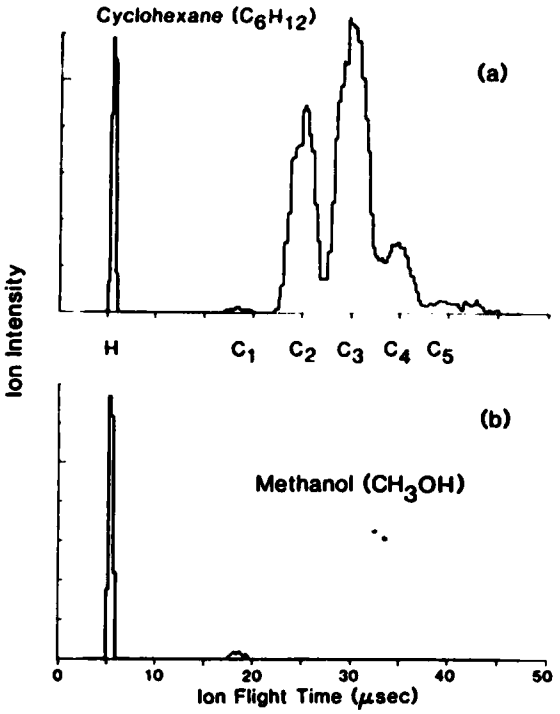

Fig. 7. Mass spectra of ions desorbed from thick films of cyclohexane and methanol (Ref. 22).

are very efficient in gas phase methanol collisions but are nonexistent for cyclopropane.

5. SUMMARY

The interatomic Auger decay mechanism for ion desorption from maximal valency compounds has been tested for a number of systems and appears to describe the ion desorption for this class of compounds. Ion desorption from covalently bonded compounds is thought to proceed by 2h or 2hle excitations which remain localized long enough for desorption to occur. This same mechanism may apply to thick molecular films but at this time cannot predict the occurrence or absence of heavy ion fragment desorption from these films.

6. ACKNOWELDGEMENTS

The authors wish to acknowledge the contributions to various aspects of this work by the following colleagues: D. Doering, E. Bertel, S. A. Flodström, D. Hanson and R. Kurtz. We wish to thank the staff of the National Bureau of Standards Synchrotron Ultraviolet Radiation Facility for their assistance in conducting these experiments. This work was supported in part by the Office of Naval Research.

FOOTNOTES AND REFERENCES

1 M. L. Knotek, V. O. Jones and V. Rehn, Phys. Rev. Lett. 43, 300 (1979).

2 T. E. Madey, Surface Sci. 33, 355 (1972). J. J. Czyzewski, T. E. Madey and J. T. Yates, Jr., Phys. Rev. Lett. 32, 777 (1974); T. E. Madey, F. P. Netzer, J. E. Houston, D. M. Hanson, and R. Stockbauer in Ref. 6 below, p. 120.

3 M. L. Knotek and P. J. Feibelman, Phys. Rev. Lett. 40, 964 (1978).

4 D. P. Woodruff, M. Traum, H. H. Farrell, N. V. Smith, P. D. Johnson, D. A. King, R. L. Benbow and Z. Hurych, Phys. Rev. B 21, 5642 (1980).

5. T. E. Madey, R. Stockbauer, F. van der Veen and D. E. Eastman, Phys. Rev. Lett., 45, 187 (1980).

6 For a comprehensive survey of different aspects of ion desorption, the reader is referred to the excellent articles in N. H. Tolk, M. M. Traum, J. C. Tully and T. E. Madey (eds.) *Desorption Induced by Electronic Transitions,* Springer Series in Chemical Physics 24 (Springer-Verlag, Berlin, 1983).

7 D. M. Hanson, R. Stockbauer and T. E. Madey, Phys. Rev. B24, 5513 (1981).

8 E. Bertel, R. Stockbauer and T. E. Madey, Surface Sci. (submitted) and references therein.

9 R. Stockbauer, D. M. Hanson, S. A. Flodström and T. E. Madey (unpublished).

10 C. C. Parks, D. A. Shirley, M. L. Knotek, G. Loubriel, R. H. Stulen, B. E. Koel and R. A. Rosenberg, Surface Sci. (submitted).

11 M. L. Knotek, R. H. Stulen, G. M. Loubriel, V. Rehn, R. A. Rosenberg and C. C. Parks, Surface Sci. (submitted).

12 R. Jaeger, J. Stöhr, J. Feldhaus, S. Brennan and D. Menzel, Phys. Rev. B23, 2102 (1981).

13 R. L. Benbow, M. R. Thuler and Z. Hurych, Phys. Rev. Lett. 49, 1264 (1983), and this volume.

14 R. Stockbauer, D. Ramaker, E. Bertel, R. Kurtz and T. E. Madey, J. Vac. Sci. Technol. (submitted).

15 R. Stockbauer, D. M. Hanson, S. A. Flodström and T. E. Madey, Phys. Rev. B26, 1885 (1982).

16 T. E. Madey, R. Stockbauer, S. A. Flodström, J. F. van der Veen, F. J. Himpsel and D. E. Eastman, Phys. Rev. B23, 6847 (1981).

17 D. E. Ramaker, in Ref. 6, p. 70.

18 P. J. Feibelman, Surface Sci. 102, L51 (1981).

19 D. M. Hanson, R. Stockbauer and T. E. Madey, J. Chem. Phys. 77, 1569 (1982).

20 R. A. Rosenberg, V. Rehn, V. O. Jones, A. K. Green, C. C. Parks, G. Loubriel and R. H. Stulen, Chem. Phys. Lett. 80, 488 (1981).

21 R. A. Rosenberg, V. Rehn, A. K. Green, P. R. LaRoe and C. C. Parks, Ref. 5, pg. 247.

22 R. Stockbauer, E. Bertel and T. E. Madey, J. Vac. Sci. Technol. A1, 1162 (1983).

OFFICE OF NAVAL RESEARCH

Contract N00014-84-F0002

TECHNICAL REPORT NO. 39

THE USE OF ANGLE RESOLVED ELECTRON AND PHOTON STIMULATED DESORPTION FOR THE DETERMINATION OF MOLECULAR STRUCTURE AT SURFACES

Theodore E. Madey and R. Stockbauer
Surface Science Division
National Bureau of Standards
Washington, DC 20234

March 30, 1984

Approved for Public Release; Distribution Unlimited

To be published in Revista Brasileira de Aplicacoes de Vacuo.

SECURITY CLASSIFICATION OF THIS PAGE (When Data Entered)

REPORT DOCUMENTATION PAGE

READ INSTRUCTIONS BEFORE COMPLETING FORM

1. REPORT NUMBER: 39	2. GOVT ACCESSION NO.
3. RECIPIENT'S CATALOG NUMBER	
4. TITLE (and Subtitle): The USE OF ANGLE RESOLVED ELECTRON AND PHOTON STIMULATED DESORPTION FOR THE DETERMINATION OF MOLECULAR STRUCTURE AT SURFACES	5. TYPE OF REPORT & PERIOD COVERED: Interim
	6. PERFORMING ORG. REPORT NUMBER
7. AUTHOR(s): Theodore E. Madey and R. Stockbauer	8. CONTRACT OR GRANT NUMBER(s): N00014-84-F0002
9. PERFORMING ORGANIZATION NAME AND ADDRESS: Surface Science Division, National Bureau of Standards, Washington, DC 20234	10. PROGRAM ELEMENT, PROJECT, TASK AREA & WORK UNIT NUMBERS
11. CONTROLLING OFFICE NAME AND ADDRESS: Office of Naval Research, Physical Science Program Office, Arlington, VA 22217	12. REPORT DATE: March 30, 1984
	13. NUMBER OF PAGES
14. MONITORING AGENCY NAME & ADDRESS(if different from Controlling Office)	15. SECURITY CLASS. (of this report): Unclassified
	15a. DECLASSIFICATION/DOWNGRADING SCHEDULE

16. DISTRIBUTION STATEMENT (of this Report)

Approved for Public Release; Distribution Unlimited

17. DISTRIBUTION STATEMENT (of the abstract entered in Block 20, if different from Report)

18. SUPPLEMENTARY NOTES

To be published in Revista Brasileira de Aplicacoes de Vacuo

19. KEY WORDS (Continue on reverse side if necessary and identify by block number)

Chemisorption; electron stimulated desorption; photon stimulated desorption; surface structure.

20. ABSTRACT (Continue on reverse side if necessary and identify by block number)

This paper is a brief review of recent data related to the use of angle-resolved electron stimulated desorption and photon stimulated desorption in determining the structures of molecules at surfaces. Examples include a variety of structural assignments based on ESDIAD (electron stimulated desorption ion angular distributions), the observation of short-range local ordering effects induced in adsorbed molecules by surface impurities, and the application of photon stimulated desorption to both ionic and covalent adsorbate systems.

DD FORM 1 JAN 73 1473 EDITION OF 1 NOV 65 IS OBSOLETE

S/N 0102-LF-014-6601

SECURITY CLASSIFICATION OF THIS PAGE (When Data Entered)

THE USE OF ANGLE RESOLVED ELECTRON AND PHOTON STIMULATED DESORPTION FOR THE DETERMINATION OF MOLECULAR STRUCTURE AT SURFACES

Theodore E. Madey and R. Stockbauer,
Surface Science Division, National Bureau of Standards, Washington, DC 20234 USA

This paper is a brief review of recent data related to the use of angle-resolved electron stimulated desorption and photon stimulated desorption in determining the structures of molecules at surfaces. Examples include a variety of structural assignments based on ESDIAD (electron stimulated desorption ion angular distributions), the observation of short-range local ordering effects induced in adsorbed molecules by surface impurities, and the application of photon stimulated desorption to both ionic and covalent adsorbate systems.

Desorption, Structure, Chemisorption

1. Introduction

Important questions which arise in studies of molecules on surfaces concern the geometrical structure of the adsorbed species: at which site is a molecule bonded to the surface, what are the orientations of the bonds between molecule and surface, and what are the bond directions of the ligands in surface molecular complexes? It is now well-established that the electron stimulated desorption ion angular distribution (ESDIAD) method and the angle-resolved photon stimulated desorption (PSD) method using synchrotron radiation are of great use in providing direct information about site location and geometrical structure of molecules on surfaces [1-5].

In these methods, electronic excitation of surface molecules by a focused electron beam or a photon beam can result in desorption

of atomic and molecular ions, neutrals, and metastable species from the surface. The ions desorb in discrete cones of emission in directions determined by the orientation of the bond which is ruptured by the excitation. For example, as illustrated in Fig. 1, ESD or PSD of adsorbed CO bound in a standing-up configuration on a metal surface

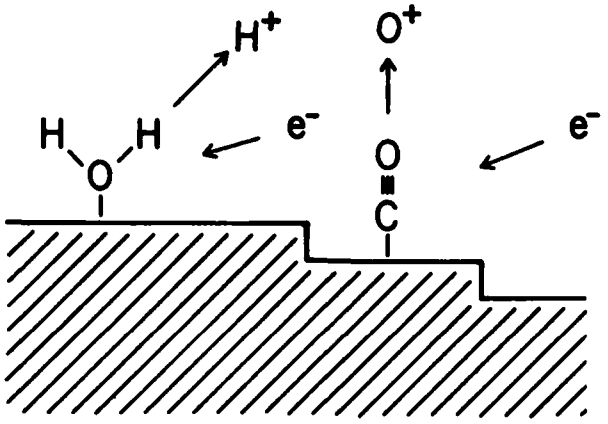

Figure 1. Schematic bonding configurations for adsorbed CO and H_2O, showing relationship between surface bond angle and ion desorption angle in ESDIAD.

will result in desorption of O^+ in the direction of the surface normal, while ESD/PSD of H^+ from H_2O adsorbed via the O atom will result in desorption of H^+ in an off-normal direction. Measurements of the patterns of ion desorption provide a direct display of the geometrical structure of surface molecules in the adsorbed layer [1-5].

In the present paper, we summarize recent experimental results detailing the utility of ESDIAD and PSD in studies of molecules on surface. In particular, we shall emphasize that

(a) ESDIAD and angle resolved PSD provide direct information about the structure of surface species without complex mathematical analysis, and

(b) these methods provide information regarding the local bonding geometry of surface species, even in the absence of long range order.

(c) PSD provides useful information about the physics of the excitation processes which lead to ion desorption, giving insights into radiation damage at surfaces.

Several reviews of ESDIAD have appeared recently [1-5], and the fundamentals of the method and experimental procedures are described extensively therein. The present paper is a shortened, updated version of References [4] and [5], and the reader is referred to those papers for more details. The physical principles of ESD and PSD are treated comprehensively in a recent volume [3].

The plan of this paper is as follows: Section 2 contains a brief discussion of experimental procedures, and the application of ESDIAD to specific molecular systems is described in Section 3. Examples include a variety of structural assignments based on ESDIAD, and the observation of short-range local ordering effects induced in adsorbed molecules by surface impurities. The emphasis will be on the structure of adsorbed molecules rather than atoms. Section 4 is a brief discussion of a major perturbation on ion trajectories due to the image potential, and the utility of PSD for determining the mechanisms of ion desorption processes is given in Section 5.

2. Experimental Procedures

An extensive discussion of experimental methods of ESD and PSD is given in [3,4] and these will not be considered in detail here. Briefly, two types of detection schemes have been employed for most of the published ESDIAD studies: an area detector with visual display [Fig. 2] and a scanning ion detector, used by Niehus [2].

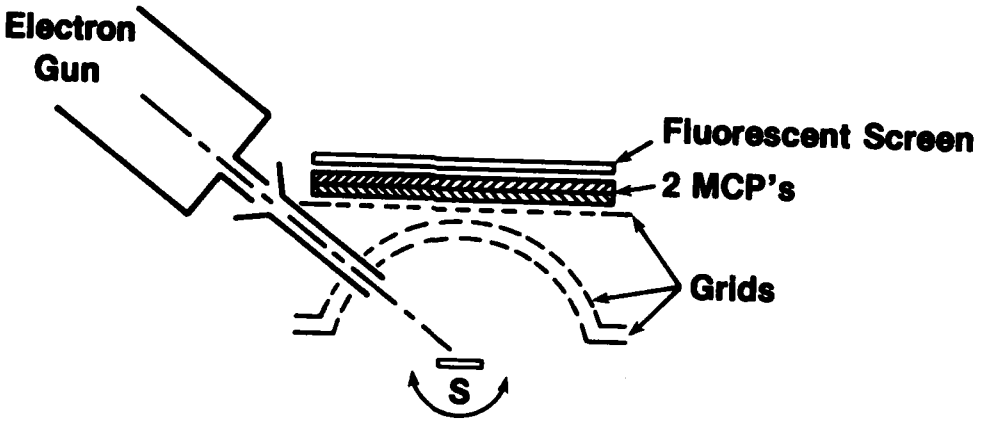

Figure 2. Schematic of NBS ESDIAD apparatus. ESDIAD patterns are displayed using the grid-microchannel plate-fluorescent screen detector array [1,4,5].

In the display-type apparatus originally developed at NBS [1,4,5] and shown in Fig. 2, a focused electron beam bombards a single crystal sample. The ion beams which desorb via ESD pass through a hemispherical grid and impinge on the front surface of a double microchannel plate (MCP) assembly. The output electron signal from the MCP assembly is accelerated to a fluorescent screen where it is displayed visually (the ESDIAD pattern) and photographed. By changing potentials, the elastic low energy electron diffraction (LEED) pattern from the sample can be studied. Mass identification of ESD ions is accomplished using a quadrupole mass spectrometer, which is also used as a detector in thermal desorption studies from the adsorbed layer.

PSD studies are performed using a source of synchrotron radiation which provides a continuously tuneable photon flux in the energy range 20 eV $< h\nu \lesssim$ 100 eV. In PSD of ions, the low signal levels and high background signals from scattered light cause special problems for angle-resolved measurements. An ellipsoidal mirror analyzer, a display-type instrument designed by EASTMAN and colleagues, has been used successfully for angle resolved PSD studies [6,7]; however, most PSD measurements reported to date do not include angle resolved measurements. At the NBS synchrotron light source, SURF-II, a double pass cylindrical mirror analyzer (CMA) is used for mass and energy analysis of PSD ions [8].

3. Experimental Results: ESDIAD

A. Calibration of the ESDIAD Method

Following the first report of ESDIAD patterns for adsorbed species, it was postulated that the direction of ion desorption was determined by the orientation of the surface bond ruptured by the electronic excitation [9]. Theoretical model calculations [10,11] yielded results which were consistent with this postulate, but a general theory of ESD angular distributions applicable to a wide class of surface systems was not (and is not) available. In order to test the postulate, the NBS group adopted an empirical approach, viz., to apply the ESDIAD method to adsorbate-substrate systems whose surface geometries have already been predicted or determined based on other structure-sensitive surface probes.

Table 1 summarizes and lists molecular adsorbates which have been studied in various laboratories using ESDIAD (see [4] for original

references). The table indicates those molecules which have been used to "calibrate" the ESDIAD method, i.e., molecules for which a structural identification has been made using methods such as high resolution electron energy loss spectroscopy (EELS), reflection-absorption infrared spectroscopy (IR), ultraviolet photoemission spectroscopy (UPS) and angle resolved UPS (ARUPS), or low energy electron diffraction (LEED).

In each case listed in Table I, the ESDIAD results are consistent with the other techniques. E.g., for standing-up CO on Ru(001), Ni(111) and W(110), the molecule is bound via the carbon atom to the metal surface with its molecular axis perpendicular to the surface; ESD O^+ (and CO^+) ions desorb in the direction perpendicular to the surface. For the bridge-bonded CO structure identified on Pd(210) using IR, the molecular axis is inclined from the perpendicular to the macroscopic surface, and ESD O^+ emission occurs in the predicted off-normal direction. A "halo" of H^+ ion emission is seen for ESD of NH_3 on Ni(111), consistent with the ARUPS identification of ammonia bonded to Ni via the N atom with the H atoms oriented away from the surface. Similar consistency is found for each of the other cases listed in Table I.

TABLE I. Structural assignments of adsorbed molecules based on ESDIAD measurements: Structures of surface molecules which have been identified using various sensitive methods as well as ESDIAD.

System	Structural Assignments	Other Methods
*CO/Ru(001)	standing-up CO	EELS, IR, ARUPS
CO/Ni(111)	standing-up CO	EELS, ARUPS
virgin-CO/W(110)	standing-up CO	UPS
CO/Pd(210)	inclined CO	IR
NH_3/Ni(111)	bonded via N atom, H atoms oriented away from surface	ARUPS
NO/Ni(111)	standing-up and inclined NO	EELS
H_2O/Ru(001)	coverage and temperature dependent structures	EELS
C_6H_{12}/Ru(001)	"chair" form of C_6H_{12} parallel to surface	EELS
WO_3(111)	inclined W-O	LEED; crystallography

*Also verified using Angle Resolved PSD

TABLE II. Other surface structures identified using ESDIAD.

System	Structures
CO/Ni(111)	standing-up CO and "inclined" CO both observed under different conditions of temperature and coverage.
virgin-CO/stepped W(110)	
α-CO on W(110)	
CO/W(100),(111)	
CO/Mo(001)	
NH_3/Ru(001)	similar to NH_3/Ni(111)
NH_3 and H_2O on oxygen-dosed Ni(111),Al(111)	azimuthal ordering

Table II contains a list of other adsorbed molecules for which structural assignments have been made using ESDIAD. In many cases, the structures were not previously suspected (e.g., inclined CO on Ni(111), Mo(100) or W(100); oxygen-stabilized ordering of NH_3 and H_2O on Ni(111) - see below, Section 3.B) but none are inconsistent with experimental results.

It appears from the evidence in Table I that for all molecular systems where we have a priori knowledge of the surface structure, the ion desorption angle observed in ESDIAD is related to the surface bond angle. In particular, it is found that the expected azimuthal angle of the surface bond is preserved in ESDIAD, but the polar angle is increased for the ion trajectory, due largely to image charge effects [1]. To date, no exceptions have been found.

B. Short-range Local Ordering in Absence of Long-range Order

In a particularly interesting application of the ESDIAD method, it has been found that traces of preadsorbed oxygen on a metal surface will induce a high degree of azimuthal order in adsorbed molecules which are disordered azimuthally on the clean surface [13].

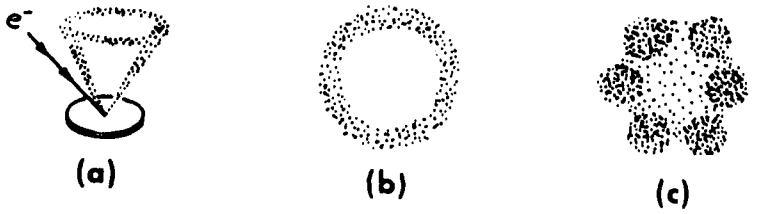

Figure 3: Schematic ESDIAD patterns for NH_3 on Ru(001).

Figure 3 schematically illustrates the ESDIAD patterns for NH_3 on Ni(111) and Ru(001) surfaces, on which NH_3 is bonded via the N atom as follows

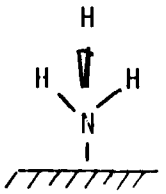

The "halo" ESDIAD pattern (3a,b) is generated by H^+ ions desorbing from an array of adsorbed NH_3 molecules which has random azimuthal orientation of the H ligands on the clean surface. In the presence of a fractional monolayer of O, the H^+ ESDIAD pattern develops discrete beams due to a local azimuthal ordering of NH_3 induced by adsorbed oxygen. Fig 3c is a schematic of the pattern characteristic of NH_3 + O on Ru(001), which is postulated to arise from a hydrogen-bonding interaction between NH_3 and O [13]:

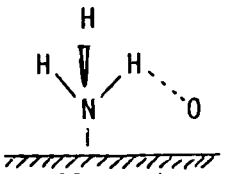

Similar azimuthal ordering effects have been seen for H_2O and NH_3 on various surfaces of Ni, Al, and Ru. More recent studies of NH_3 and H_2O on other substrates show that both electropositive and electronegative additives (e.g. O, Na) can induce locally-ordered molecular rearrangements in the adsorbed molecules [14,15].

In certain cases where H_2O forms ordered hydrogen-bonded overlayers in registry with the substrate [14], the additive can induce disorder in the layer.

Systems in which the additive induces short range order which is either absent or different on the clean surface include:

NH_3 on Ru(001) + O, Na
NH_3 on Ni(111) + O
NH_3 on Al(111) + O
H_2O on Ni(111) + O
H_2O on Ru(001) + Na

Under certain conditions of coverage, long range and short range order in the overlayer are destroyed for

H_2O on Ru(001) + O, Na

It appears that both geometrical and electronic factors are involved in the effect of surface additives on local ordering of adsorbed molecules.

4. Influence of Image Potential on Ion Trajectories

Several authors have discussed the influence of the image potential on ion trajectories [1,16]: the image potential causes an increase in the polar angle for ion desorption. CLINTON's [16] calculations indicate that an ion desorbing with an initial angle α_i with respect to the surface normal will arrive at the detector with an apparent desorption angle α_o given by

$$\cos \alpha_o = \cos \alpha_i \left[\frac{1 + V_I/[(E_K - V_I) \cos^2 \alpha_i]}{1 + V_I/(E_K - V_I)} \right]^{1/2} \qquad (1)$$

In this expression, V_I is the screened image potential at the initial ion-surface separation Z_o, and E_K is the final, measured kinetic energy of the ion. We note that V_I is a negative quantity, so that

$$|V_I/(E_K - V_I)| \leq 1 \text{ and } \alpha_o \geq \alpha_i .$$

In order for equation (1) to have a real physical solution, the following relationship must be satisfied:

$$\left| \frac{V_I}{(E_K - V_I) \cos^2 \alpha_i} - \right| \leq 1 \qquad (2)$$

This means that there will be a cut-off angle for ion desorption defined by the value of α_i for which $\alpha_o = 90°$. For values of α_i greater than the cutoff angle, the ions will follow low trajectories and be recaptured by the surface. The possibility of beam-damage induced by bombardment of surface species by low energy ESD ions is very likely.

As discussed previously [1], it appears that the major final-state perturbation of ion trajectories is in the polar direction. In general, for a perfectly planar surface or for desorption along an azimuth of symmetry, the perturbation of the azimuthal angle

should be minimal.

5. Mechanisms of ESD/PSD Processes

A number of different initial electronic excitations have been identified as contributing to ESD and PSD of ions and neutrals from surfaces, including valence electron excitations, and both shallow and deep core hole excitations. It appears on the basis of evidence to date that ESD and PSD are initiated by the same elementary excitations, and that differences which occur in spectral yield curves (ion yield vs. energy of e^-, $h\nu$) reflect differences in the physics of the excitation process for electrons and photons. The different spectral dependences of ion desorption yields are described in detail by Knotek [17] and depend on a variety of factors (energy dependence of initial excitation cross section, final states accessible, and definition of energy deposition). In general, PSD ion yields rise sharply at threshold to a peak, and fall off at higher energy as $^1/E^n$, where $2 < n < 3$. ESD ion yields rise more slowly at threshold and reach broad peaks at 3-4 times the threshold energy. Hence, the relatively sharp PSD ion yields are generally more useful for isolating and identifying desorption mechanisms than are ESD yields. In the following paragraphs, we will explore ESD/PSD desorption mechanisms for several different classes of surface species: ionically-bonded surface atoms, and covalently-bonded surface molecules.

(a) Ionic systems

Ion desorption from maximal valency, ionically-bonded surfaces is believed to proceed via an Auger decay mechanism proposed by Knotek and Feibelman (K-F) [18]. Maximal valency means that the cation is ionized down to the noble gas configuration (e.g., K^+, Ca^{2+}, Ti^{4+}, etc. in K_2O, CaO, TiO_2, etc.), and that the highest occupied level is its highest core level, of binding energy $\gtrsim$ 20 eV. There is always some degree of covalency, but to a first approximation, the valence electrons have little density at the cation. In the K-F mechanism as applied to TiO_2, for example, ion desorption can be initiated by the production of a vacancy in the highest occupied core level, Ti 3p. The vacancy is filled by an interatomic Auger process involving an electron from the O^{2-}, and the release of two additional Auger electrons from the O^{2-} can leave the oxygen positively charged. The Coulomb potential for O^+ in the presence of Ti^{4+} is replulsive, and the O^+ will desorb from the surface.

An adsorbate system to which the K-F mechanism appears applicable is the adsorption of oxygen on Ti(001), where a variety of evidence indicates that surface TiO_2 is formed [8]. Fig. 4 shows the PSD O^+ ion yield vs. photon energy, and compares it with the secondary electron yield from Ti, which is proportional to the Ti 3p ionization probability [8]. The similarity of the onsets and energy dependences of the O^+ ion yield and Ti 3p core hole excitation leads to the conclusion that ion desorption is initiated by the production of a Ti 3p core hole in accordance with the K-F model. The differences in detail of the two curves of Fig. 4 may indicate additional excitation mechanisms also. Similar evidence for the K-F process in ion desorption have been observed for W(111) [7], as well as a number of ionic solids.

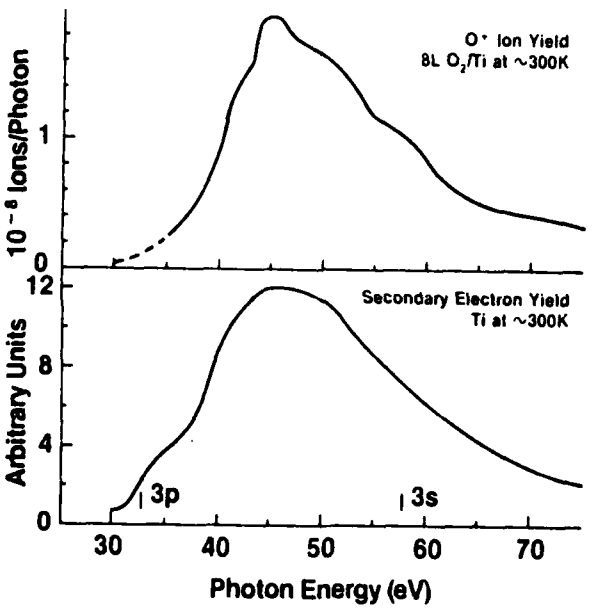

Figure 4: PSD O^+ yield vs. photon energy for oxygen adsorbed on Ti(0001); comparison with secondary electron yield [8].

(b) Covalent systems

The mechanism for ion desorption from covalently-bonded systems are less characterized. The first ESD mechanism, proposed by Menzel, Gomer and Redhead [19,20], suggested a Franck-Condon type transition to a repulsive final state from which desorption or de-excitation (and possible recapture) could occur. The exact nature of the repulsive final states are just now being elucidated by theorists. In a number of cases, the most promising candidates are two-hole states in valence

orbitals, in which the holes remain localized on the surface molecule for a long period of time ($\sim 10^{-14}$ s) that bond rupture can occur and an ion can be ejected [21].

To illustrate PSD of a covalently-bonded adsorbate, CO on Ru(001) was studied [22]. CO is bonded in molecular form to Ru, via the carbon end of the molecule. The PSD O^+ ion yield as a function of photon energy is compared with the probability of Ru core level production in Fig. 5. There is little correlation between the onsets or structure in the two curves, indicating that Ru core levels are not involved in the ion desorption process in this energy range. Ramaker has recently proposed that the peak at 41 eV in Fig. 5 is due to a $5\sigma^{-2}\ 6\sigma^{2}$ excitation, and that the 50 eV peak is due to ionization of the CO 3σ state, which then undergoes heavy mixing with 2h1e (two hole-one electron) states in the adsorbed molecule [21].

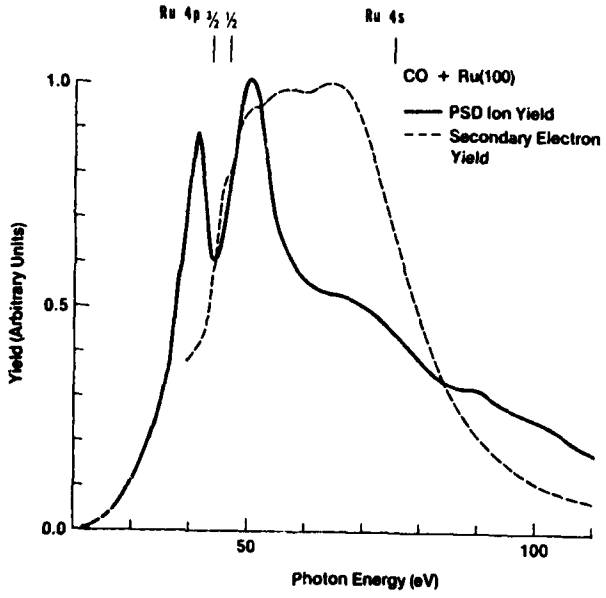

Figure 5: PSD from CO/Ru(0001).

Menzel and colleagues [23] show that excitation of deep core levels (O1s, N1s, C1s) can also lead to desorption of ions from covalently-bonded adsorbates. Adsorbate core hole ionization is quickly followed by Auger decay which ends in multiply valence-ionized adsorbate states. Certain of the "multiple-hole" states will lead to dissociation and desorption of ions.

6. Summary

We summarize the structural information obtainable using ESDIAD and PSD as follows:

1) ESDIAD provides direct evidence for the structures of surfaces molecules and molecular complexes, and in certain cases (e.g., oxides) can provide structural information about the substrate surface.
2) ESDIAD is particularly sensitive to the orientation of hydrogen ligands in adsorbed molecules. In general, electron scattering from surface H is sufficiently weak that LEED is not very useful.
3) ESDIAD is sensitive to the local bonding geometry of molecules on surfaces even in the absence of long-range translational order.
4) The identification using ESDIAD of impurity-stabilized surface structures (H_2O and NH_3 on O-dosed surfaces) is of relevance to surface reaction mechanisms, as well as to catalyst promoters and poisons.
5) Photon Stimulated Desorption, although not yet as extensively applied as ESDIAD in structural studies, has all of the capabilities of ESD. A particular advantage of PSD is the use of tuneable photon sources to excite specific surface bonds selectively.

In the future, we anticipate that ESDIAD will find wide use as a technique to complement and extend other surface-sensitive structural probes, particularly in studies of local structure in the absence of long range order. The correlation of PSD ion angular distributions with specific valence and core hole excitations in surface species should be particularly fruitful, especially for complex systems (mixed oxides, coadsorption systems, catalysis). The combination of angle-resolved PSD with SEXAFS (surface x-ray absorption fine structure) will provide an opportunity to measure both bond orientation and bond length. Finally, the angle resolved desorption of neutrals (including metastables) and negative ions will provide new insights into both structure and mechanisms of excitation.

7. Acknowledgements

The authors acknowledge, with pleasure, the contributions of various colleagues to this work: D. Doering, C. Benndorf, F. P. Netzer, F. Bertel, S. A. Flodstrom, D. Hanson, J. T. Yates, Jr.

This work was supported in part by the Office of Naval Research and the Division of Basic Energy Sciences, U.S. Department of Energy.

8. References

1) T. E. Madey, in E. Taglauer and W. Heiland (ed.) "Inelastic Particle-Surface Collisions", Springer Series in Chemical Physics 17 (Springer-Verlag, Berlin, 1981) p. 80.
2) H. Niehus, Appl. Surface Sci. 13 (1982) 292.
3) N. H. Tolk, M. M. Traum, J. C. Tully and T. E. Madey (eds.) "Desorption Induced by Electronic Transitions", Springer Series in Chemical Physics 24 (Springer-Verlag, Berlin, 1983).
4) T. E. Madey, F. P. Netzer, J. E. Houston, D. M. Hanson and R. Stockbauer, in Ref. 3, p. 120.
5) T. E. Madey, D. L. Doering, E. Bertel and R. Stockbauer, Ultramicroscopy (1983), in press.
6) J. F. van der Veen, F. J. Himpsel, D. E. Eastman and P. Heimann, Solid State Comm. 36, (1980) 99.
7) T. E. Madey, R. Stockbauer, J. F. van der Veen and D. E. Eastman, Phys. Rev. Lett. 45, (1980) 187.
8) D. M. Hanson, R. Stockbauer, and T. E. Madey, Phys. Rev. B24 (1981) 5513.
9) T. E. Madey, J. J. Czyzewski and J. T. Yates, Jr., Surface Sci. 49 (1975) 465.
10) J. I. Gersten, R. Janow and N. Tzoar, Phys. Rev. Lett. 36 (1976) 610.
11) W. L. Clinton, Phys. Rev. Lett. 39 (1977) 965.
12) F. P. Netzer and T. E. Madey, Phys. Rev. Lett. 47 (1981) 928.
13) C. Benndorf and T. E. Madey, Chemical Physics Letters, in press.
14) D. L. Doering and T. E. Madey, Surface Sci. 123 (1982) 305.
15) D. L. Doering, S. Semancik and T. E. Madey, Surface Sci. (1983).
16) W. L. Clinton, Surface Sci. 112 (1981) L791.
17) M. L. Knotek, in Ref. 3, op. cit., p. 139.
18) M. L. Knotek and P. J. Feibelman, Phys. Rev. Lett. 40 (1978) 964; Surface Sci. 90 (1979) 78.
19) D. Menzel and R. Gomer, J. Chem. Phys. 41 (1964) 3311.
20) P. A. Redhead, Can. J. Phys. 42 (1964) 886.
21) D. E. Ramaker, in Ref. 3, op. cit., p. 70.
22) T. E. Madey, R. L. Stockbauer, S. A. Flodstrom, J. F. van der Veen, F. J. Himpsel and D. Eastman, Phys. Rev. B23 (1981) 6847.
23) D. Menzel, J. Vac. Sci. Technol. 20 (1982) 538.

OFFICE OF NAVAL RESEARCH

Contract N00014-84-F0002

TECHNICAL REPORT NO. 40

INSTRUMENTATION FOR PHOTON STIMULATED DESORPTION

Roger Stockbauer
Surface Science Division
National Bureau of Standards
Washington, DC 20234

March 30, 1984

To be published in Nuclear Instruments and Methods

SECURITY CLASSIFICATION OF THIS PAGE *(When Data Entered)*

REPORT DOCUMENTATION PAGE

READ INSTRUCTIONS BEFORE COMPLETING FORM

1. REPORT NUMBER: 40	2. GOVT ACCESSION NO.
3. RECIPIENT'S CATALOG NUMBER	
4. TITLE *(and Subtitle)*: INSTRUMENTATION FOR PHOTON STIMULATED DESORPTION	5. TYPE OF REPORT & PERIOD COVERED: Interim
	6. PERFORMING ORG. REPORT NUMBER
7. AUTHOR(s): Roger Stockbauer	8. CONTRACT OR GRANT NUMBER(s): N00014-84-F0002
9. PERFORMING ORGANIZATION NAME AND ADDRESS: Surface Science Division, National Bureau of Standards, Washington, DC 20234	10. PROGRAM ELEMENT, PROJECT, TASK AREA & WORK UNIT NUMBERS
11. CONTROLLING OFFICE NAME AND ADDRESS: Office of Naval Research, Physical Science Program Office, Arlington, VA 22217	12. REPORT DATE: March 30, 1984
	13. NUMBER OF PAGES
14. MONITORING AGENCY NAME & ADDRESS*(if different from Controlling Office)*	15. SECURITY CLASS. *(of this report)*: Unclassified
	15a. DECLASSIFICATION/DOWNGRADING SCHEDULE

16. DISTRIBUTION STATEMENT *(of this Report)*

Approved for Public Release; Distribution Unlimited

17. DISTRIBUTION STATEMENT *(of the abstract entered in Block 20, if different from Report)*

18. SUPPLEMENTARY NOTES

To be published in Nuclear Instruments and Methods.

19. KEY WORDS *(Continue on reverse side if necessary and identify by block number)*

Desorption; electrostatic analyzer; photon stimulated desorption; synchrotron radiation; time-of-flight mass spectrometry.

20. ABSTRACT *(Continue on reverse side if necessary and identify by block number)*

Photon stimulated desorption (PSD) refers to the ejection of ions, atoms or molecular fragments from a surface initiated by the absorption of single photons; to date, most studies have concentrated on detection of ions. The properties of PSD which make it attractive as a surface characterization tool are its extreme surface sensitivity, the ions being ejected only from the topmost layer, and the rapidity with which the ions are ejected. Since the desorption is fast (~10^{-14} s), with respect to

(continued)

DD FORM 1 JAN 73 1473 EDITION OF 1 NOV 65 IS OBSOLETE

S/N 0102-LF-014-6601

SECURITY CLASSIFICATION OF THIS PAGE *(When Data Entered)*

Block 20. Abstract (Continued)

molecular vibrations ($\sim 10^{-12}$ s), the ion trajectory reflects the initial bonding geometry of the particle to the surface.

To study the ion desorption process, one would like to measure the mass, kinetic energy distribution, angular distribution and the yield (desorption rate vs. photon energy) of the desorbing ions. Time-of-flight analyzers measure only ion mass and yield while most electrostatic deflection analyzers measure kinetic energy and yield. The ellipsoidal mirror analyzer is unique in that it measures all four quantities simultaneously.

INSTRUMENTATION FOR PHOTON STIMULATED DESORPTION

Roger Stockbauer
Surface Science Division
National Bureau of Standards
Washington, DC 20234

Abstract

Photon stimulated desorption (PSD) refers to the ejection of ions, atoms or molecular fragments from a surface initiated by the absorption of single photons; to date, most studies have concentrated on detection of ions. The properties of PSD which make it attractive as a surface characterization tool are its extreme surface sensitivity, the ions being ejected only from the topmost layer, and the rapidity with which the ions are ejected. Since the desorption is fast ($\sim 10^{-14}$ s), with respect to molecular vibrations ($\sim 10^{-12}$ s), the ion trajectory reflects the initial bonding geometry of the particle to the surface.

To study the ion desorption process, one would like to measure the mass, kinetic energy distribution, angular distribution and the yield (desorption rate vs. photon energy) of the desorbing ions. Time-of-flight analyzers measure only ion mass and yield while most electrostatic deflection analyzers measure kinetic energy and yield. The ellipsoidal mirror analyzer is unique in that it measures all four quantities simultaneously.

I. Introduction

Photon Stimulated Desorption (PSD) is a relatively new field, the first results being published in 1979.[1] It has two characteristics which make it extremely attractive as a surface characterization tool. The first is that ions are desorbed only from the surface making it extremely surface sensitive. The second is that the desorption is very fast ($\sim 10^{-14}$ sec) with respect to molecular vibration times ($\sim 10^{-12}$ sec) so that the ions desorb in the direction of the surface bonds. Hence, angular distribution of the desorbed ions is related to the bonding geometry of the surface species.[2,3]

In general, PSD of ions is initiated by a fast, photon-induced electronic excitation of a surface species to a repulsive final state. If the final state lifetime is on the order of 10^{-14} to 10^{-15} s, electronic energy is converted into nuclear motion and the ion moves away from the surface. The probability that an ion will survive to reach the detector is related to the rate of neutralization by electron hopping from the substrate. Two of the specific mechanisms used to describe the physics of the excitation and desorption process are particularly applicable to PSD of ionic and of covalent surface species. Knotek and Fiebelman[4] proposed an interatomic Auger decay mechanism for maximal valency ionic compounds. In this model, desorption is initiated by the formation of a core hole in the metal atom. This hole would normally be filled in an Auger process involving the metal atom's valence electrons. However, since these are depleted in a maximal valency compound, this process has a low probability. Instead, a valence electron from the ligand fills the metal core hole in an interatomic Auger process with the subsequent release of one or two more valence electrons. The originally

AD-A141 319 ELECTRON EMISSION AND ION DESORPTION SPECTROSCOPY OF CLEAN AND OXIDIZED T..(U) NATIONAL BUREAU OF STANDARDS WASHINGTON DC SURFACE SCIENCE DI.. E BERTEL ET AL. 2/2

UNCLASSIFIED 30 MAR 84 TR-35 N00014-94-F-0002 F/G 7/2 NL

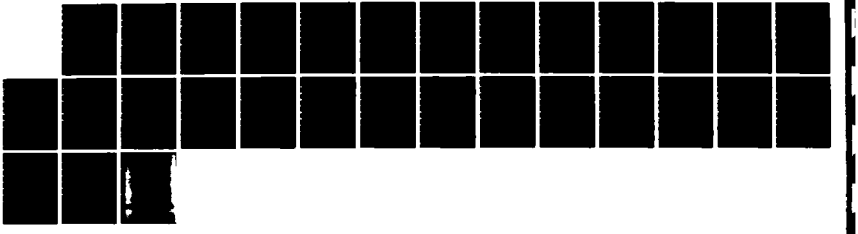

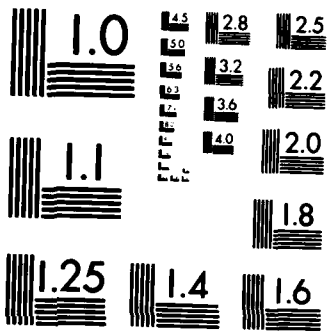

negatively-charged ligand atom is now positively charged, and is repelled from the surface by the reverse Madelung potential. The theory predicts that the ion desorption should be proportional to the core hole production and should occur no matter how the core hole is produced, i.e. whether by electron, photon or ion impact.

Verification of the theory usually involves comparing the ion yield curve with the probability of producing a core hole. The latter is given, for example, by the secondary electron yield as a function of photon energy. The similarity of the two curves is taken as an indication of the applicability of the Knotek-Feibelman theory.

A second mechanism for PSD involves two hole excited states and applies to covalent adsorbates. Here the desorption is thought to occur from states involving two hole (2h) or two hole, one electron (2h1e) excitations[5] which have a long lifetime with respect to ion desorption ($>10^{-13}$ secs).

2. PSD Analyzers

In general, PSD involves the measurement of ion mass, ion yield (ion desorption rate vs. photon energy), ion kinetic energy distribution, and ion angular distribution. The ideal analyzer would measure all of these simultaneously or at least be able to measure them sequentially. Although analyzers possessing all these capabilities exist, none is dedicated currently to PSD.

One property of the ion kinetic energy distributions can be used to great advantage. It has been generally observed that ions of different mass desorbed from the same system have different kinetic energy distributions. This allows one to distinguish the desorbing species with either mass or

energy analysis. With most instrumentation currently in use, it is difficult to measure both simultaneously. The type of ion analyzer used for PSD depends primarily on the time structure of the synchrotron light source. For large storage rings where the time between the puses of light is relatively long, a drift tube, time-of-flight (TOF) analyzer can be used. Synchrotron light sources with relatively small diameters do not have time structures which allow ion TOF measurements. For instance, SURF II at the National Bureau of Standards has one light pulse every ~9 nsec. Quadrupole or electrostatic deflection analyzers, however, are used successfully on these synchrotron sources.

Time of flight

The first PSD measurements using a drift tube, time-of-flight analyzer, were made by Knotek, Jones and Rehn.[1] Their experimental configuration consisted of a spiraltron situated about 5 cm from a surface on which impinged the synchrotron radiation. A later version of this type of analyzer is shown in Fig. 1.[6] The refinements include an electrostatic shield (1), a meshed entrance aperture (2), and a microchannel plate (MCP) array. Ions are emitted from the sample in discrete pulses due to the pulsed nature of the synchrotron light. A relatively high field between the sample and grid accelerates the ions to a fixed energy. They enter the drift tube and arrive at the MCP separated in time according to their mass to charge ratio.

The peak intensities in the TOF mass spectra are measured as a function of photon energy to obtain the ion yield curves. The signal observed at the MCP is illustrated in the upper part of Fig. 2 using the time structure of the

light from SPEAR operating in the single bunch mode.[1] Synchrotron light scattering from the sample, strikes the MCP giving rise to a train of pulses which reflects the time structure of the synchrotron. These serve as start pulses for the timing circuit. The H^+ ions arrive at the MCP 300 nsec after the light pulse, while the OH^+ ions arrive 1250 nsec after the light pulse. Since the OH^+ flight time is longer than the 780 nsec between pulses, it is observed after the second light pulse and the second H^+ signal. For large numbers of mass peaks, the overlapping spectra become difficult to disentangle. The problem is exaggerated if the synchrotron is run in multibunch mode rather than single bunch mode. This is done to increase the stored current, i.e. light output, and the resulting signal is shown in the lower part of Fig. 2. In order to disentangle the new multiply-overlapped spectra, one bunch is left out of the synchrotron pulse train to act as a marker. The missing mass peaks can now be associated with the missing light pulse and proper identification can be made.

The ions normally undergo 3-5 keV of acceleration in the TOF. This high acceleration has the advantage of compressing the TOF spectra in time, reducing the overlap problem discussed above. It also increases the mass resolution of the experiment. The resolution is limited by the width of the mass peaks which is due primarily to the kinetic energy distribution when they are formed at the surface. This spread in initial energy shows up as a spread in velocity resulting in a spread in flight time. The higher accelerating voltages reduces this spread, increasing the resolution.

This same effect has the disadvantage of not permitting use of the TOF peak width to measure this initial ion kinetic energy distribution. The high

fields reduce the widths to such an extent that residual timing jitter in the electronics can contribute significantly to the peak widths. In practice, however, it should still be able to extract some kinetic energy distribution information from the TOF peak shapes though this has not yet been attempted.

The high potentials used in these analyzers also effectively thwart any attempt to measure the angular distribution of the desorbing ions. The high potentials compress the ion beam into a relatively small area which is difficult to resolve with the MCP. In addition, the scattered light pulse which can be 2-4 orders of magnitude more intense than the ion pulse precludes the use of an area detector due to the relatively long time required for the spatial conversion (~3μ sec). A gating circuit could be used to block out the light pulse but as yet such electronics are not available as standard equipment. The use of a fluorescent screen to view the angular distributions directly would have to rely on pulsing the MCP or screen off during the light pulse.

The main advantages of the TOF analyzer are its relatively cheapness, simple construction, and operation. It easily measures ion mass and ion yields but to date has not been used for ion kinetic energy or angular distributions.

RF-Quadrupole

Perhaps the simplest means of detecting ions desorbed from a surface is to place the sample near the entrance slit of a mass spectrometer. Menzel et al.[7] have used a RF quadrupole mass analyzer located directly in front of a sample to detect PSD ions. The quadrupole selects ions of a particular mass as the photon energy is scanned producing an ion yield curve. The sample could be rotated in front of the quadrupole to obtain an angular distribution.

The system is relatively simple and inexpensive. However, it measures only one mass at a time requiring repeated photon energy scans if more than one species is desorbed from the surface. Kinetic energy distributions are also time consuming.

Electrostatic Deflection

Any electrostatic analyzer, including commercial double pass cylindrical mirror (CMA) and ellipsodial mirror analyzers normally used for photoemission studies, can be used to detect ions by simply reversing the sign of deflecting potentials and setting the electron multiplier potential to the proper voltage to detect ions.

The double pass CMA was first used successfully by Woodruff et al. at the Tantalus storage ring. This instrument was manufactured by Physical Electronics Division of Perkin-Elmer Corporation.[9] A cross sectional view and the associated electronics of an identical system currently in use at NBS[10] are shown in Fig. 3. The ions are emitted from the surface of a crystal placed at the focus of the first stage of the analyzer. The ion traverse the first stage, come to focus at the midpoint of the analyzer, traverse the second stage and arrive at the detector.

There are few internal grids in the CMA to allow gating so that ion time-of-flight mass analysis under photon impact is usually not possible. Instead, the kinetic energy analysis performed by the analyzer is used to separate the different species desorbing from the surface. As mentioned above, it has been observed that different ionic species desorbing from the same surface have different ion kinetic energy (IKE) distributions. Mass identification can be made under electron impact as shown in Fig. 3 by simply pulsing an electron

beam onto the surface for a short period and measuring the ion flight time. The ion mass is determined for each of the different peaks in the IKE distribution. It is assumed that if the IKE structure observed under photon impact is the same as under electron impact then the desorbing species will be the same.

The ion analysis is usually performed with a positive bias on the crystal. This is necessary to remove a background signal due to scattering of light from the crystal, which strikes the grid or analyzer surfaces and causes ions to desorb from these surfaces. The positive bias makes these ions appear at negative kinetic energy so that they can be distinguished from the ions desorbing from the surface. The bias has the additional effect of compressing the width of the angular distribution patterns which increases the count rate, and of shortening the ion transit time between the crystal and first grid which increases mass resolution.

Typical operating conditions for the TOF analysis through the CMA are a +20V crystal bias, 50V CMA pass energy and 500-1000 V negative potential on the front of the electron multiplier for ion conversion. The electron beam is pulsed on the sample for ~1μsec using one of the deflector plates or the extractor plate in the electron gun. Ion flight times are ~5μsec for H^+ and ~18 μsec for O^+ and typical mass resolution is 8 amu.

To summarize, the double pass CMA measures PSD ion yields and ion kinetic energy distributions. Mass analysis can be performed under electron impact. Some indications of angular distributions of the desorbed ion can be obtained by rotating the sample in front of the CMA. This is not exact since the CMA accepts a cone of emmitted ions centered on its axis. Hence, if the surface

of the sample is not perpendicular to the CMA axis, a distribution of angles will be accepted. The main advantages of the CMA are that it is commercially available and has a very good signal to noise ratio.

An electrostatic analyzer that overcomes the disadvantages of the TOF and CMA analyzers is the ellipsodial mirror analyzer described by Eastman, Donelon, Hien and Himpsel.[11] This is an electrostatic differential energy analyzer which preserves the charged particle trajectories and hence is able to measure the angular distributions. It is normally used for electron analysis but again, by reversing the potentials, is well suited for ion analysis.[12] The analyzer, illustrated in Fig. 4, consists of two series of grids and an ellipsoidal mirror. The sample is placed at one focus of the ellipse. The desorbed ions are accelerated between grids G_1 and G_2, traverse the field free region between grids G_2 and G_3, and encounter the ellipsodial mirror which acts as a low pass filter. Only those ions below a certain energy are reflected by the mirror and focused at the second focal point of the ellipse. Beyond this aperture the ions enter a retarding energy analyzer consisting of the grids G_4-G_6 which acts as a high pass filter. The ions continue on their trajectories and strike a MCP array and position-sensitive detector where they are converted to an electronic signal. The combination of low and high pass filters acts as a differential energy analyzer while the ion angular distributions are preserved.

Pulses can be applied to grids G_1 and G_5 to gate the ions allowing TOF mass analysis. In this mode, the two grids are biased so that no ions traverse the analyzer. Short pulses of the proper height are applied

sequentially to the grids allowing ions of a selected energy and mass to pass.

The ellipsodial mirror display analyzer is well suited for PSD studies. It can measure ion yield, kinetic energy, angular distributions, and ion mass simultaneously. Its primary disadvantage is its complexity and expensive construction.

An electrostatic analyzer being used by Menzel[13] also combines most of these features. It is a mirror analyzer consisting of concentric toroidal surfaces which deflect the ions much like a spherical mirror analyzer. This is followed by a truncated cone lens system. A schematic of the particle trajectories is shown in Fig. 5. The analyzer accepts ions emitted over a broad range of polar angles simultaneously but only over a narrow slice of azimuthal angles. The cross sectional view in Fig. 6 shows the focusing property of the toroidal surfaces (T_1,T_2) for ions emitted from the sample (S). The resulting ring image at K" is refocused by the conical lens to a smaller ring image (K) on an area detector. The analyzer is axially symmetric so that the polar angle of the ion is preserved.

As with the ellipsodial mirror analyzer, ion yield, kinetic energy and angular distributions can be measured, but not simultaneously. The sample or analyzer must be rotated to obtain the azimuthal distributions. As with the cylindrical mirror analyzer, the lack of internal grids prevents TOF mass determinations under photon impact. Its primary disadvantage is the difficult machining of the toroidal surfaces.

Optical Methods for Neutral Desorption

Due to relatively low absolute number of particles which desorb in PSD, most experiments to date have relied on ion desorption measurements because of the inherent high detection efficiency for ions. However, in one experiment the PSD of excited alkali atoms has been measured.[14] The method is based on detection of the optical resonance radiation from excited Na and Li atoms. A lens is used to focus the radiation from the atoms when they are 1-2 millimeters in front of the surface onto the entrance slit of an optical spectrometer placed at right angles to the sample. The spectrometer monitors the intensity of the resonance radiation as the incident photon energy is scanned.

The method has a very limited application, i.e. only to those systems for which product species desorb in excited states in sufficient number, and fluoresce within several millimeters of the surface. The identification of the desorbing species can usually be made unambiguously from the wavelength of the fluorescence. The kinetic energy of the particle can, in principle, be obtained either from the Doppler shift of the fluorescence or if the fluorescence lifetime is known, from an intensity vs. distance from surface measurement.

Laser detection methods could also be supplied to detect ground or excited state neutral species desorbed in PSD. Laser excited fluorescence which has been successfully applied to the detection of neutrals from thermal desorption[15] or multiphoton ionization could conceivably be used.

3. TOF Electronics

Timing Circuits

The measurement of the ion TOF in the analyzers discussed above can be done with several combinations of electronic components as illustrated in Fig. 7. All involve measuring the time between the desorption of the ion from the surface and its arrival at the detector. Signals are needed then to turn on (start) the timing circuits when the ion is desorbed and off (stop) when the ion is detected. The most simple timing method is a delay and gate generator. This device produces a gate pulse, at a present time (delay time) after receiving a start pulse. It is inserted between the detector and counter and allows the ion (stop) pulses to be counted only while the gate is on. To record a TOF spectra, the ion count rate is measured as a function of delay time. The yield for a particular mass ion is recorded by setting the delay to the flight time for that mass and scanning the photon energy. The method is simple and inexpensive but not efficient since only one mass can be measured at a time.

A more sophisticated method is to use a time to amplitude converter (TAC) and a pulse height analyzer (PHA). The TAC produces an output signal whose amplitude is proportional to the time between start and stop pulses. The PHA sorts pulses according to their height and displays the number of pulses (y axis) vs. pulse height (x axis) which is the flight time of the ions. The PHA display is then the TOF mass spectrum. The advantage of this system is that the TAC-PHA combination analyzes the flight time of each ion detected. Hence, the TUF of all ion species is detected simultaneously unlike the delay and gate system where only one species at a time is detected. The disadvangates

are its relatively high cost and the fact that only one ion (the first) can be analyzed per start pulse.

A similar method employing digital techniques replaces the TPHC-PHA combination with a time digitizer. This device measures the time between start and stop pulses directly and outputs it as a digital number. This is read by a computer which stores and displays the TOF spectra. Time digitizers are available as stand alone units or as CAMAC plug-ins which facilitates the computer interfacing and programming. Most of these units provide for timing several events simultaneously from one start pulse so that more than one ion can be analyzed per pulse. They are relatively inexpensive if there is a computer available and their digital output makes them ideal for computer controlled data gathering and analysis systems.

Data Analysis

There are several aspects of PSD data analysis that present unique problems. They arise first from the fact that the PSD ion desorption rate is, in general, a relatively weak process compared to photoemission. For instance, where photoemission count rates may be on the order of 10^3/sec, the ion count rate may be 10/sec. Hence, dark current and scattered light backgrounds must be subtracted from the data. Also, in order to obtain an ion yield spectra, the relative intensity of the light must be known as a function of wavelength to properly normalize the PSD data.

By far, the most serious problem arises from the fact that the ion kinetic energy distributions, in general, are independent of photon energy. Hence, ions desorbed by second order radiation from the photon monochromator

will be indistinguishable from those desorbed by the first order radiation. This problem is particularly severe when using synchrotron radiation sources since, under certain conditions, the second order radiation can be as intense as the first order radiation from the monochromator. This problem is virtually nonexistent in photoelectron emission measurements since the kinetic energy of the photoelectrons from most spectral features is proportional to the photon energy. Hence, the photoelectron spectra from the first and second order radiation are at different kinetic energies and are therefore easily separable.

The problem from overlapping PSD spectra from different orders is particularly vexing when one tries to determine PSD onsets. A threshold measurement involves determining the rise of the signal from the background. The uncertainty in the background in PSD and hence in the threshold can be considerable if the intensity of the second order light in this region is large.

The procedures used to correct the PSD ion data for monochromator transmission and second order light are given in detail elsewhere.[16]

Acknowledgments

The author acknowledges valuable discussions with T.E. Madey. This work was supported in part by the Office of Naval Research.

References

1. M.L. Knotek, V.O. Jones, and V. Rehn, Phys. Rev. Lett. 43, 300 (1979).

2. T.E. Madey and J.T. Yates, Jr., Surface Sci. 63, 203 (1977).

3. T.E. Madey, R. Stockbauer, F. van der Veen, and D.E. Eastman, Phys. Rev. Lett. 45, 187 (1980).

4. M.L. Knotek and P.J. Feibelman, Phys. Rev. Lett. 40, 964 (1978).

5. D.E. Ramaker in Desorption Induced by Electronic Transitions, eds. N.H. Tolk, M.M. Traum, J.C. Tully and T.E. Madey, Springer Series in Chemical Physics 24 (Springer-Verlag, Berlin, 1983) p. 70.

6. R. Jaeger, J. Stöhr, J. Feldhaus, S. Brennan and D. Menzel, Phys. Rev. B 23 2102 (1981).

7. D. Menzel, private communication.

8. D.P. Woodruff, M.M. Traum, H.H. Farrell, N.V. Smith, P.D. Johnson, D.A. King, R.L. Benbow and Z. Hurych, Phys. Rev. B 21 5642 (1980).

9. In order to describe this instrument adequately, it is necessary to identify it by manufacturer's name. In no instance does such identification imply endorsement by the National Bureau of Standards nor does it imply that the particular instrument is necessarily the best available for this applications.

10. D.M. Hanson, R. Stockbauer and T.E. Madey, Phys. Rev. B 24, 5513 (1981).

11. D.E. Eastman, J.J. Donelon, N.C. Hien and F.J. Himpsel, J. Nucl. Inst. Methods 172, 327 (1980).

12. J.F. van der Veen, F.J. Himpsel, D.E. Eastman and P.J. Heimann, Solid State Comm. 36, 99 (1980).

13. H.A. Engelhardt, W. Bäck, D. Menzel and H. Liebl, Rev. Sci. Instrum. 52, 835 (1981); H.A. Engelhardt, A. Zartner, and D. Menzel, Rev. Sci. Instrum. 52, 1161 (1981).

14. N.H. Tolk, M.M. Traum, J.S. Kraus, T.R. Pian, W.E. Collins, N.G. Stoffel, and G. Margaritondo, Phys. Rev. Lett. 49, 812 (1982).

15. R.R. Cavanagh and D.S. King, Phys. Rev. lett. 47, 1829 (1981).

16. T.E. Madey and R. Stockbauer in Experimental Physics - Surfaces, (R.L. Park and M.G. Lagally, eds.) Academic Press, New York (in press).

Figure Captions

Fig. 1. Geometry of time-of-flight set-up from Ref. 6. 1: shield cylinder; 2: grid; 3: microchannel plate assembly.

Fig. 2. Upper: Temporal relationship of photon and ion pulses detected (Ref. 1) for a synchrotron light source operating in single bunch mode. Lower: Same but for six bunch mode with one bunch missing.

Fig. 3. Schematic of a CMA used for simultaneous mass (by time-of-flight) and energy analysis of ions from electron stimulated desorption.

Fig. 4. Schematic of ellipsodial mirror display analyzer (Ref. 11).

Fig. 5. Trajectories of ions in a toroidal mirror analyzer and truncated cone lens (Ref. 13).

Fig. 6. Cross sectional view of the toroidal mirror analyzer and lens (Ref. 13).

Fig. 7. Timing circuit for ion time-of-flight measurements.

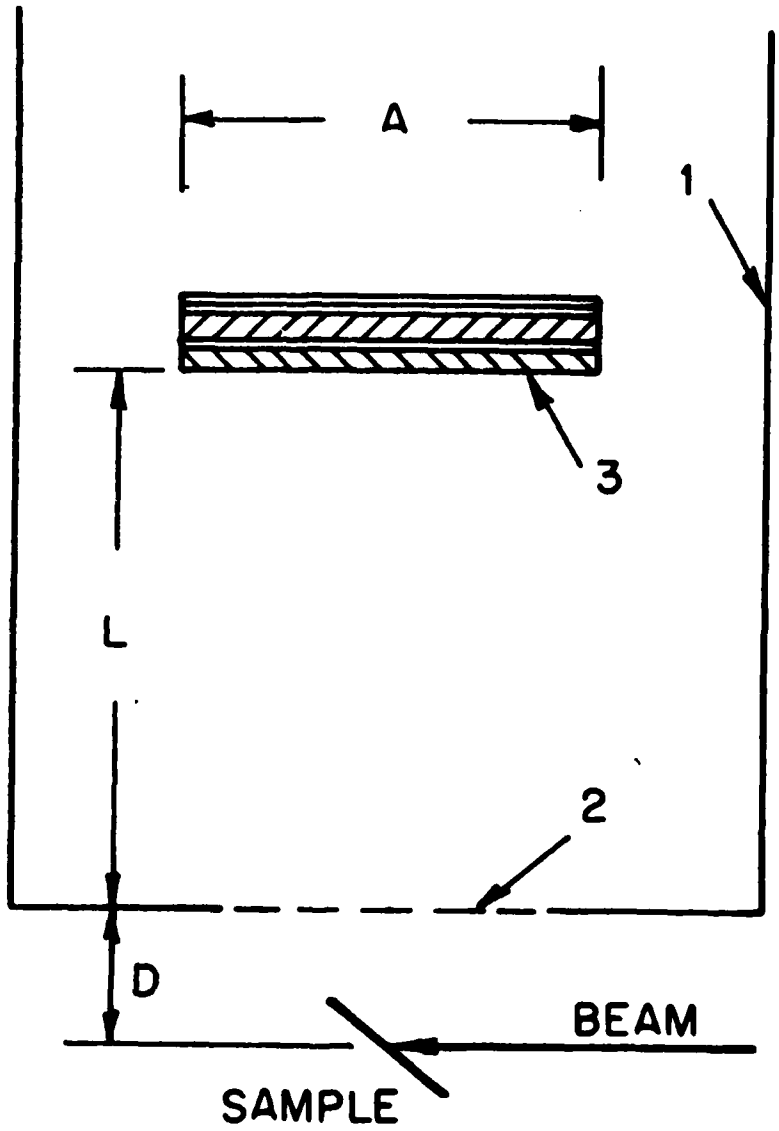

Fig 1

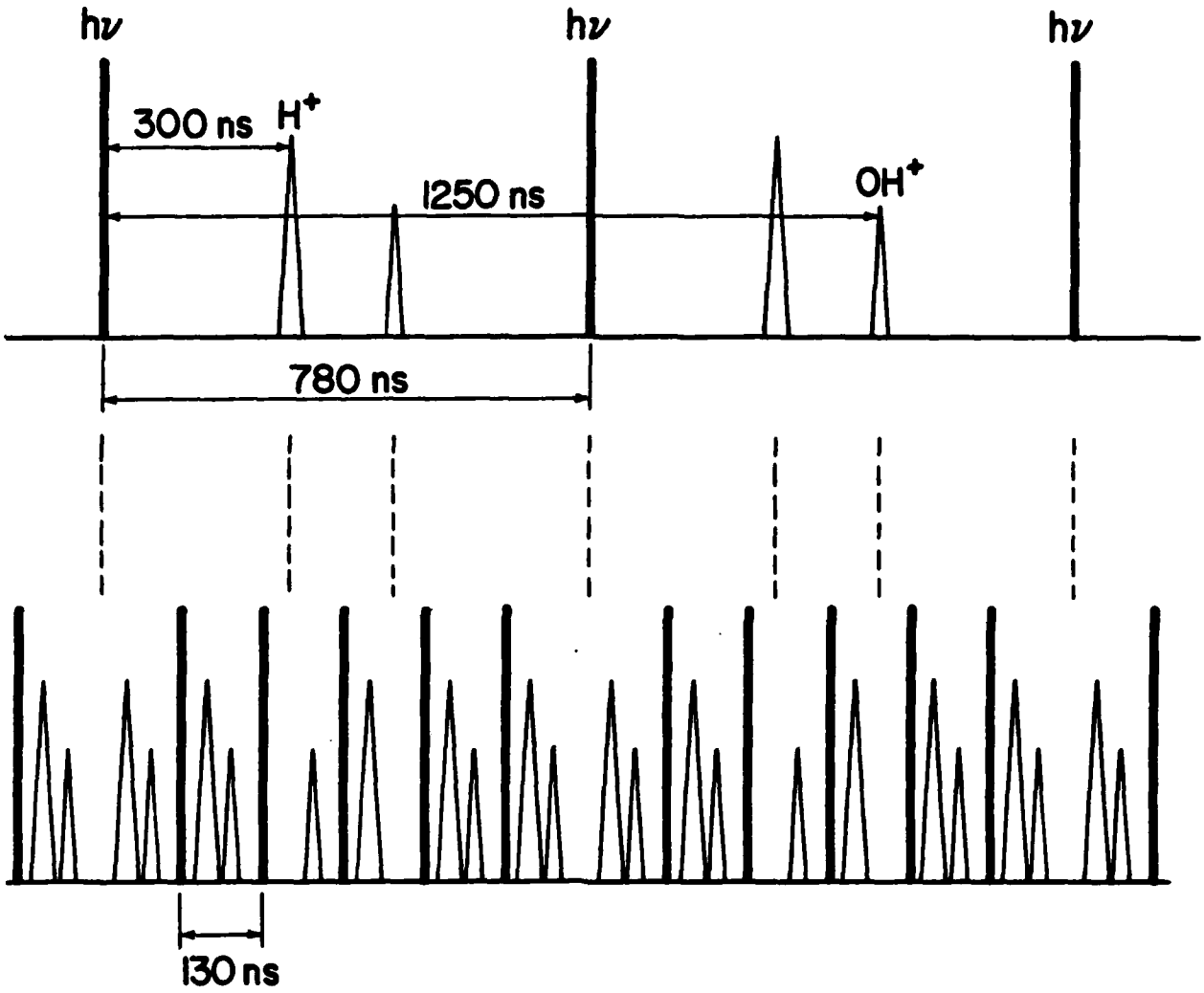

Fig. 2

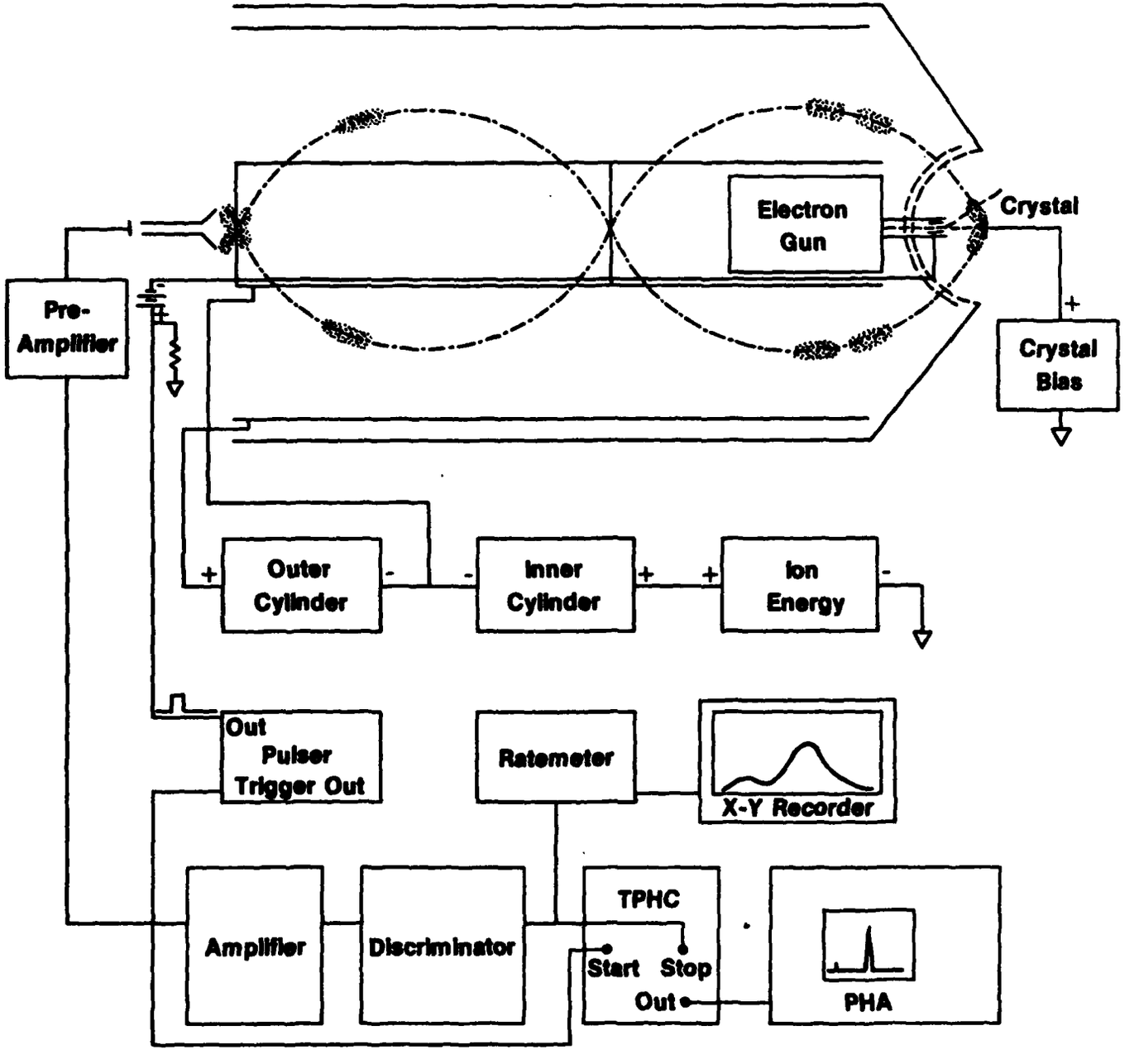
Electron Gun
Crystal
Pre-Amplifier
Crystal Bias
+
Outer Cylinder
-
-
Inner Cylinder
+
+
Ion Energy
-
Out Pulser Trigger Out
Ratemeter
X-Y Recorder
Amplifier
Discriminator
TPHC
Start
Stop
Out
PHA

Fig. 3

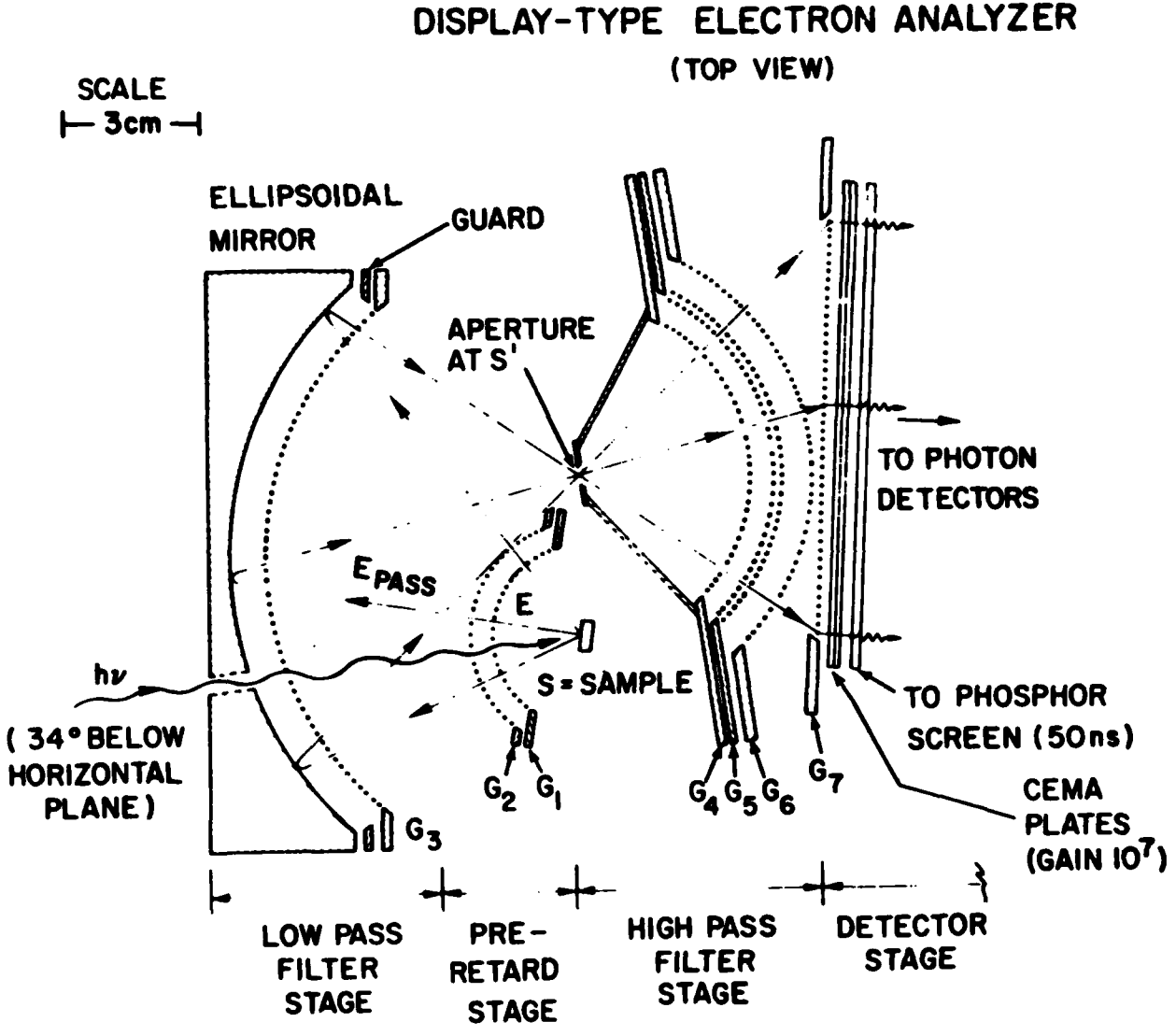
DISPLAY-TYPE ELECTRON ANALYZER
(TOP VIEW)
SCALE
⊢ 3cm ⊣
ELLIPSOIDAL MIRROR
GUARD
APERTURE AT S'
TO PHOTON DETECTORS
E PASS
E
hν
(34° BELOW HORIZONTAL PLANE)
S = SAMPLE
TO PHOSPHOR SCREEN (50ns)
CEMA PLATES (GAIN 10^7)
G_1
G_2
G_3
G_4
G_5
G_6
G_7
LOW PASS FILTER STAGE
PRE-RETARD STAGE
HIGH PASS FILTER STAGE
DETECTOR STAGE

Fig. 4

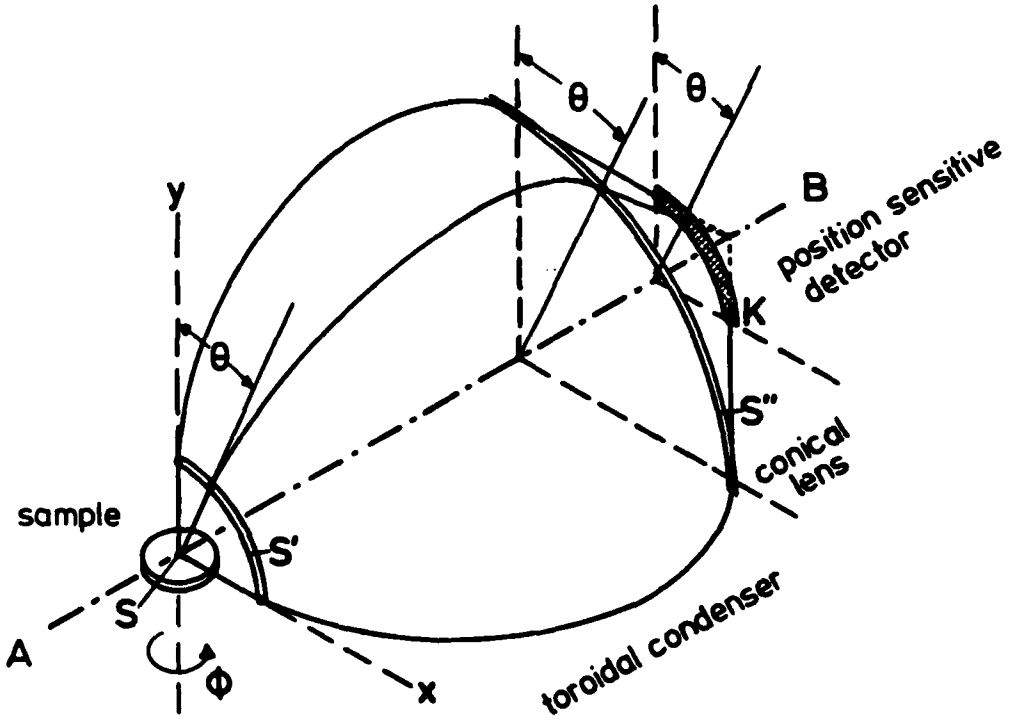
θ
θ
θ
y
B
position sensitive
detector
K
S"
conical
lens
sample
S'
S
A
Φ
x
toroidal condenser

Fig. 5

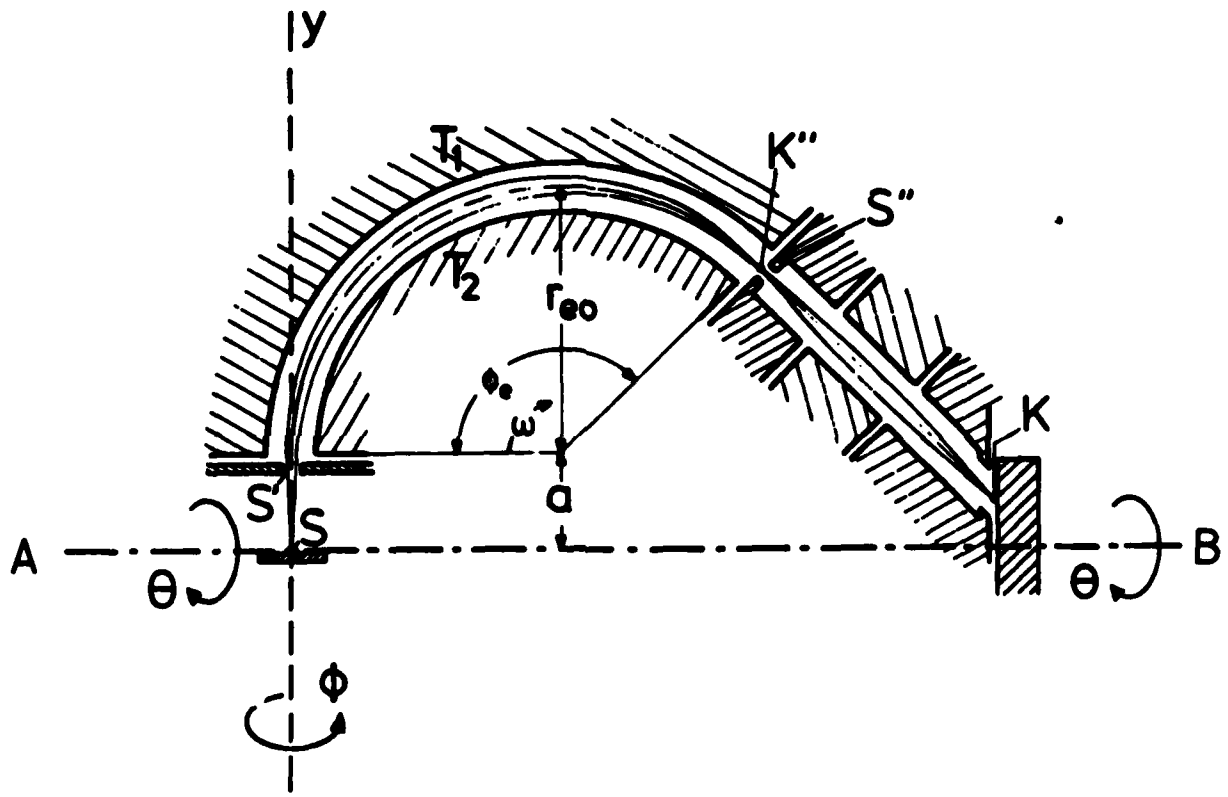

Fig. 6

Timing Circuits

Delay and Gate

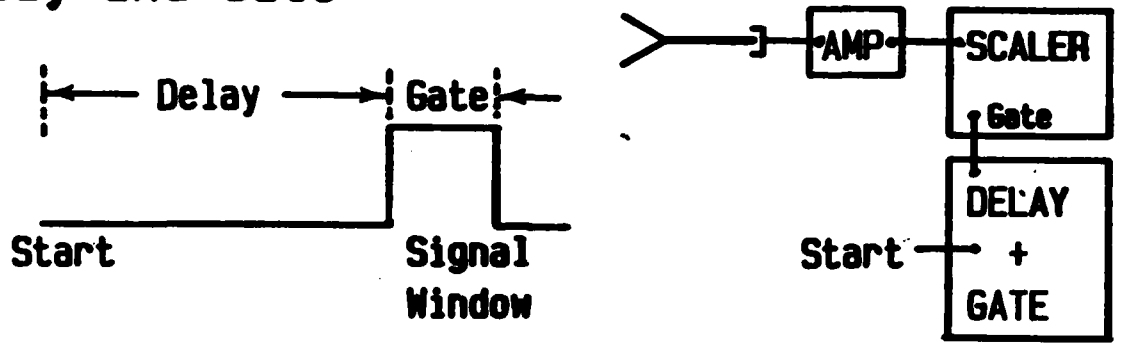

TAC-PHA

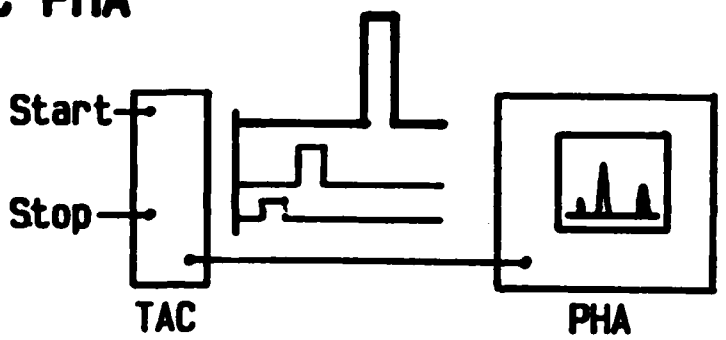

Time Digitizer

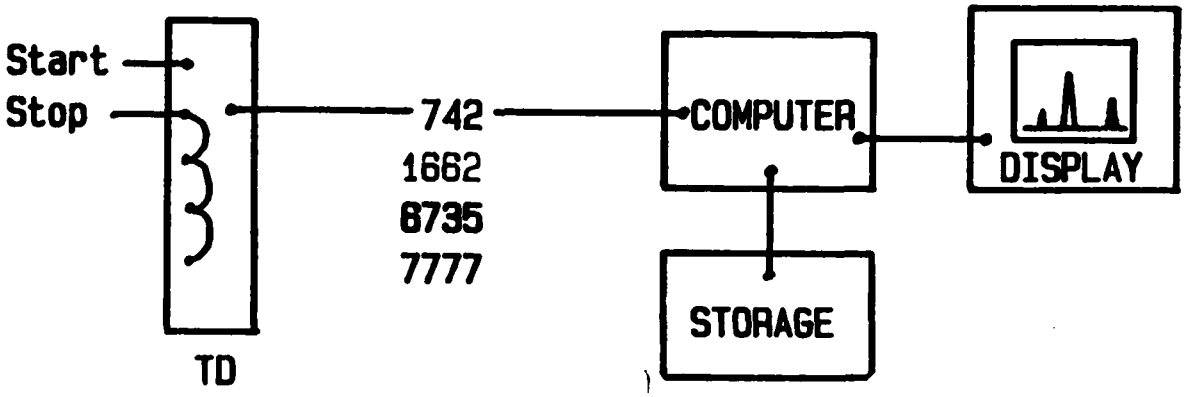

Fig. 7

OFFICE OF NAVAL RESEARCH

Contract N00014-84-F0002

TECHNICAL REPORT NO. 41

Mechanism for Photon Stimulated Desorption of O^+ from Cr(110)

R. Stockbauer, D. E. Ramaker, E. Bertel,
R. L. Kurtz and T. E. Madey
Surface Science Division
National Bureau of Standards
Washington, DC 20234

March 30, 1984

To be published in the Journal of Vacuum Science and Technology

SECURITY CLASSIFICATION OF THIS PAGE (When Data Entered)

REPORT DOCUMENTATION PAGE		READ INSTRUCTIONS BEFORE COMPLETING FORM
1. REPORT NUMBER 41	2. GOVT ACCESSION NO.	3. RECIPIENT'S CATALOG NUMBER
4. TITLE (and Subtitle) Mechanisms for Photon Stimulated Desorption of O^+ from Cr(110)		5. TYPE OF REPORT & PERIOD COVERED Interim
		6. PERFORMING ORG. REPORT NUMBER
7. AUTHOR(s) R. Stockbauer, D. E. Ramaker, E. Bertel, R. L. Kurtz and T. E. Madey		8. CONTRACT OR GRANT NUMBER(s) N00014-84-F0002
9. PERFORMING ORGANIZATION NAME AND ADDRESS Surface Science Division National Bureau of Standards Washington, DC 20234		10. PROGRAM ELEMENT, PROJECT, TASK AREA & WORK UNIT NUMBERS
11. CONTROLLING OFFICE NAME AND ADDRESS Office of Naval Research Physical Science Program Office Arlington, VA 22217		12. REPORT DATE March 30, 1984
		13. NUMBER OF PAGES
14. MONITORING AGENCY NAME & ADDRESS(if different from Controlling Office)		15. SECURITY CLASS. (of this report) Unclassified
		15a. DECLASSIFICATION/DOWNGRADING SCHEDULE

16. DISTRIBUTION STATEMENT (of this Report)

Approved for Public Release; Distribution Unlimited

17. DISTRIBUTION STATEMENT (of the abstract entered in Block 20, if different from Report)

18. SUPPLEMENTARY NOTES

To be published in the Journal of Vacuum Science and Technology

19. KEY WORDS (Continue on reverse side if necessary and identify by block number)

Chromium; chromium oxide; desorption; oxidation; photoemission; photon stimulated desorption; direct recombination.

20. ABSTRACT (Continue on reverse side if necessary and identify by block number)

The interaction of oxygen with Cr(110) has been studied using synchrotron radiation techniques. A major objective of this work has been to determine the mechanism of electron and photon stimulated desorption (ESD/PSD) of O^+ from the surface of a non-maximal-valency, covalent oxide. The mechanism identified in this study is an extension of the Knotek-Feibelman Auger decay model of ion desorption (1), because the driving force is the Coulomb correlation of a localized 2 hole state rather than the instability of the ion in the Madelung potential (2).

DD FORM 1 JAN 73 1473 EDITION OF 1 NOV 65 IS OBSOLETE

S/N 0102-LF-014-6601

SECURITY CLASSIFICATION OF THIS PAGE (When Data Entered)

Summary Abstract

Mechanisms for Photon Stimulated Desorption of O^+ from Cr(110)

R. Stockbauer, D.E. Ramaker, E. Bertel, R.L. Kurtz and T.E. Madey

Surface Science Division

National Bureau of Standards

Washington, D.C. 20234

The interaction of oxygen with Cr(110) has been studied using synchrotron radiation techniques. A major objective of this work has been to determine the mechanism of electron and photon stimulated desorption (ESD/PSD) of O^+ from the surface of a non-maximal-valency, covalent oxide. The mechanism identified in this study is an extension of the Knotek-Feibelman Auger decay model of ion desorption (1), because the driving force is the Coulomb correlation of a localized 2 hole state rather than the instability of the ion in the Madelung potential (2).

Measurements were made using synchrotron radiation from the NBS SURF-II facility (25 eV $\lesssim h\nu \lesssim$ 75 eV) (3). The surface was characterized using various electron spectroscopies, including constant final state (CFS) secondary yield spectra, UPS, AES, and ELS, as well as electron and photon stimulated desorption of ions and ESD ion angular distributions (ESDIAD).

The interaction of oxygen with Cr(110) at 300 K leads to dissociative chemisorption at low exposures ($\lesssim$ 1-2L), followed by rapid formation of an oxide film as the exposure increases (4). In several studies, the data indicate that the stoichiometry of the stable oxide which forms on Cr(110) is in the range Cr_2O_3 to CrO_2 (5); there does not appear to be evidence for the formation of the maximal valency CrO_3 oxide (4-6). The present UPS data substantiate this conclusion.

PSD of O^+ ions having a most probable kinetic energy of $\sim$ 4 eV is observed for oxygen exposures $\gtrsim$ 1 Langmuir. ESDIAD data indicate that O^+ desorbs from Cr(110) in a normal direction, for all oxygen exposures (0-50 L) and adsorption temperatures (80-700 K) used in this work. For all oxygen exposures and adsorption temperatures, the O^+ ion yield vs. photon energy is similar to Fig. 1a for the lightly-oxidized Cr(110) surface (7): the yield increases from a threshold near 43 eV to a single sharp peak at 51 eV, and decreases at higher photon energies (the sharp structure above 55 eV is due to noise).

Figure 1b is the 2.5 eV CFS spectrum corresponding to the same thin oxide layer as Fig. 1a; this CFS curve is essentially a measure of the Cr 3p photoabsorption spectrum for the surface region. The CFS spectrum exhibits a pronounced shoulder at $\sim$ 45 eV and a peak at 60 eV which are absent in the PSD O^+ yield curve. The peaks at $\sim$ 51 eV are similar for both curves. Shoulders are also seen at $\sim$ 45 eV in CIS curves for photoemission from the Cr d band and the oxide valence band of the lightly-oxidized Cr(110) (8).

For the Knotek-Feibelman mechanism (1) of ion desorption from maximal valency oxides, the ion yield curve is expected to be similar in form to the CFS photoabsorption curve (core hole excitation cross section for the cation). In the O/Cr case, however, it is clear that there is structure in the Cr secondary electron yield (Fig. 1b) which is absent in the PSD O^+ yield curve (Fig. 1a); not all of the possible Cr 3p excitations lead to ion desorption.

Based on O K ELS data for Cr_2O_3 (9), Cr K XAS data for Cr_2O_3 and atomic Cr SXA data, we suggest that the shoulder at 45 eV in Fig. 1b is due to excitation to $2t_{2g}$ and $3e_g$ orbitals (which are primarily localized Cr 3d orbitals), and the peak at 51 eV corresponds to excitations to a $2t'_{2g}$ orbital. The $2t_{2g}$ and $3e_g$ orbitals will be dominated by resonant photoemission decay, and hence will not initiate desorption. In contrast, excitation into the $2t'_{2g}$ orbital will

decay by direct recombination as well as by Auger processes (i.e. where the excited electron either escapes before the Auger decay, or remains a spectator (satellite)), and hence can produce desorption.

Just below the Fermi level, UPS data reveal two main valence bands which can be identified as the Cr 3d and O valence bands (v_o and v_1) with electron density

$$v_o = c\ 3d$$

$$v_1 = a\ 3d + b\ O_{2p}.$$

In addition, a satellite feature is seen at a higher apparent binding energy than the valence band, v_1. Normal Auger decay of the core hole creates the valence band holes v_o^{-2}, $v_o^{-1}v_1^{-1}$, and v_1^{-2} with the relative intensity c^2, ac, and a^2. These relative intensities assume that the Cr intra-atomic Auger process dominates the Auger decay. Only the v_1^{-2} final state (or the $v_1^{-2}\ 2t'_{2g}$ state in the case of the satellite) is thought to be responsible for the O^+ desorption, because v_1 is a bonding orbital, albeit localized strongly on the O atom (b>>a). Recent cluster calculations for H/Ni (10) indicated a strong repulsive potential only for two holes in a bonding orbital. It is assumed that this is also required for O/Cr. The strong localization on the O atom decreases the covalent interaction beween neighboring v_1 bond orbitals and consequently increases the v_1^{-2} lifetime for the desorption process (2). In this picture, the desorption results from the Coulomb correlation of a localized 2-hole covalent antibonding state that was created by a metal-atom, intra-atomic Auger process. This is in sharp contrast to the Knotek-Feibelman model for ionic systems which assumes an inter-atomic Auger process in a maximal valency system.

References

1) M. Knotek and P.J. Feibelman, Phys. Rev. Lett. 40, 964 (1978); Surface Sci. 90, 70 (1979).

2) D.E. Ramaker, J. Vacuum Sci. Technol. A1(2), 1137 (1983).

3) D.M. Hanson, R.L. Stockbauer, and T.E. Madey, Phys. Rev. B 24, 5513 (1981).

4) Y. Sakisaka, H. Kato, and M. Onchi, Surface Sci. 120, 150 (1982).

5) G. Gewinner, J.C. Peruchetti, A. Jaegle, and A. Kalt, Surface Sci. 78, 439 (1978).

6) F. Watari and J.M. Cowley, Surface Sci. 105, 240 (1981).

7) The surface was heated to 450 K while dosing with 25 L of O_2, then cooled to 80 K for another 10 L dose; it was then annealed at 300 K, and cooled to 80 K for the measurements. (1L = $1x10^{-6}$ Torr s)

8) E. Bertel, R. Stockbauer and T.E. Madey, to be published.

9) L.A. Grunes, R.D. Leapman, C.N. Wilker, R. Hoffmann, and A.B. Kunz, Phys. Rev. B25, 7157 (1982).

10) C.F. Malius, R.H. Stulen, and J.O. Noell, Phys. Rev. Lett. 48, 1429 (1982).

Figure Caption

(a) O^+ PSD ion yield for lightly oxidized Cr(110), corrected for monochromator transmission and second order radiation.

(b) Constant Final State secondary electron yield curve for lightly oxidized Cr(110), corrected as above.

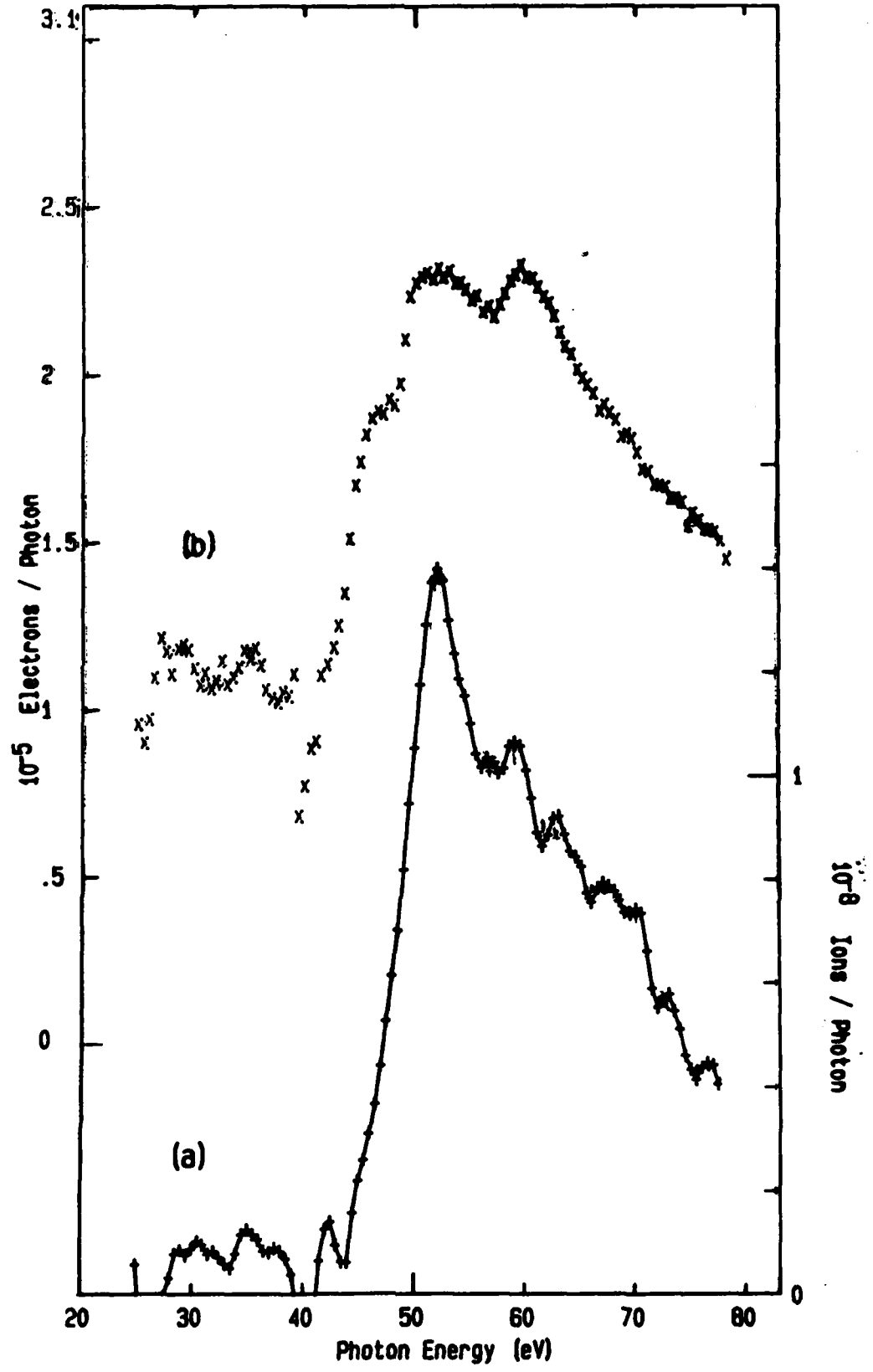
3.1
2.5
2
1.5
1
.5
0
10^{-5} Electrons / Photon
(b)
(a)
1
0
10^{-8} Ions / Photon
20
30
40
50
60
70
80
Photon Energy (eV)